Groeien met Groen Staal

EXMENTE

Reducing Electric Furnace Material Physical Property Infrastructure

Theory Manual

2025-09-17

Revision 2

Document Purpose

The purpose of this manual is to empower readers to pursue new innovations in the field of pyrometallurgical material property modelling by equipping them with knowledge and understanding of the models available in auxi-mpp.

Target Audience

This user manual is intended for the Groeien met Groen Staal (GGS) consortium involved in developing new Reducing Electric Furnace (REF) technologies, particularly the Theme II partners. It guides users through the underlying theory the material physical property models in auxi-mpp is based on.

The Theme II partners include process, metallurgical, chemical, and mechanical engineers from Tata Steel Netherlands, along with PhD students and their supervisors from TU Delft, TU Eindhoven, and the University of Twente.

Document Overview

The manual is divided into four parts.

Part I (Executive Summary) provides an overview of the purpose, contents, and outcomes of this manual. Part II (Slag Material Properties) covers the theory and validation of the models that describe slag physical properties. Part III (Liquid Alloy Material Properties) covers the theory and validation of the models that describe liquid alloy physical properties. Finally, Part IV (Appendices) contains definitions of terms and abbreviations used throughout the document.

Disclaimer

This Report has been prepared for the purpose set out in the brief provided to Ex Mente by GGS by Groeien met Groen Staal: WP-II.6 (GGS) and was not prepared for any third party or for any other purpose than that detailed in the engagement terms with GGS.

The contents of this document relate specifically to the project referenced herein, and Ex Mente cannot accept responsibility for use of the contents of this document other than for its intended purpose.

The information contained in this document is current as of the date of the Report, and may not reflect any event or circumstance which occurs after the date of the Report. The opinions contained herein are expressed in good faith and whilst every care has been taken in preparing this Report in accordance with standards of engineering practice (customary in the engineering profession for services of a similar nature), Ex Mente shall not, in any event, be liable for any indirect or consequential damages, including, without limitation, loss of profit or interruption of business arising from the recipient's use of this document or the contents hereof.

Document Identification

Distribution Statement	This document is distributed under the MIT License. Ex Mente retains copyright.
Project Label **Project Name**	NLG-176-603 Material Data Framework
Document Name **Document Number** **Release Date**	Reducing Electric Furnace Material Physical Property Infrastructure - Theory Manual NLG-176-603-DOC-1228 Rev. 2 2025-09-17
Compiled For	Groeien met Groen Staal: WP-II.6 Contact person: Vinod Dhiman Tel.: +31 (0)251 49 35 62 E-mail: Vinod.Dhiman@tatasteeleurope.com
Compiled By	Ex Mente Technologies (Pty) Ltd Postal address: P.O. Box 10214, Centurion, 0046, SOUTH AFRICA Tel.: +27 87 808 1903 E-mail: info@ex-mente.co.za Website: www.ex-mente.co.za

Document Authorisation

Release	Name	Signature
Author	Hanno Muire	Hanno Muire Digitally signed by Hanno Muire Date: 2025.09.18 11:10:54 +02'00'
Author	Stefan Koning	Stefan Koning Digitally signed by Stefan Koning Date: 2025.09.18 11:26:38 +02'00'
Reviewer	Dr Johan Nell	Johan Nell Digitally signed by Johan Nell Date: 2025.09.18 10:30:10 +02'00'
Approver	Dr Johan Nell	Johan Nell Digitally signed by Johan Nell Date: 2025.09.18 10:30:20 +02'00'

Document History

Revision	Release Date	Description
Rev. 2	2025-09-17	Third formal release to GGS.
Rev. 1	2025-07-01	Second formal release to GGS.
Rev. 0	2025-02-18	First formal release to GGS.
Draft 1	2025-02-14	Draft 1 release for internal review.

Contents

List of Figures

List of Tables

Part I

Executive Summary

Chapter 1

Introduction

The pyrometallurgy industry plays an important role in the global economy but faces growing challenges that demand innovative solutions. These challenges include stricter environmental regulations, such as the EU's target of a 30% reduction in CO_2 emissions by 2030, alongside the rising global demand for high-grade steel and increased reliance on lower-quality ores due to the depletion of high-grade resources. Consequently, traditional Blast Furnace-Basic Oxygen Furnaces (BF-BOFs) must be replaced with more efficient smelting technologies, such as the proposed REF process unit, to help the industry adapt.

Innovation requires advancements in existing tools, particularly in pyrometallurgy. There is a growing need to describe processes more fundamentally through improved material property models, process models, and multiphysics models. These improved models can assist the industry in developing new REF process units more quickly and cost-effectively.

This manual supports the GGS Theme II partners in developing new REF processes with well documented theory on material property models. The property models documented here are implemented in an open-source python package called auxi-mpp. This manual therefore gives the theoretical background and insight necessary to arrive at better innovations using the models available in auxi-mpp.

Chapter 2

Focus

This iteration of the manual describes physical property models for slags and liquid alloys. The covered properties include density (molar volume), viscosity, and electrical conductivity for both material types, as well as diffusivity for slags and thermal conductivity for liquid alloys.

Future versions will expand to include material physical property models for gases, single pellet, and multiphase materials like pellet beds, all accessible through auxi-mpp.

The models take temperature, pressure, composition, and for multi-component models also phase constituent activities, as inputs. The underlying theory for each property model is explained to help readers understand its operation and the specific component systems for which it is valid. The models have been validated against extracted model and experimental data to demonstrate accurate implementation in auxi-mpp.

Chapter 3

Highlights

3.1 Slag Material Properties

Density Model (Thibodeau): The Thibodeau density model, which estimates slag density via molar volume, has been successfully implemented in auxi-mpp. This model is fundamentally based on the structural Q-species concept, accounting for variations in melt composition and temperature. The auxi-mpp implementation demonstrates good agreement with literature models and experimental data for unary, binary, ternary, and quaternary Fe-free systems. For Fe-bearing systems, while parameters have been refitted due to changes in Fe bond fraction parameters in the underlying Modified Quasi-chemical Model (MQM) model, further refinement is still required to fully align with extracted literature model data.

Electrical Conductivity Models:

1. **Thibodeau Electrical Conductivity (ThibodeauEC) Model**: This structural model uses the Nernst-Einstein relationship and relies on the molar volume and diffusivity models to estimate electrical conductivity . The auxi-mpp implementation of this model closely reproduces literature and experimental data for unary, binary, and ternary Fe-free systems. For Fe-bearing systems, there is an increasing deviation from literature data as the fraction of iron oxides increases. This is likely due to a parameter change for FeO in the underlying thermodynamic database.

2. **Hundermark Electrical Conductivity Models**: This unified, semi-empirical model is particularly useful for Fe-bearing slags, although it can apply to others. For non-Fe bearing systems, auxi-mpp's implementation generally reproduces literature models well, with some exceptions for Al2O3-containing systems. Fe-bearing systems, current auxi-mpp estimates deviate slightly from literature data as the amount of iron oxides increases. This is thought to be caused by updated thermodynamic parameters for FeO in the FactSage database.

Diffusivity Model (Thibodeau): This model calculates diffusivity from slag polymerisation and is integral to the electrical conductivity calculation within the ThibodeauEC model. While not independently validated due to a lack of direct literature data for comparison, its successful incorporation and indirect validation through the accurate performance of the Thibodeau electrical conductivity model indicate its correctness.

Viscosity Model (Grundy-Kim-Brosch): The Grundy-Kim-Brosch viscosity model has been implemented and successfully validated against literature models and experimental data across unary, binary, and multicomponent systems. For multicomponent Fe-bearing systems, auxi-mpp generally performs well; however, visible deviations from literature for systems like $CaO-Fe_2O_3-SiO_2$ and $Al_2O_3-CaO-Fe_2O_3-SiO_2$ were observed, where auxi-mpp's results align more closely with FactSage 8.3, suggesting potential inaccuracies in the original literature data or changes in underlying thermodynamic databases.

3.2 Liquid Alloy Material Properties

Density Models: Several models for liquid alloy density have been implemented in auxi-mpp. The primary model, based on volumetric thermal expansion, has been successfully validated for unary metallic elements, the binary Fe-Ni system, and the ternary Cu-Fe-Ni system, showing good agreement with experimental data. Supported unary elements for the volumetric thermal expansion model include: Al, Sb, Bi, Cd, Cr, Co, Cu, Ga, Hf, In, Fe, Pb, Mo, Ni, Nb, Si, Ag, Ta, Tl, Sn, Ti, W, V, Zn, and Zr. Additional empirical models for binary alloys containing non-metallics (e.g., Fe-C, Fe-S) and specific commercial alloys (e.g., stainless steel 304) have also been implemented and validated where data was available.

Electrical Conductivity Model (Polynomial Fit): Due to the complexity of modelling liquid alloys with transition metals, an empirical approach using polynomial fits to experimental resistivity data has been implemented. The models for unary (Fe, Ni, Si), binary (Fe-C, Fe-Si, Fe-Mn, Fe-Ni), and ternary (Fe-C-Si) systems have been validated. Second-degree polynomials are generally recommended as they provide a good balance of accuracy and stability, avoiding the overfitting issues seen with higher-order fits.

Viscosity Models: Two distinct viscosity models have been implemented.

1. Andrade-Type Model: For unary liquid metals, this model has been successfully validated against recommended reference data across all supported elements. Supported elements include: Al, Sb, Bi, Cd, Co, Cu, Ga, In, Fe, Pb, Hg, Ni, Si, Ag, Tl, Sn, and Zn.
2. Deng Model: This linear, empirical model for binary and multi-component iron-based alloys (Fe-C-X, where X = Si, Mn, P, S, or Ti) shows good agreement with experimental data across all validated systems.

Thermal Conductivity Model (Wiedemann-Franz Law): Thermal conductivity is estimated by applying the Wiedemann-Franz law to the electrical conductivity polynomial models. Validation against the Fe-Ni system, the only one with sufficient experimental data, indicates that the model underestimates thermal conductivity by 20–38%, a finding consistent with other literature. Users should be aware that the fundamental assumptions of the Wiedemann-Franz law are violated for pig iron compositions, and the model should be used with caution.

Part II

Slag Material Properties

Background

Slags are integral to pyrometallurgical processes, serving crucial roles in metal extraction, purification, and environmental control. These molten materials, predominantly composed of metal oxides, form during the smelting, refining, and alloying of metals. Slags not only facilitate the separation of metals from their ores but also play a significant role in controlling reactions, heat transfer, and minimising environmental impacts such as emissions and waste generation. Controlling the slag properties is therefore essential for optimal yields and minimal waste. To effectively control slag properties, it is important to understand the underlying principles that govern them.

The physical properties of slags are intricately interconnected, primarily due to the slag's structure. This structure, specifically the degree of polymerisation (Q) of the silicate network, acts as the fundamental characteristic influencing the slag's properties like diffusivity (D), viscosity (μ), electrical conductivity (σ), thermal conductivity (κ), and density (ρ) (Mysen and Richet 2019).

A highly polymerised network, characterised by long, interconnected chains of silicate tetrahedra, restricts the movement of all slag components. This restricted movement results in higher μ, as the slag becomes more resistant to flow. Similarly, D decreases, as the interconnected network hinders the movement of ions. σ is also reduced, as the movement of charge-carrying cations is impeded by the tightly bound structure. κ is increased, as the interconnected structure presents a lower resistance to the flow of phonons, resulting in higher thermal conductivity.

Conversely, a less polymerised network with more non-bridging oxygen atoms, allows for greater freedom of movement. This leads to lower μ, higher D, increased σ, but decreased κ. The molar volume ($\bar{V}$) and ρ is also affected by Q, as the arrangement of silicate tetrahedra and the packing of cations influence the overall volume occupied by the slag.

The structure of silicate melts is characterised by the three types of bridging oxygen atoms. A free oxygen separates a metal-metal (M – M) pair, a non-bridging oxygen separates a metal-silicon (M – Si) pair, and a bridging oxygen separates a silicon-silicon (Si – Si) pair. From the Si atom's perspective, silicon atoms are always tetrahedrally bonded to four oxygen ions such that the basic silicate melts mainly consist of M^{q+}, O^{2-}, and $SiO_4{}^{4-}$. As the silica content increases beyond the orthosilicate composition, the $SiO_4{}^{4-}$ tetrahedra begin to polymerise, forming more bridging oxygens and gradually creating a three-dimensional network.

The degree of polymerisation of a slag is described by the Q^{n}-species which is the fraction of $SiO_4{}^{4-}$ ions that contains n bridging oxygens. In pure SiO_2, all four oxygens surrounding each silicon are bridging oxygens, with the Q^4-species fraction being 1.0, whereas an isolated $SiO_4{}^{4-}$ ion is a Q^0-species (Kim et al. 2012a).

The structure of a slag is significantly affected by both temperature (T) and composition (x). Increasing T generally leads to a decrease in polymerisation, as the thermal energy breaks the bonds between silicate tetrahedra, resulting in shorter chains and a more fluid slag. x also plays a crucial role, with network-forming oxides like SiO_2 and Al_2O_3 promoting polymerisation by forming extensive interconnected networks. Conversely, network-modifying oxides such as CaO, MgO, Na_2O, and K_2O disrupt the network by breaking the Si – O – Si bonds, resulting in shorter chains and a less polymerised structure. Al_2O_3 is also amphoteric and may act as a network modifier depending on the availability of other network-modifying oxides, such as CaO or Na_2O, to charge compensate for Al^{3+} ions.

In short, the specific type and concentration of these oxides, along with T, ultimately determine the structure and resulting physical properties of slag.

Chapter 4

Density

4.1 Thibodeau Density Model

A model developed by Thibodeau et al. (2016a).

4.1.1 Introduction

The density is closely related to the molar volume of a slag, it is essentially the reciprocal thereof. Estimation of the density is therefore not limited to models strictly for density, as molar volume models will achieve the same goal. Hence, the structural molar volume model developed by Thibodeau et al. (2016a) was implemented with the intention to estimate slag density.

4.1.2 Model Overview

This model is based on the concept of silicate tetrahedral Q-species. Q-species represent different structural units defined by silicon tetrahedra with varying numbers of bridging oxygens (oxygen atoms shared between two tetrahedra), non-bridging oxygens (oxygen atoms bonded to only one silicon atom), and free oxygens (oxygen atoms not bonded to silicon).

The original literature model uses the MQM found in ChemApp for Python and the FactSage FToxid database to calculate the quantity of each Q-species in a given melt (Thibodeau et al. 2016a). Each Q-species is assigned a molar volume that changes linearly with temperature. The model calculates the total molar volume of the melt by summing the contributions from each Q-species and free oxide species. This allows the model to account for the non-linear behaviour of molar volume in silicate melts that arises from the changing distribution of Q-species with composition and temperature.

It is important to note that this model is formulated strictly for liquid slag systems – the user should therefore ensure that his/her system is above the liquidus temperature before performing calculations. Also, we recommend the model to be used within the validation ranges specified in Table 4.2. The validation ranges are based on selected figures from the original articles. To peruse the full range of systems the model were validated for, the user is directed to the original article.

Finally, for systems containing Fe, the correct ratio of Fe(II) and Fe(III) has to be provided. This means the user needs to know the oxidation environment of the system, and from that estimate this ratio before passing it on to the model.

4.1.3 Model Formulation

Molar volume for a multicomponent system is typically expressed with Equation (4.1).

$$\bar{V}_{\text{slag}} = \frac{\sum_i \bar{m}_{\text{i}} \cdot x_{\text{i}}}{\rho_{\text{slag}}} \tag{4.1}$$

However, the molar volume of the metal oxide melt (slag) can also be expressed as the sum of molar volumes for each phase constituent scaled by its mole fraction in the slag, according to Equation (4.2).

$$\bar{V}_{\text{slag}} = \sum_i \bar{V}_{\text{i}} \cdot x_{\text{i}} \tag{4.2}$$

Thibodeau et al. (2016a) and Thibodeau et al. (2016b) developed more fundamental, structure-based equations based on Equations (4.1) and (4.2) to model the molar volume in binary and multicomponent slag systems containing $Li_2O - Na_2O - K_2O - MgO - CaO - MnO - PbO - Al_2O_3 - SiO_2$. This model was further extended to include FeO and Fe_2O_3 in Thibodeau et al. (2016c), demonstrating its applicability across a wide range of SiO_2-based slag systems. The following information describes the model and its implementation.

Unary

The molar volume of a unary system is simply calculated as a linear combination of a pure oxide's parameters at a specific temperature, as shown in Equation (4.3).

$$\bar{V}_{\text{slag}}^{T} = \text{a} + \text{b}T \tag{4.3}$$

Binary

The level of oxygen in slag determines the types and quantities of bonding scenarios that develop between non-oxygen atoms. There are types of bonding scenarios corresponding to the three possible structural states for oxygen shown in Equation (4.4). O^0 represents a bridging oxygen; Si – O – Si, O^{-2} refers to a free oxygen; M – O – M, and O^- denotes a non-bridging oxygen; Si – O – M.

$$\text{O}^0 + \text{O}^{2-} \rightleftharpoons 2\text{O}^- \tag{4.4}$$

If we are dealing with one mole of slag, the total moles of oxygen per mole of slag is calculated by summing the oxygen contributions from each species in the slag system, as shown in Equation (4.5).

$$n_{\mathrm{t}} = x_{\mathrm{M_2O}} + x_{\mathrm{MO}} + 3x_{\mathrm{M_2O_3}} + 2x_{\mathrm{MO_2}} \tag{4.5}$$

The number of bridging oxygen atoms is calculated using Equation (4.6), which incorporates the bond fraction of Si – O – Si contacts and can be obtained from the MQM model found in ChemApp for Python. Likewise, Equation (4.7) is used to determine the number of M – O – M contacts.

$$n_{\mathrm{O^0}} = x_{\mathrm{Si-Si}} \cdot n_{\mathrm{t}} \tag{4.6}$$

$$n_{\mathrm{M-M}} = x_{\mathrm{M-M}} \cdot n_{\mathrm{t}} \tag{4.7}$$

Now, the number of Si – O^0 bonds per mole of solution is simply twice the number of bridging oxygens; $2n_{\mathrm{O^0}}$. The average number of bridged oxygens per silicon atom is therefore $2n_{\mathrm{O^0}}/x_{\mathrm{SiO_2}}$. Assuming that all Si atoms are tetrahedrally coordinated with four oxygens, the probability that one of the oxygens will be bridging is therefore a quarter of this, as given by Equation (4.8).

$$P_{\mathrm{O^0}} = \frac{1}{4} \cdot \frac{2n_{\mathrm{O^0}}}{x_{\mathrm{SiO_2}}} = \frac{n_{\mathrm{O^0}}}{2x_{\mathrm{SiO_2}}} \tag{4.8}$$

If the probability of an oxygen in a Q-species being a bridging oxygen is known, the probability to have a given Q^{n} (where $\mathrm{n} = 0, 1, 2, 3,$ or 4) can be calculated with Equation (4.9);

$$W_{\mathrm{n}} = \frac{4!}{(4-\mathrm{n})!\mathrm{n}!} P_{\mathrm{O^0}}^{\mathrm{n}} (1 - P_{\mathrm{O^0}})^{(4-\mathrm{n})} \quad \mathrm{n} = 0, 1, 2, 3, \text{or } 4 \tag{4.9}$$

The amount of each Q-species per mole of slag can be determined from their probabilities to form, calculated with Equation (4.10). This is achieved by multiplying W_{n} with $x_{\mathrm{SiO_2}}$, since the latter gives the mole fraction of all Q-species combined;

$$n_{\mathrm{Q^n}} = W_{\mathrm{n}} \cdot x_{\mathrm{SiO_2}} \text{ for } \mathrm{n} = 0, 1, 2, 3, \text{or } 4 \tag{4.10}$$

The molar volume is then calculated by Equation (4.11) as a linear combination of the molar volume for each species, weighted by the amount of the associated species present.

$$\bar{V}_{\mathrm{slag}}^{T} = n_{\mathrm{Q^4}} \bar{V}_{\mathrm{SiO_2}}^{T} + \sum_{\mathrm{n}=0}^{3} n_{\mathrm{Q^n}} \bar{V}_{\mathrm{Q^n}}^{T} + n_{\mathrm{M-M}} \bar{V}_{\mathrm{M-M}}^{T} \tag{4.11}$$

In Equation (4.11), the species specific molar volume is calculated with Equation (4.12), where the two empirical parameters a and b were fitted to the pure oxide slags, assuming that their molar volumes varies linearly with temperature.

$$\bar{V}_{\mathrm{i}} = \mathrm{a_i} + \mathrm{b_i} T \tag{4.12}$$

Multicomponent

To calculate the molar volume for multicomponent systems, Equation (4.11) was adapted to account for the different cations that Si can be connected to and for the different ways in which the cations can connect to each other. This is given in Equation (4.13). The molar volume of a given Q-species is therefore calculated as a linear combination of the different non-bridging oxygen, Si – M$_i$, scenarios. The contribution from free oxygen contacts, $\bar{V}_{\mathrm{M_i-M_j}}$, are taken as the average of their pure oxides' molar volumes as per Equation (4.14).

$$\bar{V}^T_{\mathrm{slag}} = n_{\mathrm{Q^4}}\bar{V}^T_{\mathrm{SiO_2}} + \sum_{\mathrm{n=0}}^{3} n_{\mathrm{Q^n}} \frac{\sum_i x_{\mathrm{Si-M_i}}\bar{V}^T_{\mathrm{Q^n}}}{\sum_i x_{\mathrm{Si-M_i}}} + \sum_i \sum_j n_{\mathrm{M_i-M_j}}\bar{V}^T_{\mathrm{M_i-M_j}} \tag{4.13}$$

$$\bar{V}^T_{\mathrm{M_i-M_j}} = \frac{\bar{V}^T_{\mathrm{M_i}} + \bar{V}^T_{\mathrm{M_j}}}{2} \tag{4.14}$$

Density

Once the molar volume is known, the density can be calculated. The density can be calculated from molar volume with Equation (4.15).

$$\rho_{\mathrm{slag}} = \frac{\sum_i \bar{m}_{\mathrm{i}} x_{\mathrm{i}}}{\bar{V}_{\mathrm{slag}}} \tag{4.15}$$

If the molar volume model proofs to be accurate, accurate density values can be calculated from it.

4.1.4 Variable Declarations

The parameters used in Equation (4.12) is tabulated in Table 4.1

Table 4.1: Empirical model parameters for molar volume calculation of SiO_2 slags.

	Q^3		Q^2		Q^1		Q^0		Pure Oxide	
Oxides	a	b×10^3	a	b×10^3	a	b×10^3	a	b×10^3	a	b×10^3
SiO_2	-	-	-	-	-	-	-	-	27.3	0.00
Li_2O	29.96	2.80	35.73	5.00	41.66	6.50	48.18	8.20	13.52	3.30
Na_2O	34.41	3.50	43.11	8.00	53.22	10.0	63.78	13.0	25.32	5.95
K_2O	38.17	6.00	54.75	12.00	68.92	16.50	87.63	21.00	37.85	8.83
MgO	30.42	1.00	34.79	2.40	37.66	4.00	42.34	5.00	14.05	0.70
CaO	32.60	1.70	35.60	3.50	42.60	6.00	50.70	7.00	19.54	0.85
MnO	31.00	1.60	34.50	3.50	38.80	6.50	43.00	7.00	16.09	0.95
PbO	39.00	1.00	44.50	3.00	56.00	5.00	65.00	8.30	23.86	3.21
Al_2O_3	35.98	0.00	36.89	0.00	47.69	0.00	50.30	0.00	11.15	0.47
FeO*	29.90	3.50	31.10	2.00	40.80	5.20	48.70	6.70	13.46	1.17
Fe_2O_3*	40.60	0.00	48.20	0.00	82.60	0.00	44.20	0.00	10.05	1.38

* The model parameters for FeO and Fe_2O_3 had to be refitted due to a change in Fe parameters used in the MQM model of ChemApp for Python.

4.1.5 Assumptions

The structural molar volume model for oxide slags is based on several key assumptions.

1. It relies on accurately estimated molar volumes of pure liquid oxide components.
2. It assumes that the molar volume of each component, including pure oxides and Q-species, changes linearly with temperature.
3. The model uses Q-species as the fundamental structural units, assuming they are the minimal units needed to explain silicate melt volumes.
4. It considers the excess molar volume from medium-range structures formed by Q-species to be negligible.
5. It assumes that the MQM, with the FactSage FToxid database, accurately calculates bond fractions.
6. It assumes a single liquid melt without solid phases or liquid miscibility gaps.
7. It assumes Al_2O_3 to be a network modifier.
8. It assumes other potentially important anions (e.g. S^{2-}, $SO_4{}^{2-}$, $CO_3{}^{2-}$, etc.) will not disrupt the oxygen network.

4.1.6 Model Validation

Molar Volume, Fe-free Systems

The Thibodeau density model implemented in auxi-mpp, was evaluated by comparing its inverse (molar volume) against both the literature model and experimental data. Data were extracted directly from figures in Thibodeau et al. (2016a) and Thibodeau et al. (2016b). The models were validated for the systems and temperatures shown in Table 4.2.

Table 4.2: Molar Volume Validation Ranges

Model	Systems	Composition (mol mol^{-1})	Temperature (K)
Unary	SiO_2	pure substance	$0 - 3000$
	Al_2O_3	pure substance	$2000 - 3250$
	MgO	pure substance	$300 - 4000$
	CaO	pure substance	$300 - 3500$
Binary	$Al_2O_3 - SiO_2$	$x_{Al_2O_3} = 0 - 1$	2073
	$CaO - SiO_2$	$x_{CaO} = 0 - 1$	$1773, 1973$
	$MgO - SiO_2$	$x_{MgO} = 0 - 1$	1973
Ternary	$CaO - MgO - SiO_2$	$x_{MgO} = 0 - 1$, $x_{SiO_2}/x_{CaO} = 1$	$1723, 1873$
	$CaO - MgO - SiO_2$	$x_{CaO} = 0 - 1$, $x_{SiO_2}/x_{MgO} = 2$	$1723, 1873$
	$Al_2O_3 - MgO - SiO_2$	$x_{SiO_2} = 0 - 1$, $x_{MgO}/x_{Al_2O_3} = 1$	$1873, 1973$
	$Al_2O_3 - MgO - SiO_2$	$x_{MgO} = 0 - 0.5$, $x_{SiO_2} = 0.5$	$1873, 1973$
	$Al_2O_3 - CaO - SiO_2$	$x_{SiO_2} = 0 - 1$, $x_{CaO}/x_{Al_2O_3} = 1$	$1773, 1873$
	$Al_2O_3 - CaO - SiO_2$	$y_{Al_2O_3,CaO,SiO_2} = 0 - 1$	1873
	$CaO - MgO - SiO_2$	$y_{CaO,MgO,SiO_2} = 0 - 1$	1873
Quaternary	$Al_2O_3 - CaO - MgO - SiO_2$	$y_{Al_2O_3,CaO,SiO_2} = 0 - 0.9$, $y_{MgO} = 0.1$	1873
	$Al_2O_3 - CaO - MgO - SiO_2$	$y_{CaO,MgO,SiO_2} = 0 - 0.8$, $y_{Al_2O_3} = 0.2$	1873
	$Al_2O_3 - CaO - MgO - SiO_2$	$y_{CaO,MgO,SiO_2} = 0 - 0.7$, $y_{Al_2O_3} = 0.3$	1873

The auxi-mpp model agrees well with the literature model across unary, binary, ternary and quaternary systems. Figure 4.1 shows that auxi-mpp aligns with the literature model ("2016: Thibodeau et al.") for unary systems, plotting molar volume against temperature.

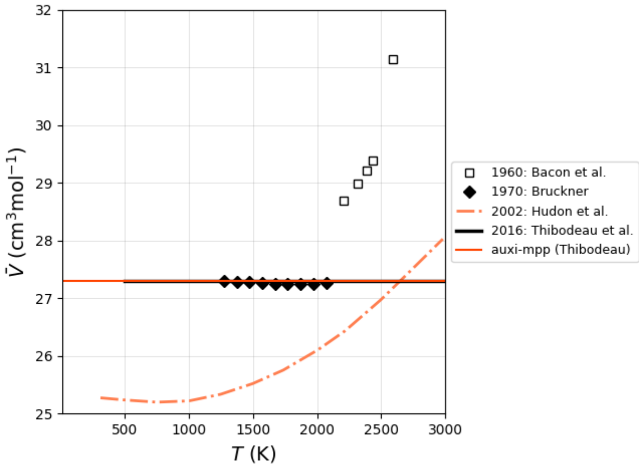

(a) SiO_2

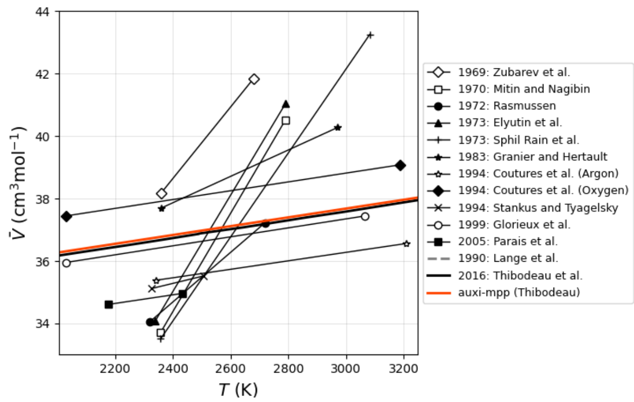

(b) Al_2O_3

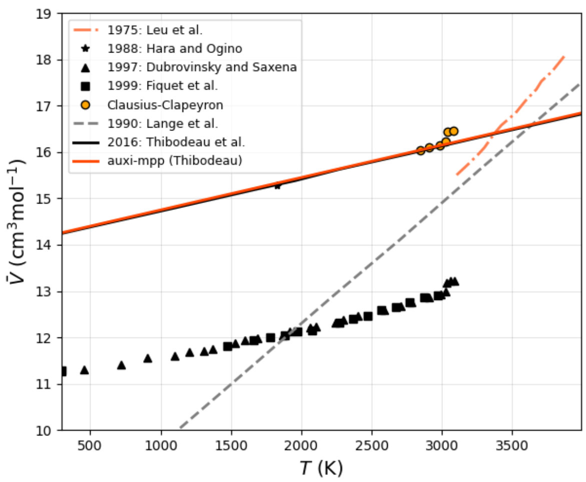

(c) MgO

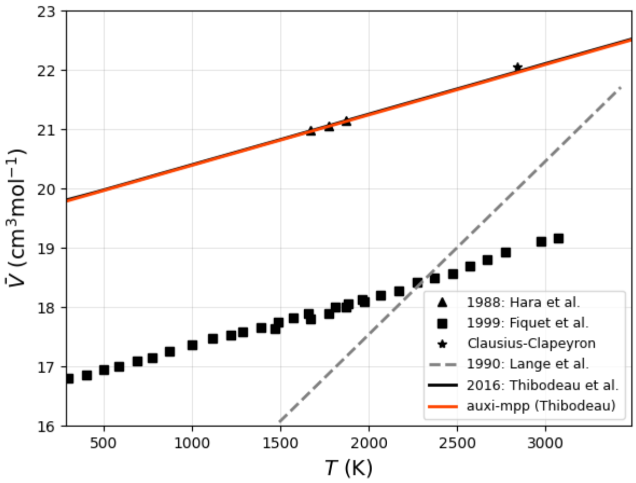

(d) CaO

Figure 4.1: Molar volume vs temperature of unary systems.

Similarly, Figure 4.2 and Figure 4.3 confirm this agreement for binary and ternary systems, where molar volume is plotted against mole fraction.

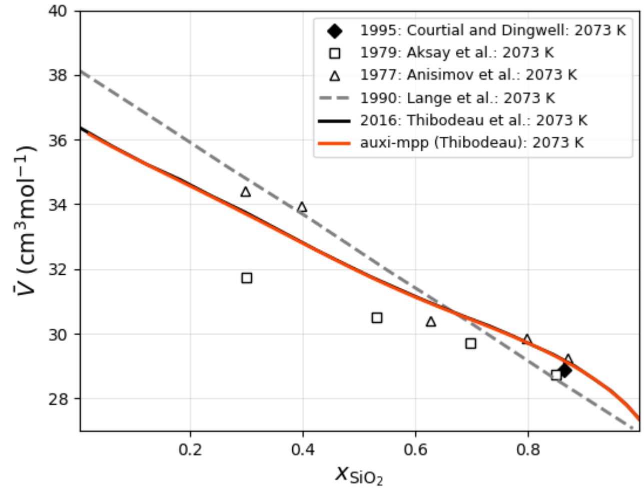

(a) $Al_2O_3 - SiO_2$

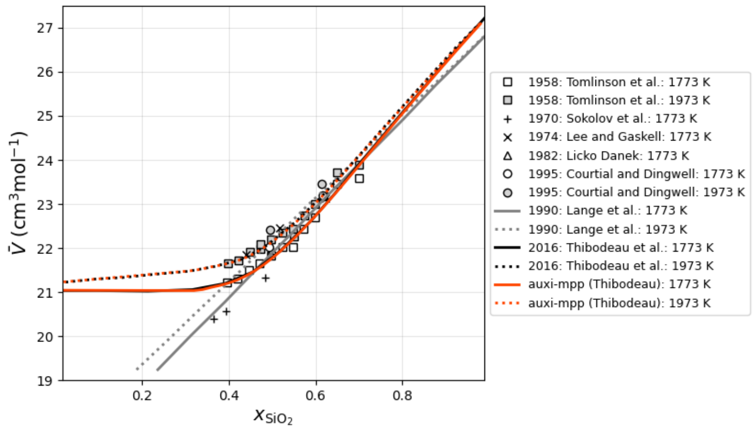

(b) $CaO - SiO_2$

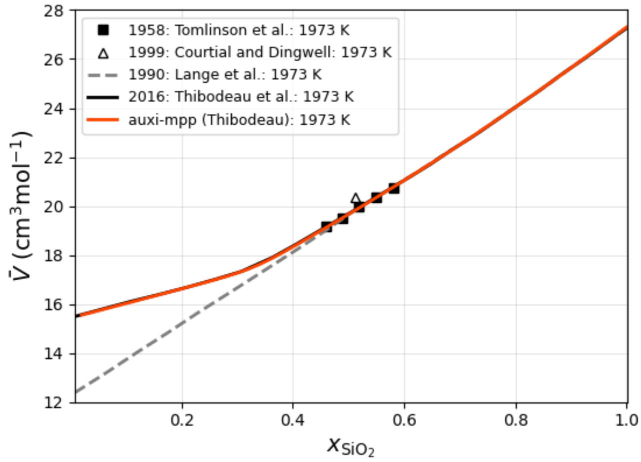

(c) $MgO - SiO_2$

Figure 4.2: Molar volume vs mole fraction of binary systems.

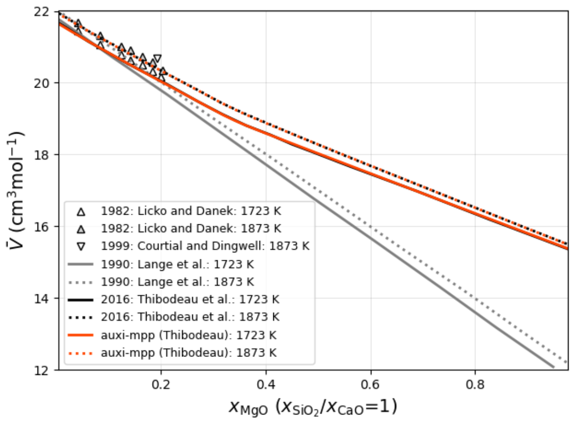

(a) $CaO-MgO-SiO_2$

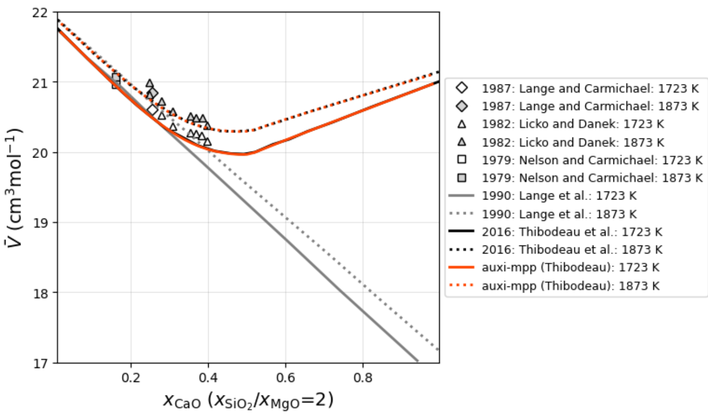

(b) $CaO-MgO-SiO_2$

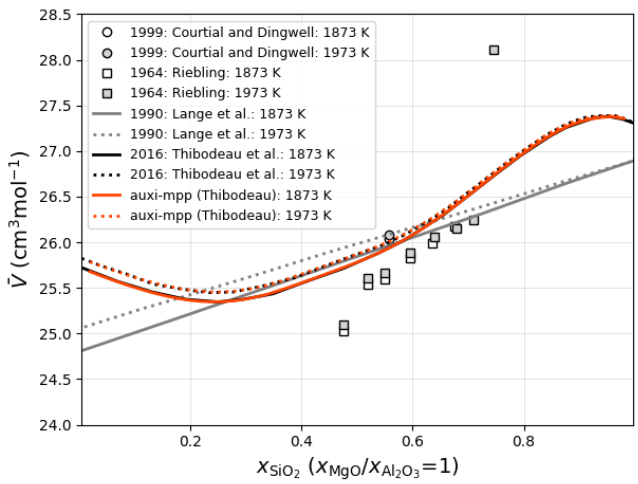

(c) $Al_2O_3-MgO-SiO_2$

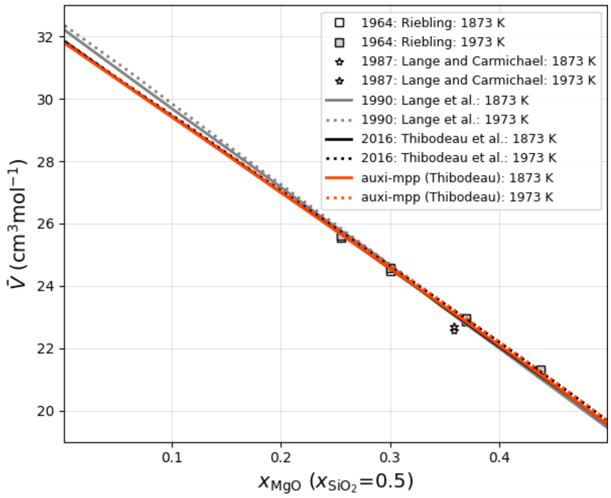

(d) $Al_2O_3-MgO-SiO_2$

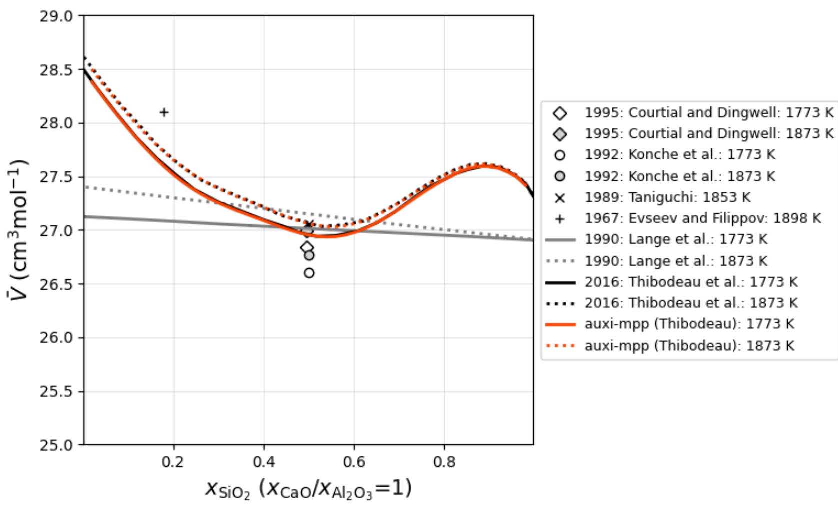

(e) $Al_2O_3-CaO-SiO_2$

Figure 4.3: Molar volume vs mole fraction for the ternary systems.

auxi-mpp was also validated for $Al_2O_3-CaO-MgO-SiO_2$. In Figure 4.4, the ternary diagrams display the molar volume contour lines as calculated by Thibodeau et al. (2016b). For each point on the contour line, the composition were extracted and used to calculate the molar volume using auxi-mpp to see if the contour line's value could be reproduced.

The green points in Figure 4.4 indicate auxi-mpp's estimations that lies within a 1% error threshold compared to the value of the contour line.

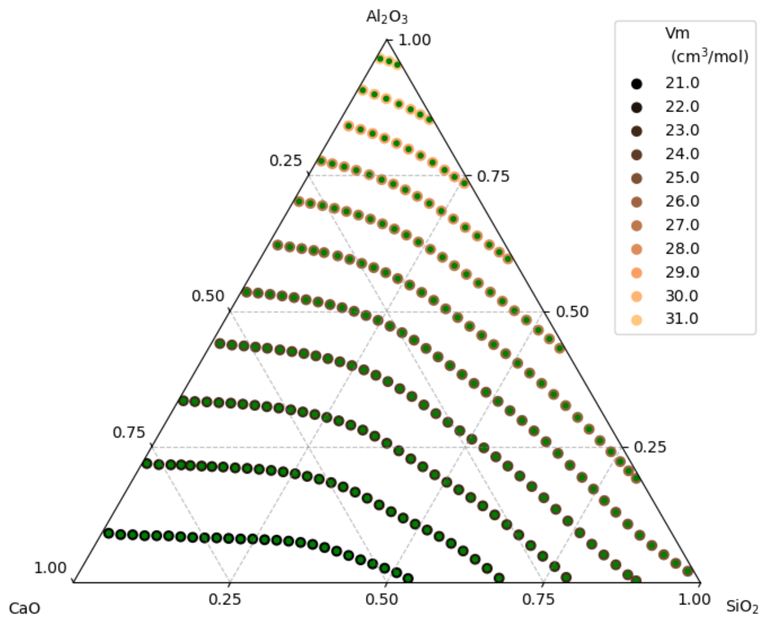

(a) $Al_2O_3 - CaO - MgO - SiO_2$ system at 1873 K and $y_{\mathrm{MgO}} = 0.1$

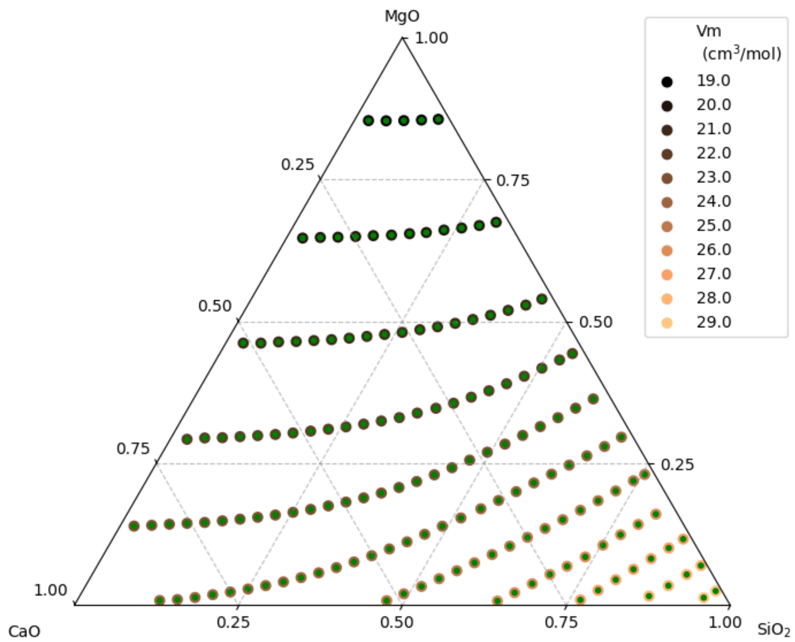

(b) $Al_2O_3 - CaO - MgO - SiO_2$ system at 1873 K and $y_{\mathrm{Al_2O_3}} = 0.3$

Figure 4.4: Molar volume vs mole fraction for quaternary systems.

Finally, Figure 4.5 gives an oversight of how auxi-mpp compares with literature for ternary and quaternary systems.

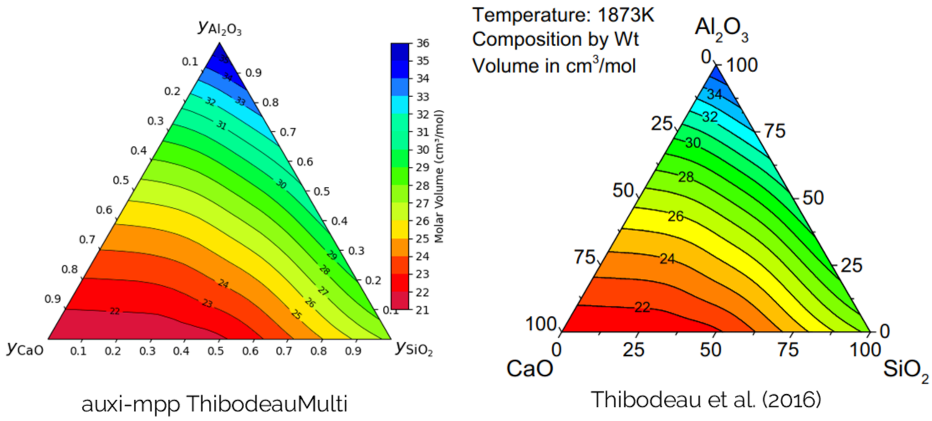

(a) $Al_2O_3 - CaO - SiO_2$

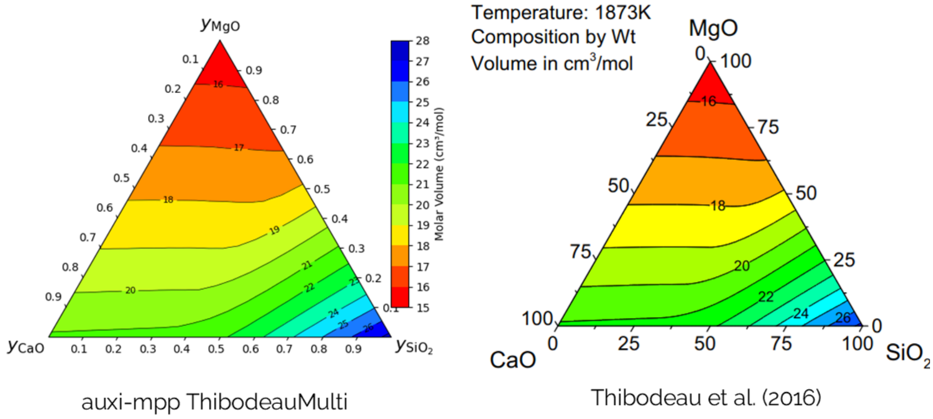

(b) $CaO - MgO - SiO_2$

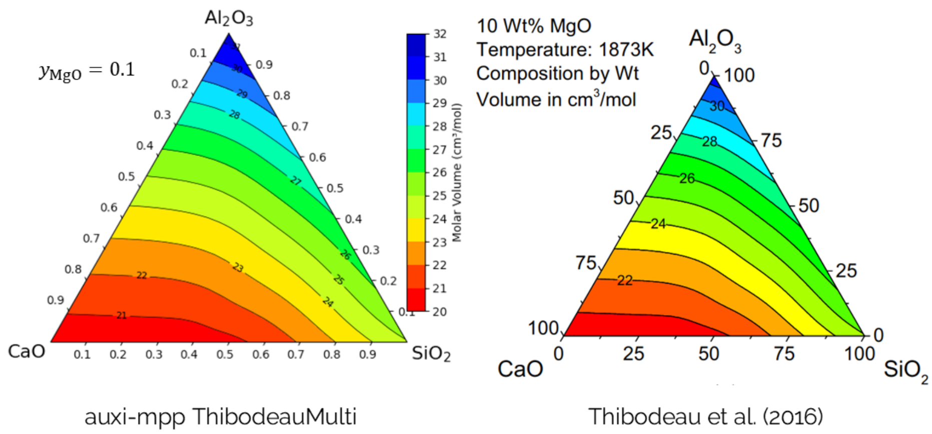

(c) $Al_2O_3 - CaO - MgO - SiO_2$

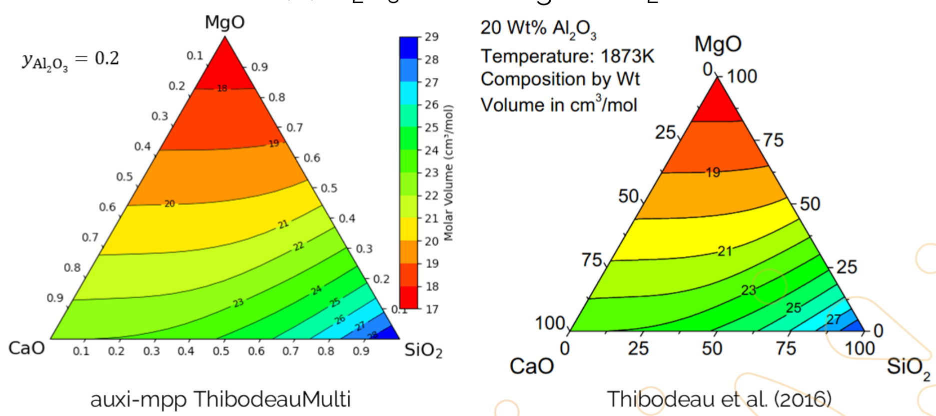

(d) $Al_2O_3 - CaO - MgO - SiO_2$

Figure 4.5: Comparing auxi-mpp's contour plots with literature.

Molar Volume, Fe-bearing Systems

The original parameters were refitted due to a change in the Fe parameters used in the MQM model of ChemApp for Python which resulted in a change in bond fraction estimates. This is shown with Figure 4.6 for the fraction of non-bridging oxygens in the SiO_2 – FeO system compared to SiO_2 – CaO and SiO_2 – MgO systems.

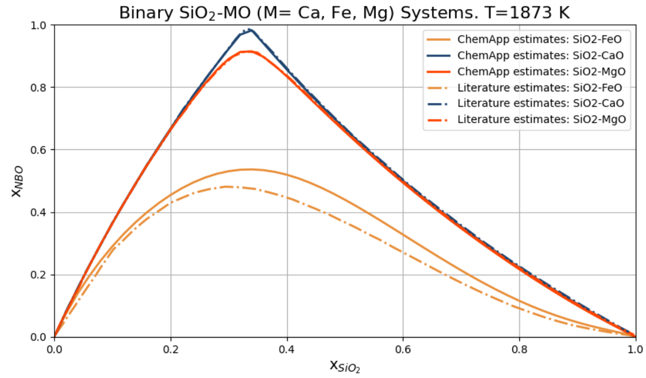

Figure 4.6: Fraction of non-bridging oxygens for binary systems.

Correlation plots were generated for the following Fe-bearing systems using both the original and the updated parameters for FeO and Fe_2O_3 from Table 4.1. There is still deviation between the extracted model data and estimated model data from auxi-mpp with respect to temperature as shown in Figure 4.8. Further refinement of the parameters are required and will be addressed in a later update.

1. FeO – SiO_2 (Hypothetical)
2. Fe_2O_3 – SiO_2 (Hypothetical)
3. Fe_2O_3 – FeO – SiO_2
4. CaO – Fe_2O_3 – FeO – SiO_2

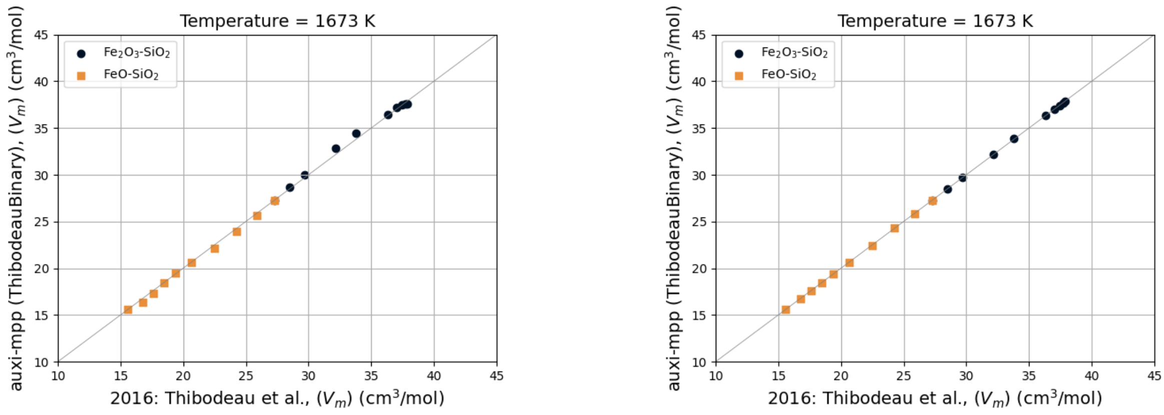

(a) (b)

Figure 4.7: auxi-mpp vs Thibodeau (2014) for correlation plots for hypothetical Fe-bearing binary systems, original (left) and updated (right) for FeO and Fe_2O_3 parameters.

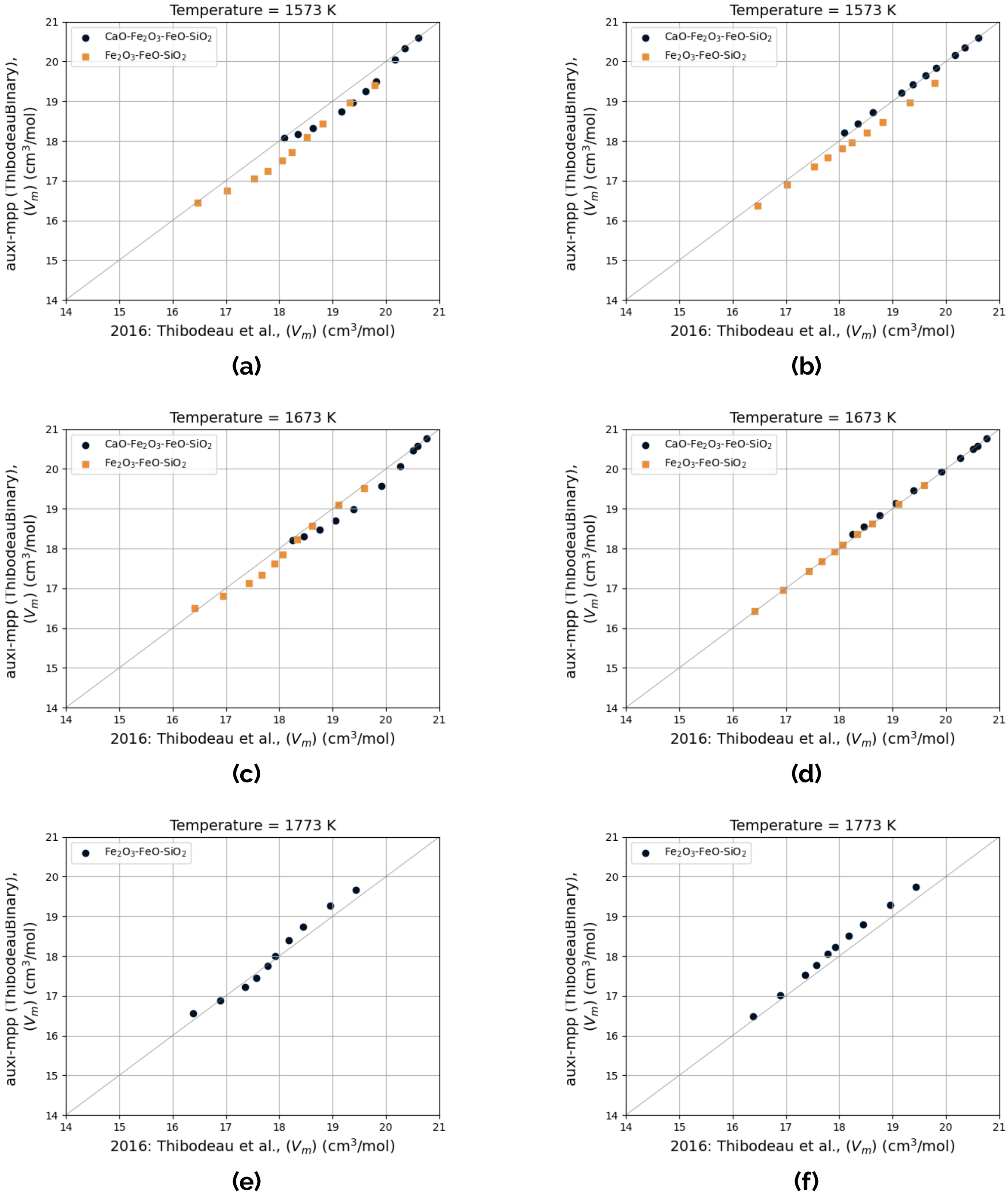

Figure 4.8: auxi-mpp vs Thibodeau (2014) correlation plots, original (left) and updated (right) for FeO and Fe_2O_3 parameters.

Chapter 5

Electrical Conductivity

5.1 Thibodeau Electrical Conductivity Model

A model developed by Thibodeau (2016).

5.1.1 Introduction

The electrical conductivity model is a structural model that uses the Nernst-Einstein relationship to predict the electrical conductivity of oxide melts. The model is built on the concept of ionic conduction, where cations act as charge carriers, and their movement is influenced by the slag's polymerisation. The electronic contribution are also accounted for when iron oxides are present.

5.1.2 Model Overview

The model relies on Thibodeau's molar volume (density) model, Chapter 4, to calculate the degree of polymerisation (Q), enabling it to account for variations in melt composition. Its parameters for individual cations are derived from unary and binary silicate systems, allowing it to estimate the electrical conductivities of higher-order systems without additional parameters.

The model deals with the role of ionic conduction in the electrical conductivity of all oxide melts and only accounts for an electronic contribution from iron oxides. When these melts contain substantial amounts of iron oxide and manganese oxide (transition metal oxides), they can host significant quantities of both divalent and trivalent Fe and Mn cations. In such instances, the contribution of electronic conduction must also be considered.

It is important to note that this model is formulated strictly for liquid slag systems – the user should therefore ensure that his/her system is above the liquidus temperature before performing calculations. Also, we recommend the model to be used within the validation ranges specified in Table 5.1. The validation ranges are based on selected figures from the original article as well as Thibodeau's dissertation.

5.1.3 Model Formulation

This model is based on the work of Thibodeau (2016) and Thibodeau (2014). It mainly estimates the total electrical conductivity based on ionic conduction (see Equation (5.1)), assuming that only iron oxides contribute to electronic conduction. The electronic contribution due to iron oxides are estimated using Equation (5.3).

$$\sigma_{\text{ionic}} = \sum_i \sigma_{\text{i}} \tag{5.1}$$

For each cationic species, electrical conductivity is defined as per Equation (5.2), indicating a dependence on molar volume and diffusivity;

$$\sigma_{\text{i}} = \frac{n_{\text{i}} x_{\text{i}} z_{\text{i}}^2 F^2}{\bar{V} RT} D_{\text{i}} \tag{5.2}$$

The molar volume and diffusion coefficient values are obtained from the models described in Chapter 4 and Chapter 6, respectively.

For iron oxides, Equation (5.3) are used to estimate the electronic contribution.

$$\sigma_{\text{electronic}} = \frac{A}{T} D_{\text{Fe}^{2+}} c_{\text{Fe}}^2 y(1-y) \tag{5.3}$$

Here, A has a value of 4×10^{14}, c_{Fe} is the total iron concentration and y is the fraction of Fe^{2+}. The total electrical conductivity is then as shown in Equation (5.4).

$$\sigma_{\text{total}} = \sigma_{\text{ionic}} + \sigma_{\text{electronic}} \tag{5.4}$$

5.1.4 Assumptions

Equation (5.2) makes several assumptions.

1. It assumes that all cations are available to carry charge, meaning there are no neutral species or complexes.
2. It is assumed that the mechanism for ionic conductivity is the same as tracer diffusion.
3. It assumes that the velocity of an ion is determined solely by the forces acting on that specific ion. Thus, the electric field does not influence the medium through which the cations diffuse.
4. It is assumed that only iron oxides contribute to electronic conduction.

5.1.5 Literature Inaccuracies

The contour mapping of electrical conductivity shown in Thibodeau (2016) Figure 34 is likely incorrect. auxi-mpp were successfully validated against all Cartesian plots in Thibodeau (2016), but could not reproduce their contour mapping – see Figure 5.4. Figure 5.4a shows all composition slices for which auxi-mpp were successfully validated, yet the contour plot for $Al_2O_3 - CaO - SiO_2$ differs. Single point calculations for several selected compositions on Figures 5.4b to 5.4c also consistenty agreed with auxi-mpp's contour mapping. Finally, the same method to create the ternary plots in Figure 5.4 were used to create those in Figure 4.5 where there were no issues.

5.1.6 Model Validation

The Thibodeau electrical conductivity (ThibodeauEC) model implemented in auxi-mpp was validated against the literature model and experimental data extracted from Thibodeau (2016). The systems and temperatures for which the models were validated are given in Table 5.1.

Table 5.1: Electrical Conductivity Thibodeau Model Validation Ranges

Model	Systems	Composition	Temperature (K)
Unary	SiO_2	pure substance	$1500-3000$
	Al_2O_3	pure substance	$2200-3200$
	MgO	pure substance	$2000-3400$
	CaO	pure substance	$1800-3400$
Binary	$Al_2O_3 - SiO_2$	$x_{Al_2O_3} = 0-1$	$1873, 1973, 2073$
	$CaO - SiO_2$	$x_{CaO} = 0.2-0.7$	$1823, 1873, 1923$
	$MgO - SiO_2$	$x_{MgO} = 0.2-0.8$	$1873, 1973, 2073$
Ternary	$Al_2O_3 - CaO - SiO_2$	$y_{Al_2O_3} = 0-1$, $y_{CaO}/y_{SiO_2} = 1$	$1673, 1773, 1873$
	$Al_2O_3 - CaO - SiO_2$	$y_{CaO} = 0-0.9$, $y_{SiO_2} = 0.1$	$1673, 1773, 1873$
	$Al_2O_3 - CaO - SiO_2$	$y_{CaO} = 0-0.8$, $y_{SiO_2} = 0.2$	$1673, 1773, 1873$
	$Al_2O_3 - CaO - SiO_2$	$y_{CaO} = 0-0.7$, $y_{SiO_2} = 0.3$	$1673, 1773, 1873$
	$Al_2O_3 - CaO - SiO_2$	$y_{CaO} = 0-0.6$, $y_{SiO_2} = 0.4$	$1673, 1773, 1873$
	$Al_2O_3 - CaO - SiO_2$	$y_{CaO} = 0-0.95$, $y_{Al_2O_3} = 0.05$	$1673, 1773, 1873$
	$Al_2O_3 - CaO - SiO_2$	$y_{CaO} = 0-0.9$, $y_{Al_2O_3} = 0.1$	$1673, 1773, 1873$
	$Al_2O_3 - CaO - SiO_2$	$y_{CaO} = 0-0.8$, $y_{Al_2O_3} = 0.2$	$1673, 1773, 1873$
	$Al_2O_3 - MgO - SiO_2$	$y_{MgO} = 0-0.5$, $y_{SiO_2} = 0.5$	$1873, 1973, 2073$
	$CaO - MgO - SiO_2$	$x_{MgO} = 0-0.4$, $x_{CaO}/x_{SiO_2} = 1$	$1773, 1823, 1873$
	$Al_2O_3 - CaO - SiO_2^‡$	$y_{Al_2O_3,CaO,SiO_2} = 0-1$	1873
	$CaO - MgO - SiO_2^‡$	$y_{CaO,MgO,SiO_2} = 0-1$	1873
Quaternary‡	$Al_2O_3 - CaO - MgO - SiO_2$	$y_{CaO,MgO,SiO_2} = 0-0.9$, $y_{Al_2O_3} = 0.1$	1873
	$Al_2O_3 - CaO - MgO - SiO_2$	$y_{Al_2O_3,CaO,SiO_2} = 0-0.9$, $y_{MgO} = 0.1$	1873
Iron Containing	$Fe_2O_3 - FeO - SiO_2$	$x_{SiO_2} = 0.2-0.5$, Fe sat.	$1573, 1673, 1773$
	$Fe_2O_3 - FeO - MgO - SiO_2$	$x_{MgO} = 0-0.65$, $x_{SiO_2} = 0.35$, Fe sat.	$1673, 1723, 1773$
	$Fe_2O_3 - FeO - MgO - SiO_2$	$x_{MgO} = 0-0.6$, $x_{SiO_2} = 0.4$, Fe sat.	$1673, 1723, 1773$
	$Fe_2O_3 - FeO - CaO - SiO_2$	$x_{CaO} = 0-0.67$, $x_{SiO_2} = 0.33$, Fe sat.	$1573, 1673, 1773$
	$Fe_2O_3 - FeO - CaO - SiO_2$	$x_{CaO} = 0-0.575$, $x_{SiO_2} = 0.425$, Fe sat.	$1573, 1673, 1773$

‡ See Figure 5.4

For Fe-free systems, auxi-mpp's ThibodeauEC model closely reproduces the literature model, which itself shows good agreement with experimental data (Thibodeau 2016).

See Figures 5.1 to 5.4 for model performance for unary, binary, ternary and quaternary systems.

For Fe-bearing systems there is a increasing deviation from literature the greater the fraction of iron oxides present. We assume this to be due to a parameter change for FeO in the FactSage's database, as is also mentioned in Section 4.1.6. The effect are presented in Figure 5.5.

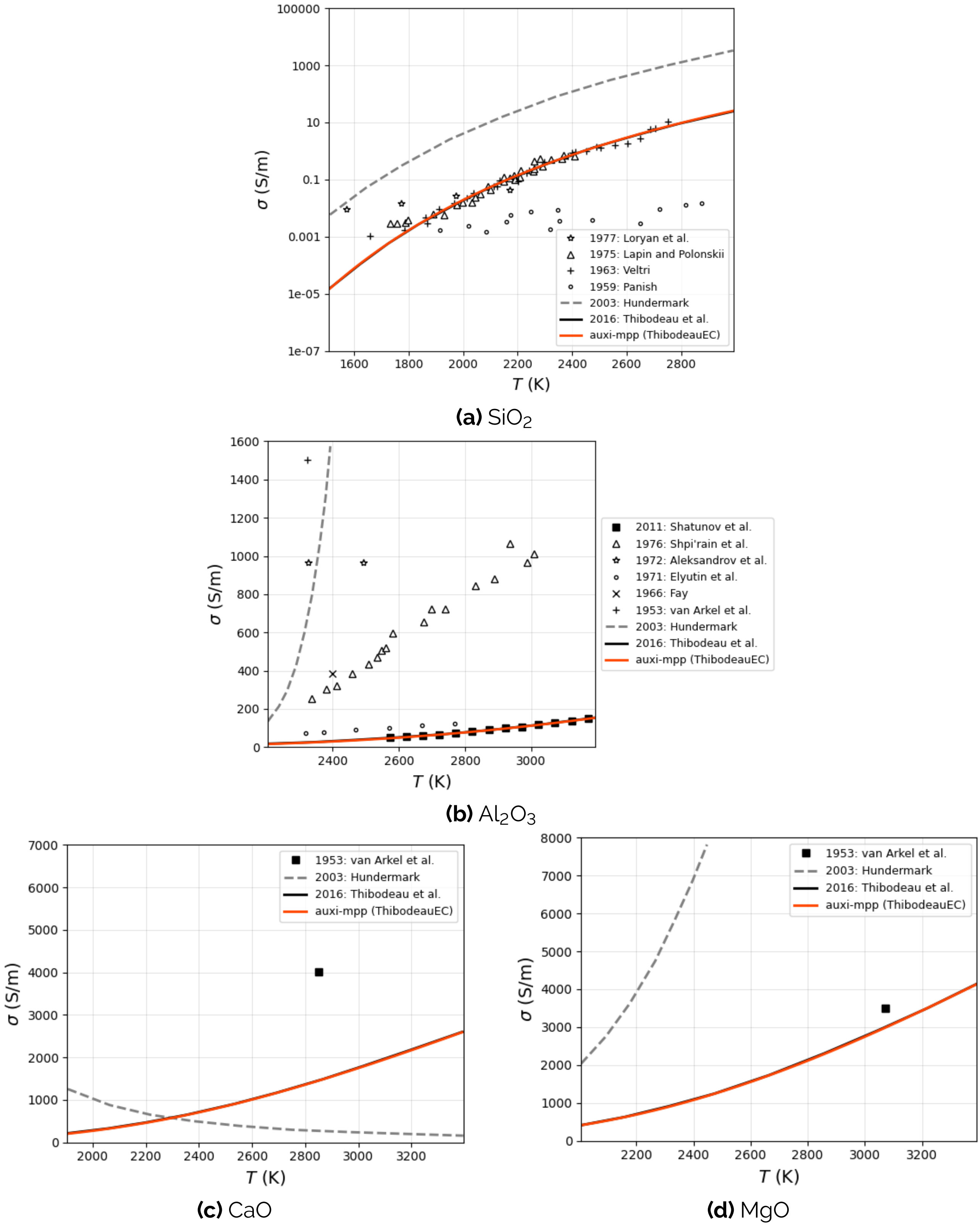

Figure 5.1: Electrical conductivity vs temperature for unary systems.

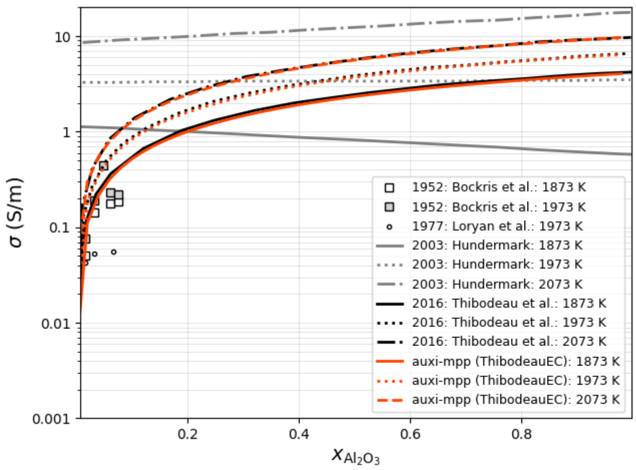

(a) $Al_2O_3 - SiO_2$

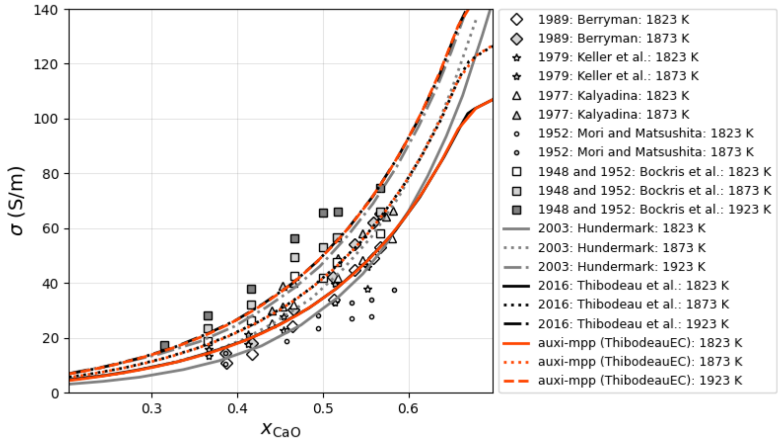

(b) $CaO - SiO_2$

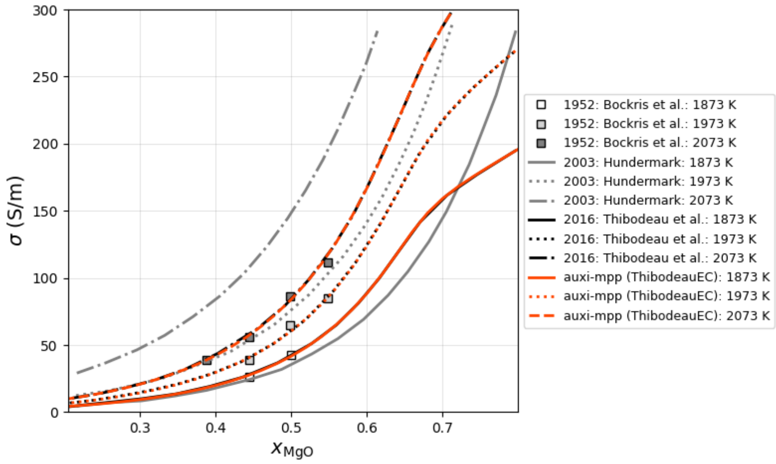

(c) $MgO - SiO_2$

Figure 5.2: Electrical conductivity vs mole fraction of binary systems.

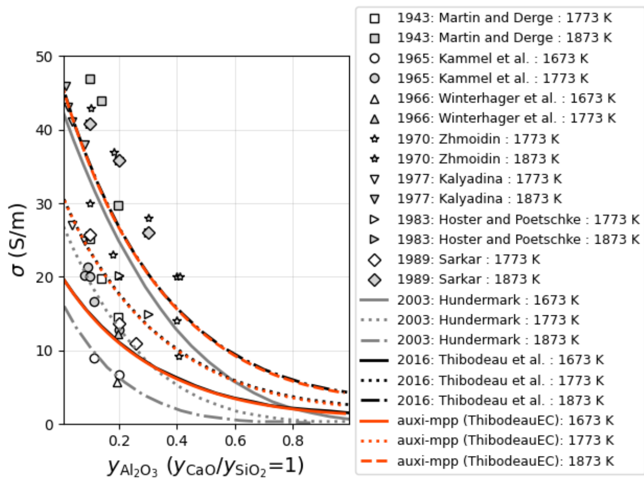

(a) $Al_2O_3 - CaO - SiO_2$

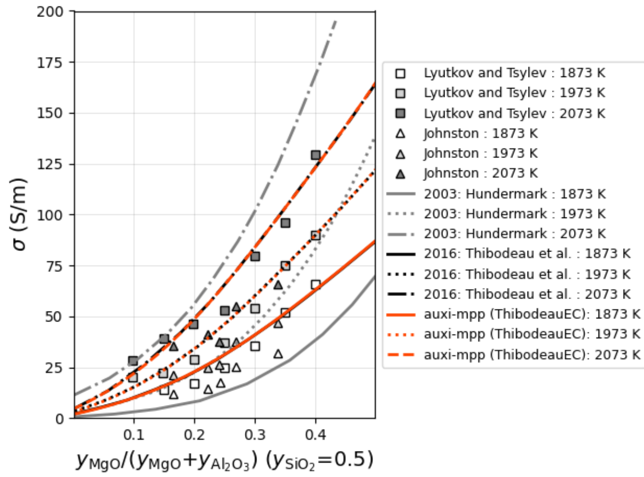

(b) $Al_2O_3 - MgO - SiO_2$

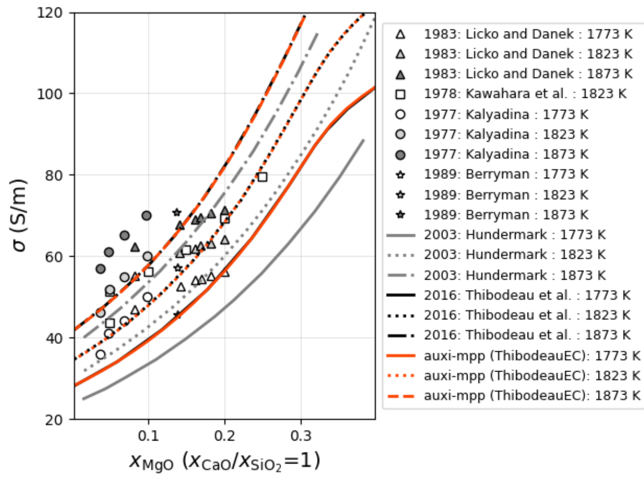

(c) $CaO - MgO - SiO_2$

Figure 5.3: Electrical conductivity vs mole fraction of ternary systems.

When reproducing the contour mapping of electrical conductivity for ternary and quaternary systems, as shown in Figure 5.4, there is not an exact agreement with literature, however.

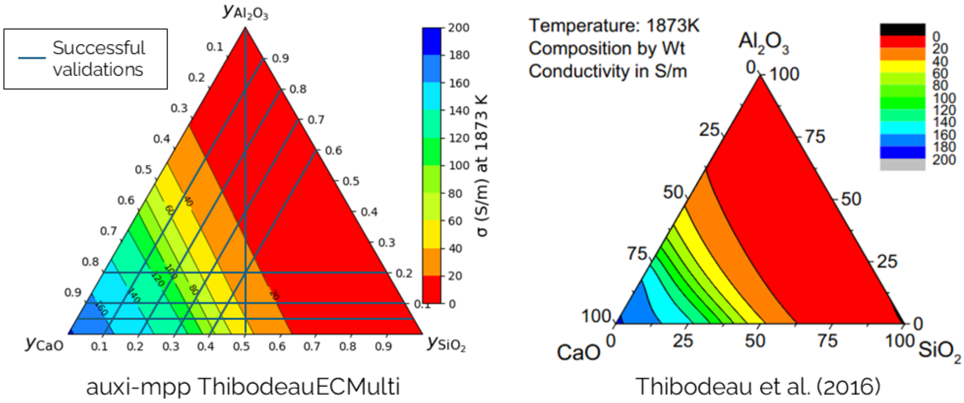

(a) $Al_2O_3 - CaO - SiO_2$

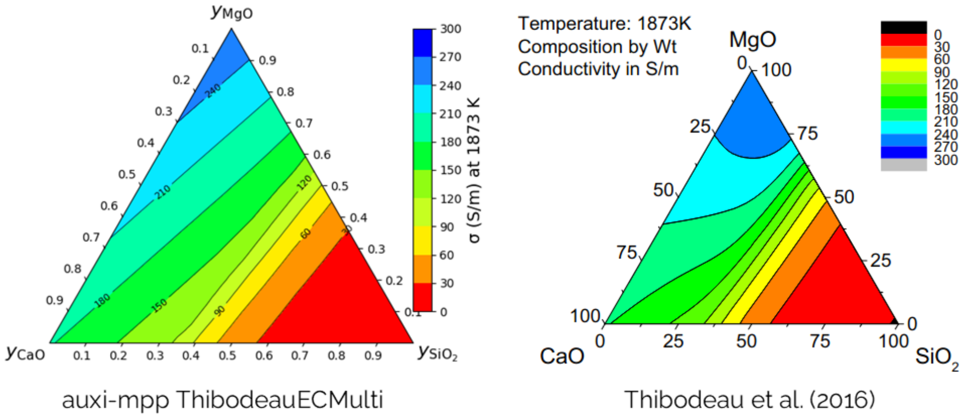

(b) $CaO - MgO - SiO_2$

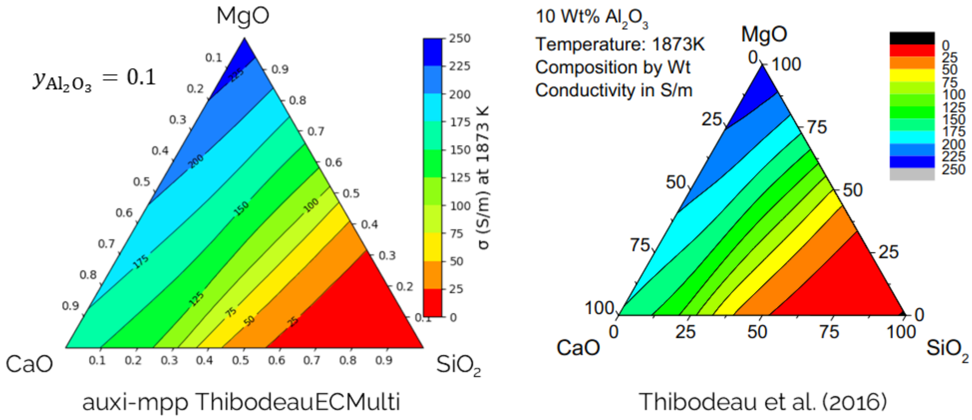

(c) $Al_2O_3 - CaO - MgO - SiO_2$

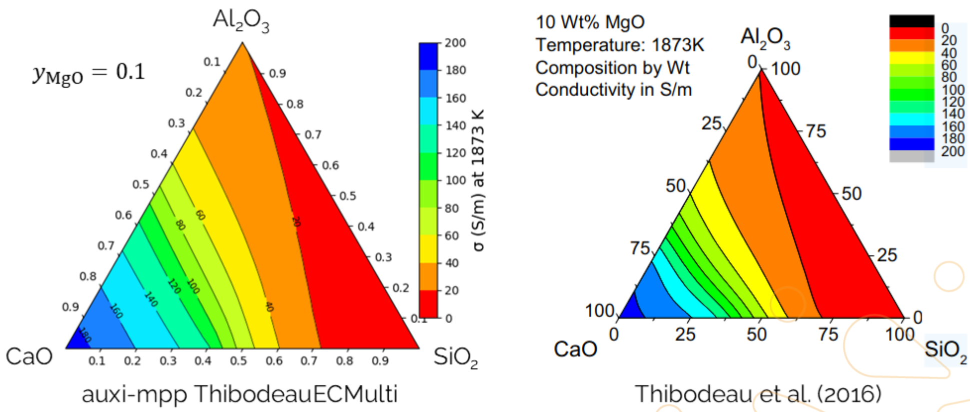

(d) $Al_2O_3 - CaO - MgO - SiO_2$

Figure 5.4: Comparing auxi-mpp's contour mapping of electrical conductivity with literature.

We believe this to be a mistake in the literature plots for a few good reasons. Figure 5.4a shows all composition slices for which the model were successfully validated against Thibodeau's own figures. There were no Cartesian plot in Thibodeau (2016) that auxi-mpp could not reproduce. Secondly, the method used to create the plots could exactly reproduce the contour mapping for ternary and quaternary systems for molar volume – see Figure 4.5. This also confirms that there are no issues with the bond fractions used. Finally, calculations performed on selected points in Figures 5.4b to 5.4d consistently agreed with auxi-mpp's mapping. Nevertheless, the contour mappings are relatively close to that in literature.

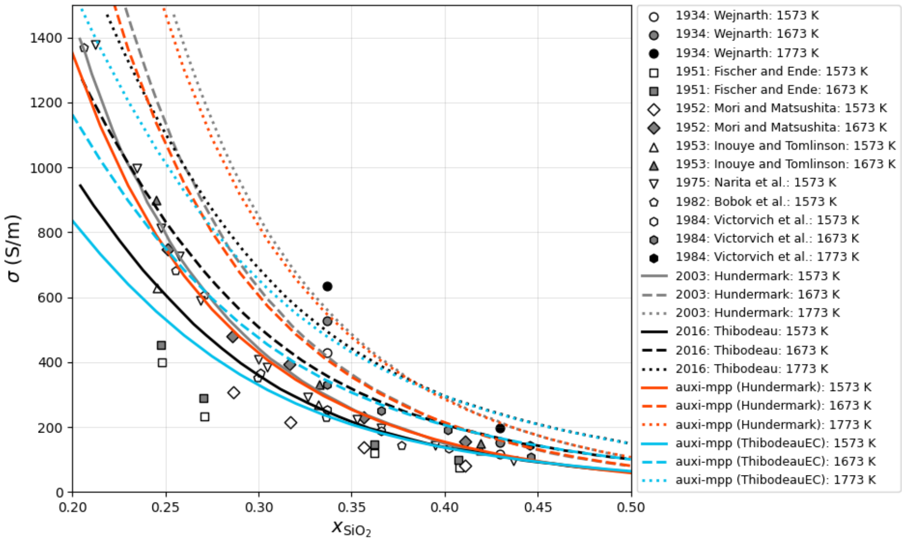

(a) $Fe_2O_3 - FeO - SiO_2$

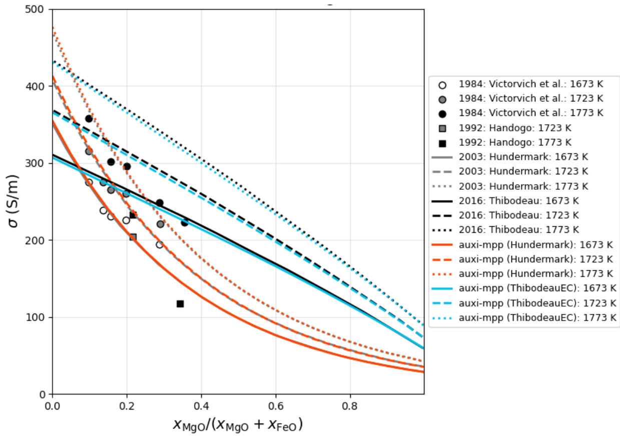

(b) $Fe_2O_3 - FeO - MgO - SiO_2$ ($x_{SiO_2} = 0.35$)

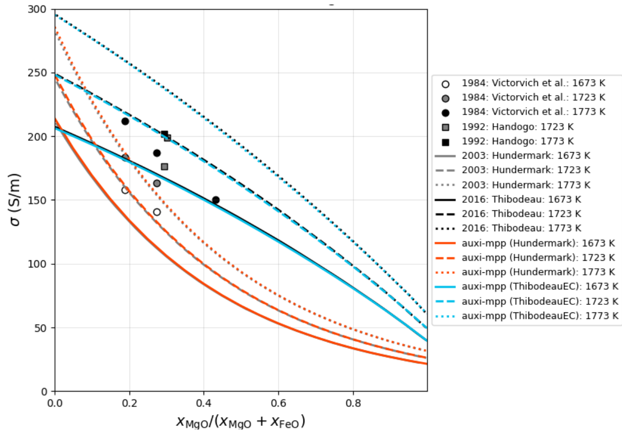

(c) $Fe_2O_3 - FeO - MgO - SiO_2$ ($x_{SiO_2} = 0.40$)

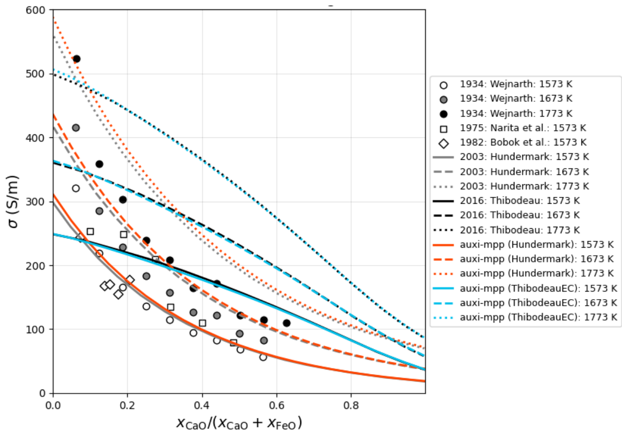

(d) $CaO - Fe_2O_3 - FeO - SiO_2$ ($x_{SiO_2} = 0.33$)

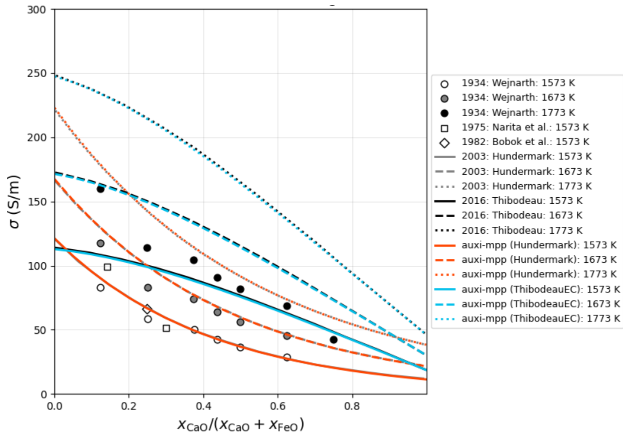

(e) $CaO - Fe_2O_3 - FeO - SiO_2$ ($x_{SiO_2} = 0.425$)

Figure 5.5: Electrical conductivity vs mole fraction of iron containing systems at iron saturation conditions.

Issues

There likely was a parameter change in FactSage's database for FeO, resulting in a different equilibrium ratio between FeO and Fe_2O_3, and thus also different bond fractions. If we apply Thibodeau's electrical conductivity model to Fe-bearing systems, we no longer obtain the results we were meant to obtain. Luckily, the deviation is not significant enough to render the model unusable.

5.2 Hundermark Electrical Conductivity Models

Models developed by Hundermark (2003).

5.2.1 Introduction

The unified model for estimating the electrical conductivity of melter-type slags, developed by Hundermark (2003), originated from challenges in the electrical control of furnaces used by South African platinum producers. The initial design was an iron-free model for $Al_2O_3 - CaO - MgO - SiO_2$ slags, based on the principle of ionic conduction as the sole operating mechanism. This foundational work was later integrated with data from iron-containing systems to create the comprehensive unified model.

5.2.2 Model Overview

Hundermark's unified model estimates the electrical conductivity of melter-type slags based on their composition, temperature, and oxidation state (Hundermark 2003). It is applicable to slags containing two or more of the following components: Al_2O_3, CaO, FeO_x, MgO, and SiO_2. The model is particularly useful for Fe-bearing slags where other models, like Thibodeau's, have shown to be unreliable (Thibodeau 2014). While empirical, the model provides reasonably accurate estimates for a wide range of slag systems, achieving an average correlation coefficient of 0.9743 with experimental values.

The model was developed by integrating two separate datasets. The first part was a foundational Fe-free model for the $Al_2O_3 - CaO - MgO - SiO_2$ system represented by Equation (5.5). This initial model, which assumed that ionic conduction is the sole mechanism, used multiple linear regressions to correlate slag composition with conductivity, yielding a correlation coefficient of 0.8358 for temperatures between 1623 to 2023 K.

The second part incorporated data from Fe-containing systems. By combining both datasets, the unified model, represented by eq. (5.6), explicitly accounts for the fractions of ferrous (Fe^{2+}) and ferric (Fe^{3+}) ions, allowing it to estimate conductivity changes with varying slag oxidation states.

It is important to note that this model is formulated strictly for liquid slag systems – the user should therefore ensure that his/her system is above the liquidus temperature before performing calculations. Also, we recommend the model to be used within the validation ranges specified in Table 5.2. The validation ranges are based on selected figures from the original articles. To peruse the full range of systems the model were validated for, the user is directed to the original article.

Finally, for systems containing Fe, the correct ratio of Fe(II) and Fe(III) has to be provided. This means the user needs to know the oxidation environment of the system, and from that estimate this ratio before passing it on to the model.

5.2.3 Model Formulation

The model formulation is the foundational Fe-free model is given by Equation (5.5), while the unified model, which includes the contribution of ferrous and ferric ions, is represented by Equation (5.6).

$$\ln \sigma = \left(31.6 - \frac{68048}{T}\right) x_{\mathrm{Al_2O_3}} + \left(-2.2 - \frac{9006}{T}\right) x_{\mathrm{CaO}} + \left(10.5 - \frac{15049}{T}\right) x_{\mathrm{MgO}} + \left(17.1 - \frac{40544}{T}\right) x_{\mathrm{SiO_2}} \tag{5.5}$$

$$\ln \sigma = \left(19.9 - \frac{47348}{T}\right) x_{\mathrm{Al_2O_3}} + \left(15.4 - \frac{24087}{T}\right) x_{\mathrm{CaO}} + \left(9.2 - \frac{14151}{T}\right) x_{\mathrm{MgO}} + \left(-0.5 - \frac{7478}{T}\right) x_{\mathrm{SiO_2}} + \left(10.0 - \frac{9140}{T}\right) x_{\mathrm{FeO}_x} \cdot x_{\mathrm{Fe^{2+}}} + \left(65.4 - \frac{82447}{T}\right) x^2_{\mathrm{FeO}_x} \cdot x_{\mathrm{Fe^{2+}}} \cdot x_{\mathrm{Fe^{3+}}} + \left(-2.6 + \frac{6642}{T}\right) x_{\mathrm{FeO}_x} \cdot x_{\mathrm{Fe^{3+}}} \tag{5.6}$$

Where σ represents the electrical conductivity, with units of $\mathrm{S\,cm^{-1}}$, x_i is the mole fraction of component i, and T is the temperature in Kelvins. x_{FeO_x} is the equivalent mole fraction of the total ferrous and ferric oxide in the slag, while $x_{\mathrm{Fe^{2+}}}$ and $x_{\mathrm{Fe^{3+}}}$ refer to the ferrous and ferric fractions, respectively.

In auxi-mpp, Equation (5.5) is used when there is no iron in the system, and the unified model given by Equation (5.6) is used when iron is present.

5.2.4 Assumptions

Several assumptions were made in the development of the Hundermark model, which are important to consider when applying the model. These assumptions include:

1. A primary assumption for the Fe-free model is that ionic conduction is the only mechanism operating in these Fe-free systems and it results solely from the movement of cations like Mg^{2+} and Ca^{2+}.
2. The Fe-free model assumes that the temperature dependence of the conductivity obeys the Arrhenius relationship. Furthermore, it was observed and incorporated into the model that the activation energy for conduction and the natural logarithm of the pre-exponential factor are linearly related, following a compensation law.
3. The Fe-free model is specifically developed for slags containing Al_2O_3, CaO, MgO, and SiO_2 in a temperature range of 1623 to 2023 K.
4. The models are fundamentally semi-empirical, meaning they are based on observed relationships and regressions techniques rather than being derived purely from first principles of slag structure or ion transport mechanisms.
5. The unified model is specifically designed for slags containing two or more of Al_2O_3, CaO, FeO_x, MgO, and SiO_2 components, and a temperature range of 1623 to 2023 K.
6. Only electrical conductivity data for fully molten slags (above their liquidus temperature) were considered for the models' development to avoid inconsistencies arising from the presence of solid phases.

5.2.5 Literature Inaccuracies

To validate the implemented Hundermark model, we had to test it against the model performance as presented by Thibodeau (2016) and Thibodeau (2014), due to a lack of performance figures in Hundermark's documentation. The performance validated against is therefore not from the original author, adding a layer of uncertainty to it. We reason that this extra link in the chain is the cause of the deviation seen when validating systems containing Al_2O_3. We discovered that when Al_2O_3's temperature coefficient in Equation (5.5) is entered as 69048 instead of 68048, the model's performance match with that presented by Thibodeau (2016), as shown in Figures 5.6 and 5.7.

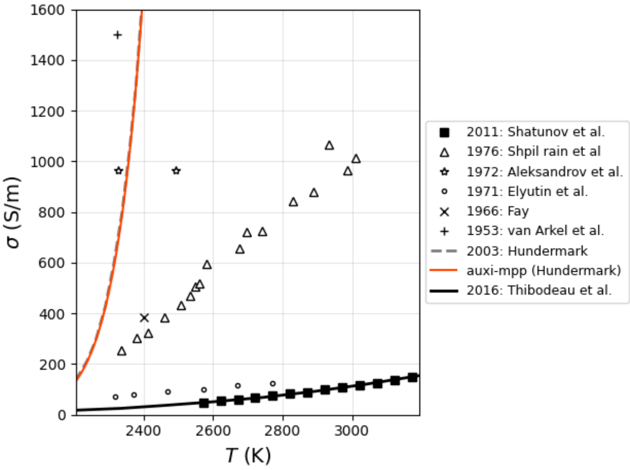

(a) Al_2O_3

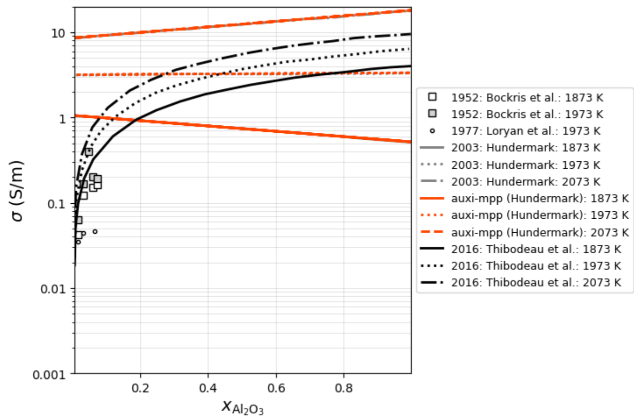

(b) $Al_2O_3 - SiO_2$

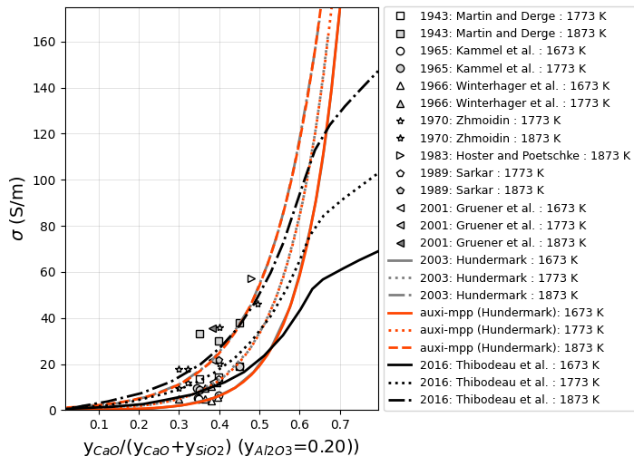

(c) $Al_2O_3 - CaO - SiO_2$

Figure 5.6: Hundermark's performance with Al_2O_3's temperature coefficient as 69048, instead of 68048.

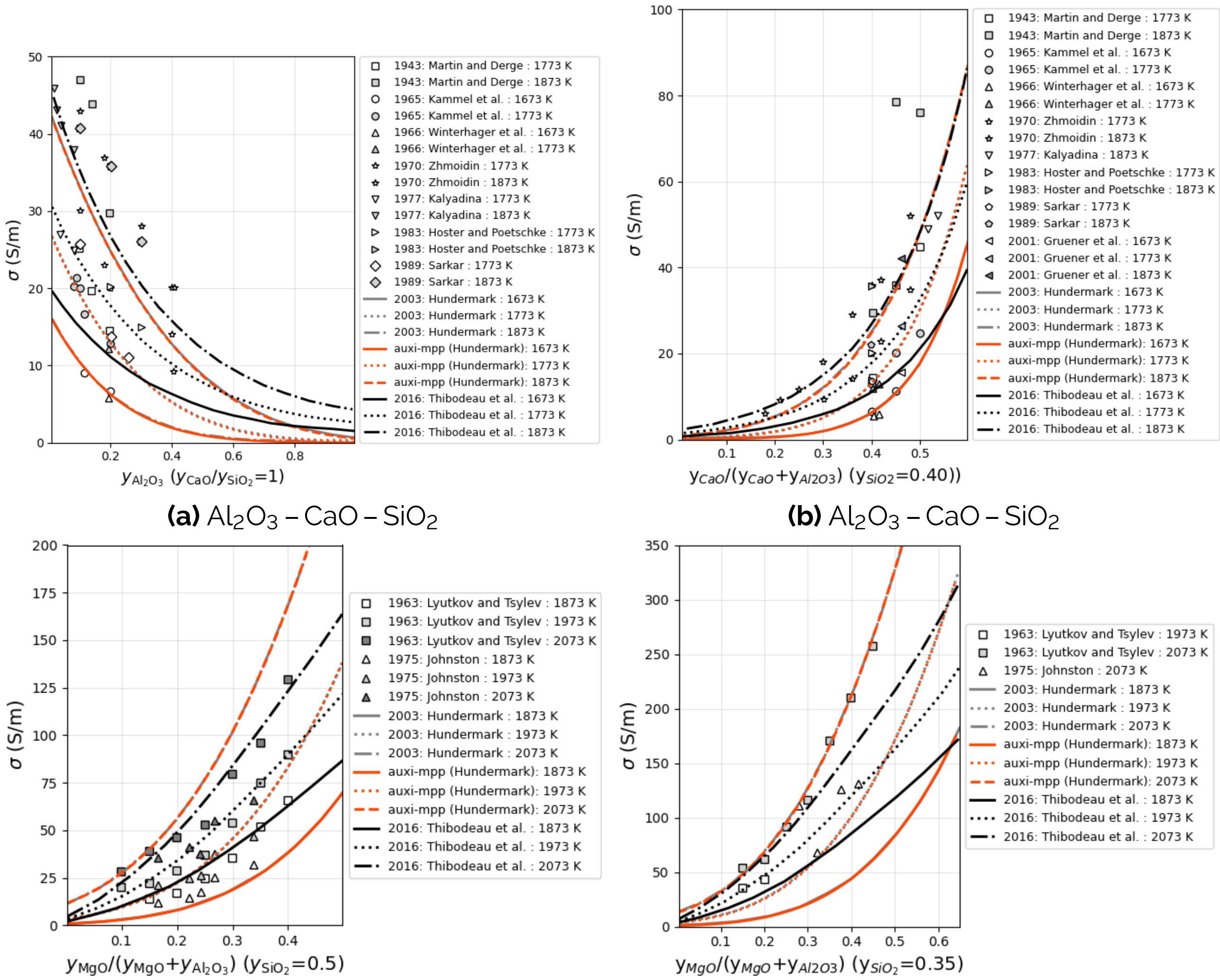

(a) $Al_2O_3 - CaO - SiO_2$ (b) $Al_2O_3 - CaO - SiO_2$

(c) $Al_2O_3 - MgO - SiO_2$ (d) $Al_2O_3 - MgO - SiO_2$

Figure 5.7: Hundermark's performance with Al_2O_3's temperature coefficient as 69048, instead of 68048.

As the original value for this coefficient, as determined by Hundermark himself, is 68048, we will assume this to be the correct value, and thus assume that Thibodeau made an error here.

5.2.6 Model Validation

Hundermark's electrical conductivity model, implemented in auxi-mpp, was validated against literature model data and experimental data extracted from Thibodeau (2016) and Thibodeau (2014), as Hundermark (2003) did not offer such plots for validation. The systems and temperatures for which the models were validated are given in Table 5.2.

Table 5.2: Electrical Conductivity Hundermark Model Validation Ranges

Model	Systems	Composition	Temperature (K)
Unary	SiO_2	pure substance	$1500 - 3000$
	Al_2O_3	pure substance	$2200 - 2400$
	MgO	pure substance	$2000 - 2450$
	CaO	pure substance	$1800 - 3400$
Binary	$Al_2O_3 - SiO_2$	$x_{\mathrm{Al_2O_3}} = 0 - 1$	$1873, 1973, 2073$
	$CaO - SiO_2$	$x_{\mathrm{CaO}} = 0.2 - 0.7$	$1823, 1873, 1923$
	$MgO - SiO_2$	$x_{\mathrm{MgO}} = 0.2 - 0.8$	$1873, 1973, 2073$
Ternary	$Al_2O_3 - CaO - SiO_2$	$y_{\mathrm{Al_2O_3}} = 0 - 1$, $y_{\mathrm{CaO}}/y_{\mathrm{SiO_2}} = 1$	$1673, 1773, 1873$
	$Al_2O_3 - CaO - SiO_2$	$y_{\mathrm{CaO}} = 0 - 0.8$, $y_{\mathrm{SiO_2}} = 0.2$	$1673, 1773, 1873$
	$Al_2O_3 - CaO - SiO_2$	$y_{\mathrm{CaO}} = 0 - 0.6$, $y_{\mathrm{SiO_2}} = 0.4$	$1673, 1773, 1873$
	$Al_2O_3 - MgO - SiO_2$	$y_{\mathrm{MgO}} = 0 - 0.65$, $y_{\mathrm{SiO_2}} = 0.35$	$1873, 1973, 2073$
	$Al_2O_3 - MgO - SiO_2$	$y_{\mathrm{MgO}} = 0 - 0.5$, $y_{\mathrm{SiO_2}} = 0.5$	$1873, 1973, 2073$
	$CaO - MgO - SiO_2$	$x_{\mathrm{MgO}} = 0 - 0.4$, $x_{\mathrm{CaO}}/x_{\mathrm{SiO_2}} = 1$	$1773, 1823, 1873$
Iron Containing	$Fe_2O_3 - FeO - SiO_2$	$x_{\mathrm{SiO_2}} = 0.2 - 0.5$, Fe sat.	$1573, 1673, 1773$
	$Fe_2O_3 - FeO - MgO - SiO_2$	$x_{\mathrm{MgO}} = 0 - 0.65$, $x_{\mathrm{SiO_2}} = 0.35$, Fe sat.	$1673, 1723, 1773$
	$Fe_2O_3 - FeO - MgO - SiO_2$	$x_{\mathrm{MgO}} = 0 - 0.6$, $x_{\mathrm{SiO_2}} = 0.4$, Fe sat.	$1673, 1723, 1773$
	$Fe_2O_3 - FeO - CaO - SiO_2$	$x_{\mathrm{CaO}} = 0 - 0.67$, $x_{\mathrm{SiO_2}} = 0.33$, Fe sat.	$1573, 1673, 1773$
	$Fe_2O_3 - FeO - CaO - SiO_2$	$x_{\mathrm{CaO}} = 0 - 0.575$, $x_{\mathrm{SiO_2}} = 0.425$, Fe sat.	$1573, 1673, 1773$

For the validation of systems containing Al_2O_3, we accept that Thibodeau (2016) likely made a simple error in the temperature coefficient for Al_2O_3 in Equation (5.5), as explained in Section 5.2.5. With that said, for Fe-free systems auxi-mpp's implementation of Hundermark's Fe-free model closely reproduces the literature model for all systems tested. See Figures 5.8 to 5.10 for model performance for unary, binary and ternary systems.

On the other hand, auxi-mpp's implementation of Hundermark's unified model, which incorporates iron, slightly deviates from literate the greater the fraction of iron oxides present. We assume this to be due to a parameter change for FeO in the FactSage's database, as is also mentioned in Section 4.1.6. The effect are presented in Figure 5.11.

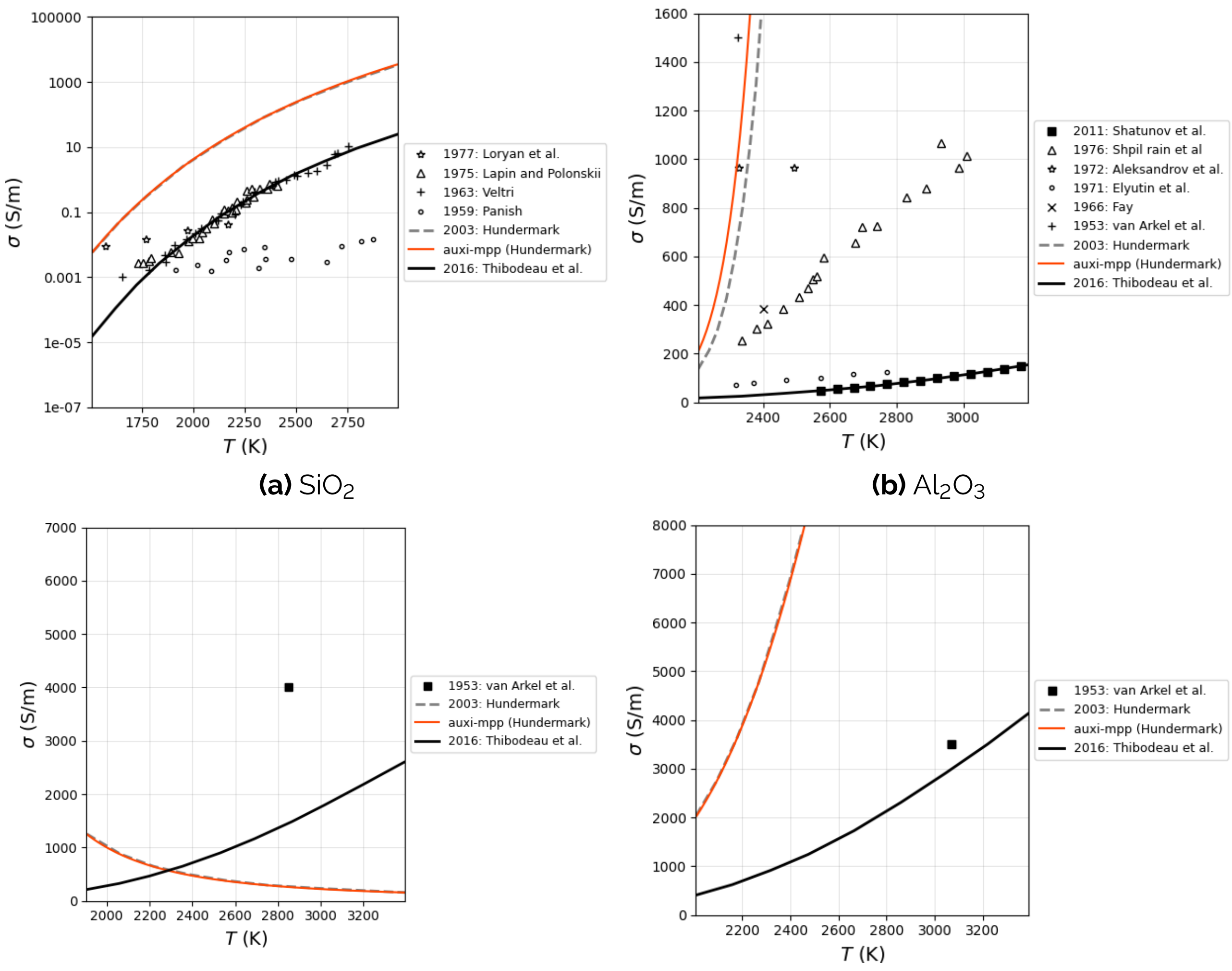

(a) SiO_2 **(b)** Al_2O_3

(c) CaO **(d)** MgO

Figure 5.8: Electrical conductivity vs temperature for unary systems.

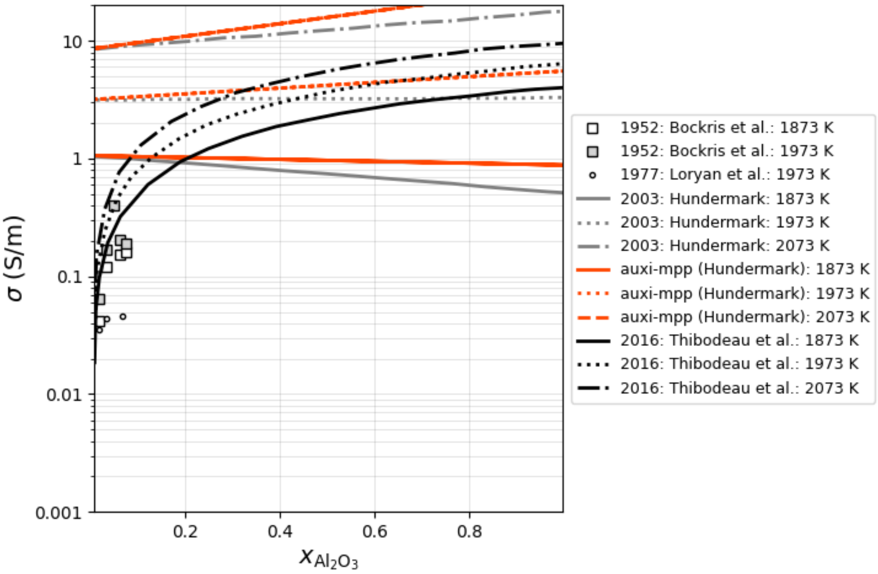

(a) $Al_2O_3 - SiO_2$

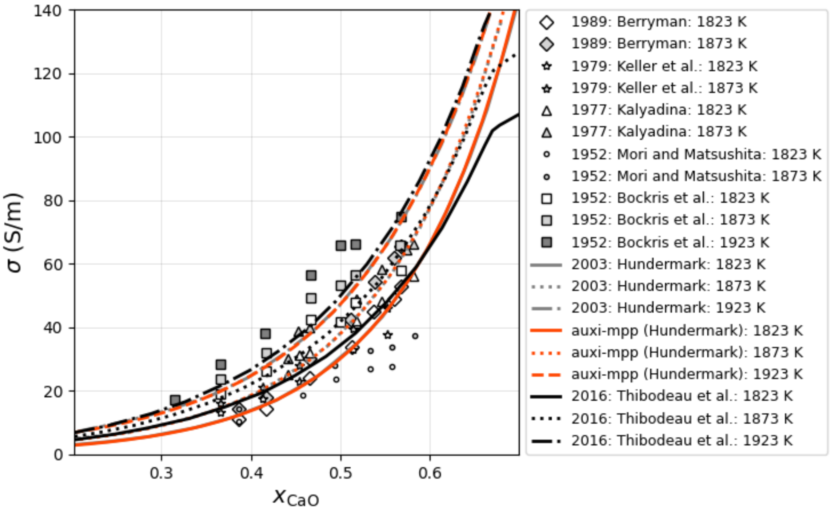

(b) $CaO - SiO_2$

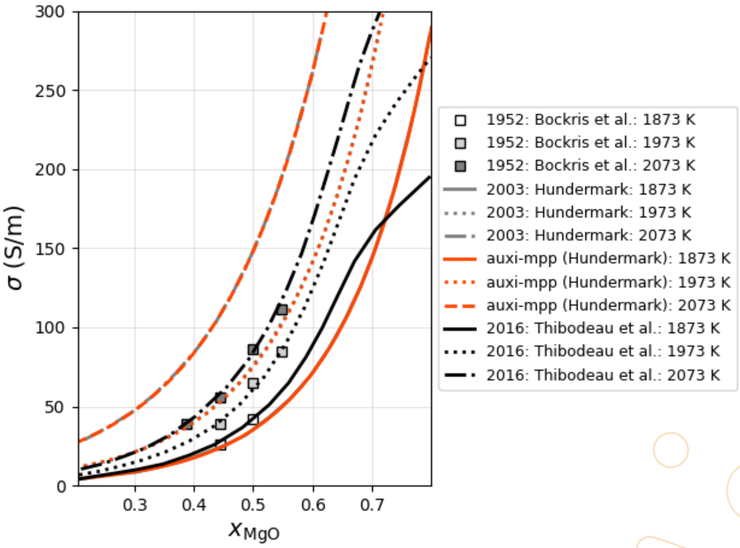

(c) $MgO - SiO_2$

Figure 5.9: Electrical conductivity vs mole fraction of binary systems.

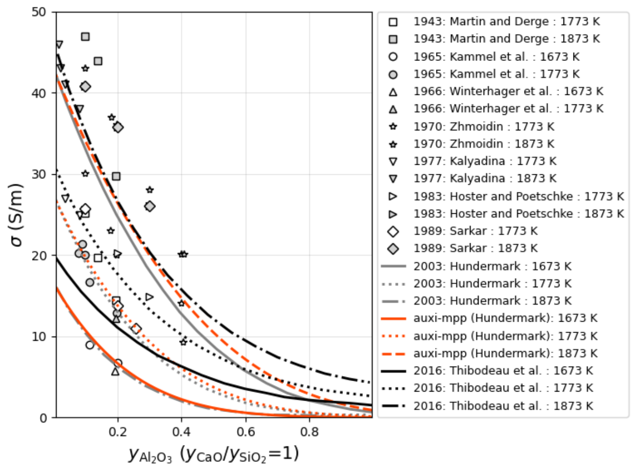

(a) $Al_2O_3 - CaO - SiO_2$

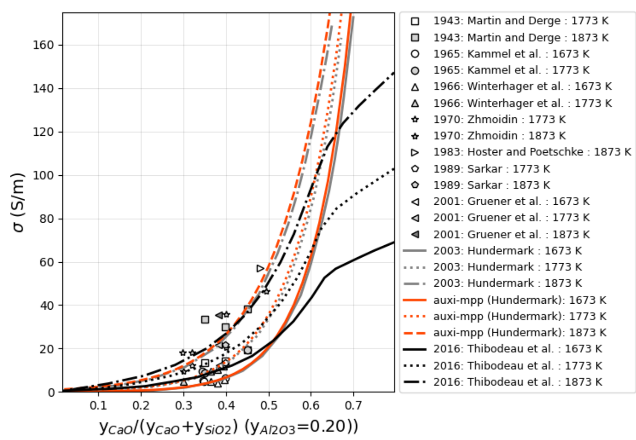

(b) $Al_2O_3 - CaO - SiO_2$

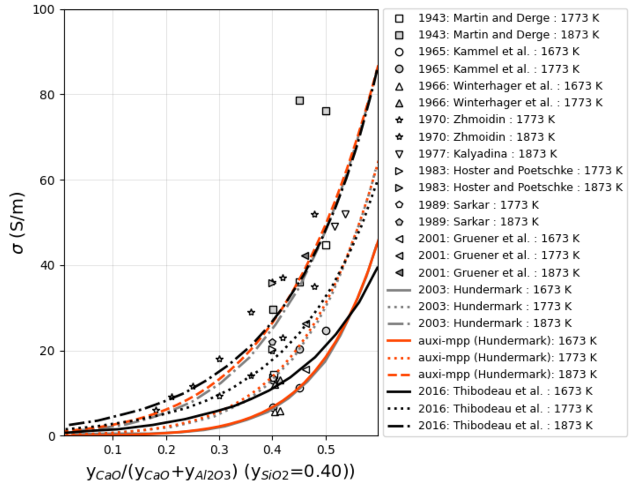

(c) $Al_2O_3 - CaO - SiO_2$

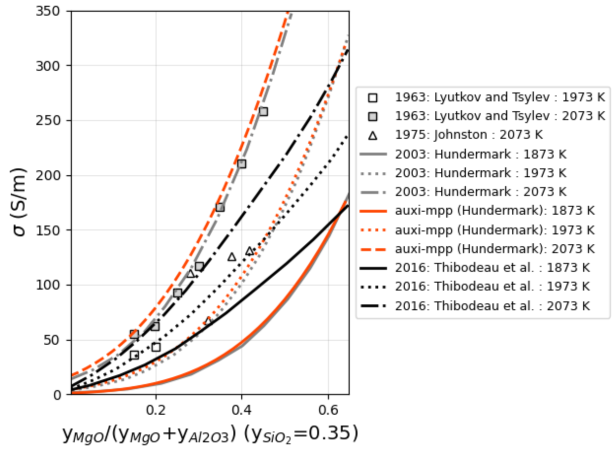

(d) $Al_2O_3 - MgO - SiO_2$

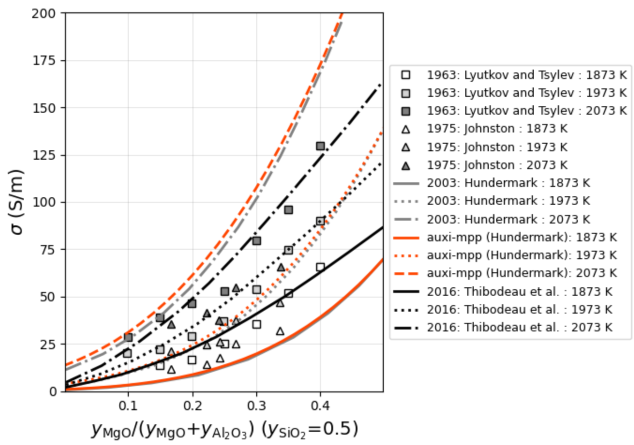

(e) $Al_2O_3 - MgO - SiO_2$

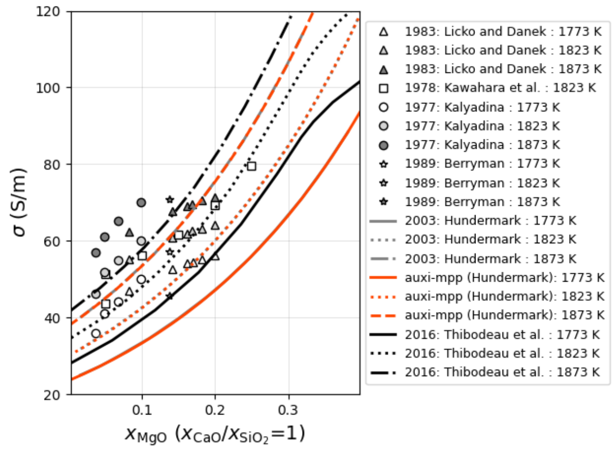

(f) $CaO - MgO - SiO_2$

Figure 5.10: Electrical conductivity vs mole fraction of ternary systems that does not contain iron.

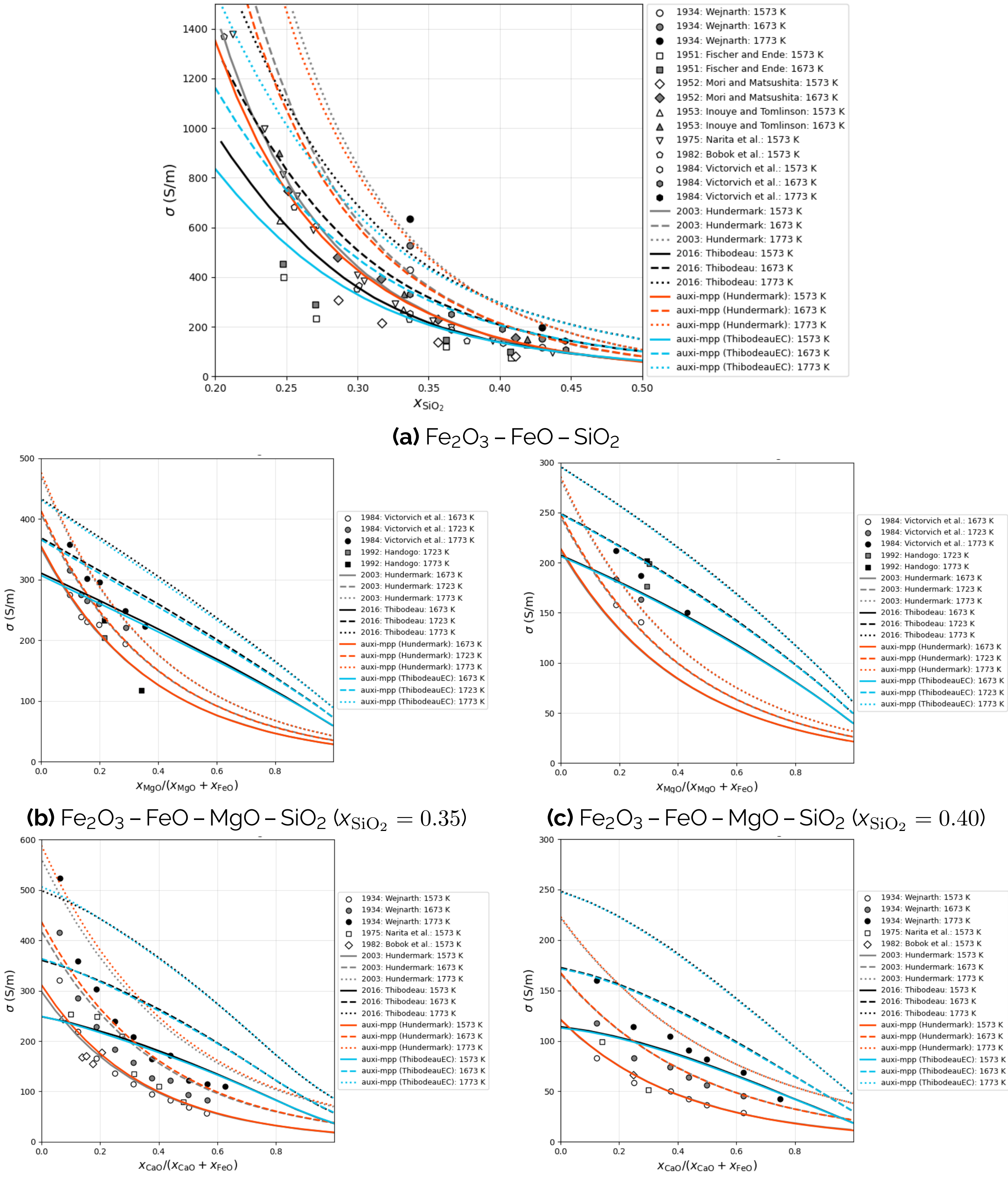

(a) $Fe_2O_3 - FeO - SiO_2$

(b) $Fe_2O_3 - FeO - MgO - SiO_2$ ($x_{SiO_2} = 0.35$)

(c) $Fe_2O_3 - FeO - MgO - SiO_2$ ($x_{SiO_2} = 0.40$)

(d) $CaO - Fe_2O_3 - FeO - SiO_2$ ($x_{SiO_2} = 0.33$)

(e) $CaO - Fe_2O_3 - FeO - SiO_2$ ($x_{SiO_2} = 0.425$)

Figure 5.11: Electrical conductivity vs mole fraction of iron containing systems at iron saturation conditions.

Issues

There likely was a parameter change in FactSage's database for FeO, resulting in a different equilibrium ratio between FeO and Fe_2O_3. If we then maintain the coefficients of Hundermark's model, we no longer obtain the results we were meant to obtain. Luckily, the deviation is not significant enough to render the model unusable.

Chapter 6

Diffusivity

6.1 Thibodeau Diffusivity Model

A model implemented by Thibodeau (2016).

6.1.1 Introduction

As with all physical properties, the diffusivity is also affected by the structure of the slag. The higher the polymerisation, the more rigid the slag structure and therefore the more difficult particles will diffuse through it. A model that calculates diffusivity (diffusion coefficients) from slag polymerisation is thus presented here.

6.1.2 Model Overview

Variations in slag composition affecting polymerisation are accounted for using bond fractions, calculated with the MQM model in ChemApp for Python and data from FactSage's FToxid database. The model's parameters for individual cations are determined using data from unary and binary silicate systems, and is capable of estimating the electrical conductivity of higher-order systems without additional parameters.

The bond fractions with the model parameters are then used to scale the activation energy that dictates the rate of diffusion. This is done in an Arrhenius-like equation which is similar to Equation (6.1). Arrhenius-like equations are typically used to calculate temperature dependence for reaction rates.

$$D = A\exp\left(-\frac{E}{RT}\right) \tag{6.1}$$

It is important to note that this model is formulated strictly for liquid slag systems – the user should therefore ensure that his/her system is above the liquidus temperature before performing calculations. Finally, for systems containing Fe, the correct ratio of Fe(II) and Fe(III) has to be provided. This means the user needs to know the oxidation environment of the system, and from that estimate this ratio before passing it on to the model.

6.1.3 Model Formulation

The diffusivity used in the calculation of the electrical conductivity described in Equation (5.2), is determined in Equation (6.2) with parameters for systems containing network formers such as SiO_2 and Al_2O_3.

$$D_{\mathrm{i}} = A_{\mathrm{i}} \exp\left(-\frac{B_{\mathrm{i}} + C_{\mathrm{i-SiSi}} x_{\mathrm{Si-Si}} + C_{\mathrm{i-SiAl}} x_{\mathrm{Si-Al}} + C_{\mathrm{i-AlAl}} x_{\mathrm{Al-Al}}}{RT}\right) \tag{6.2}$$

The bond fractions ($x_{\mathrm{i-j}}$) calculated from the MQM model are combined with the parameters A_{i}, B_{i}, and C_{i} from Thibodeau (2016).

This model is limited to the following cations; Mg^{2+}, Ca^{2+}, Mn^{2+}, Pb^{2+}, Fe^{2+}, Fe^{3+},Al^{3+}, and Si^{4+}.

6.1.4 Variable Declarations

The parameters used in the model are extracted from Thibodeau (2014) and are given in Table 6.1.

Table 6.1: Electrical Conductivity Parameters (Thibodeau 2014)

	A_{i} (cm^2 s^{-1})	B_{i} (kJ mol^{-1})	$C_{\mathrm{i-SiSi}}$ (kJ mol^{-1})	$C_{\mathrm{i-AlAl}}$ (kJ mol^{-1})	$C_{\mathrm{i-AlSi}}$ (kJ mol^{-1})
Mg^{2+}	0.03448	118.6	42.1	10.0	10.0
Ca^{2+}	0.02600	115.0	35.0	35.0	35.0
Mn^{2+}	0.05421	104.2	55.4	20.0	20.0
Pb^{2+}	0.00936	65.4	90.4	90.4	90.4
Fe^{2+}	0.04200	95.0	-	-	-
Fe^{3+}	0.00358	158.3	-	-	-
Al^{3+}	0.00358	158.3	-	-	-
Si^{4+}	5.22600	380.9	-	-	-

6.1.5 Assumptions

In this diffusivity model, the following assumptions were made.

1. It is assumed that the activation energy of the ionic conductivity is linearly increasing with the bond fractions of Si – Si and Al – Al.
2. It is assumed that that $C_{\mathrm{i-SiAl}}$ will be equal to $C_{\mathrm{i-AlAl}}$, instead of the average between $C_{\mathrm{i-AlAl}}$ and $C_{\mathrm{i-SiSi}}$. This is because it will be significantly more likely for the cations to take the lower energy route, which is on the Al side of the bond.
3. It is assumed that Al_2O_3 behaves like a network former, despite its amphoteric behaviour.
4. Parameters for Fe^{3+} were fixed to the same values as Al^{3+} as there was no data available capable of providing a better first estimate.

6.1.6 Simplifications

For applying Equation (6.2), interactions between diffusing network modifier cations are neglected. This simplifies the model, allowing it to estimate diffusion coefficients of higher-order systems from unary and binary parameters without additional parameters.

6.1.7 Model Validation

This model is not independently used or implemented due to lack of literature data for comparison. However, Chapter 5's electrical conductivity estimates incorporate the diffusivity model's results. This model was successfully validated and thereby indirectly validates the diffusivity model.

Chapter 7

Viscosity

7.1 Grundy-Kim-Brosch Viscosity Model

Model developed by Grundy et al. (2008b), Grundy et al. (2008b), Kim (2011), and Brosh et al. (2012).

7.1.1 Introduction

The Grundy-Kim-Brosch viscosity model, which accounts for silicate structure estimated using the MQM model with ChemApp for Python and the FactSage FToxid database, is currently implemented for unary through multi component systems containing SiO_2, CaO, MgO, Al_2O_3, FeO and Fe_2O_3.

7.1.2 Model Overview

The principle equation implemented in the model to calculate the viscosity (μ) for a slag is an Arrhenius-like equation, Equation (7.1). It is a function of both temperature and composition where μ is the viscosity in Pa s, R is the gas constant and T is the temperature in Kelvin.

$$\ln(\mu) = A + \frac{E}{RT} \tag{7.1}$$

The parameters A and E depends on the slag composition. For unary systems the compound specific A and E parameters are simply plugged into Equation (7.1) together with the system temperature. However, with silicate binary or multicomponent systems, A and E are not only determined by the pure substance character, but also by the interaction between the components and by the degree of polymerisation.

It is important to note that this model is formulated strictly for liquid slag systems – the user should therefore ensure that his/her system is above the liquidus temperature before performing calculations. Also, we recommend the model to be used within the validation ranges specified in Table 7.3 and Figure 7.8. The validation ranges are based on selected figures from the original articles. To peruse the full range of systems the model were validated for, the user is directed to the original article.

Finally, for systems containing Fe, the correct ratio of Fe(II) and Fe(III) has to be provided. This means the user needs to know the oxidation environment of the system, and from that estimate this ratio before passing it on to the model.

7.1.3 Unary and Binary Model Formulation

Unary Model

For unary systems, Equation (7.1) is used directly, where A and E are unique to each component. For systems containing two or more components, the structure of the slag becomes more complex, requiring A and E to be estimated based on several structural contributions.

Binary Model

Starting with the Arrhenius-like equation, Equation (7.1), instead of using a single parameter for A and E, these are weighted based on different structural contributions. For binary sytsems, A is calculated as in Equation (7.2);

$$A = A_{\mathrm{M}} x_{\mathrm{M}}^{\not{\$}_0} + x_{\mathrm{Si}}^{\not{\$}_0} [A^{*}_{\mathrm{SiO_2}} + A^{\mathrm{E}}_{\mathrm{SiO_2}} p^{40} + A_{\mathrm{M-Si}} x_{\mathrm{M}}^{\not{\$}_0} + A^{\mathrm{R}}_{\mathrm{M-Si}} (p^4 - p^{40})] \tag{7.2}$$

and E is calculated as in Equation (7.3);

$$E = E_{\mathrm{M}} x_{\mathrm{M}}^{\not{\$}_0} + x_{\mathrm{Si}}^{\not{\$}_0} [E^{*}_{\mathrm{SiO_2}} + E^{\mathrm{E}}_{\mathrm{SiO_2}} p^{40} + E_{\mathrm{M-Si}} x_{\mathrm{M}}^{\not{\$}_0} + E^{\mathrm{R}}_{\mathrm{M-Si}} (p^4 - p^{40})] \tag{7.3}$$

where p is a probability factor used to estimate the degree of polymerisation in the system, and is calculated in Equation (7.4).

Estimating Polymerisation

Silicate melt structure is defined by the bridging behaviour of oxygen atoms, influencing the polymerisation of SiO_4 tetrahedra into three-dimensional networks. The degree of polymerisation, quantified by the average number of bridging oxygens around silicon, can be estimated from bond fractions calculated using the MQM. The first step to estimate the degree of polymerisation is to know the probability for a given Si atom to form one Si – Si bridge. This propapility is given by p in Equation (7.4).

$$p = \frac{2n_{\mathrm{Si-Si}}}{2n_{\mathrm{Si-Si}} + \sum_M n_{\mathrm{Si-M}}} \tag{7.4}$$

$$= \frac{x_{\mathrm{Si-Si}}}{2x_{\mathrm{Si-Si}} + \sum_M x_{\mathrm{Si-M}}} \tag{7.5}$$

As a first approximation, p can be calculated by dividing the total number of Si – Si bridges from all silicon atoms by the combined total of Si – Si and Si – M bridges. Each Si – Si bridge is counted twice since an O^0 bond emanates from each silicon atom in the bridge.

The probability that a given silicon atom is a Q^4-species is p^4, as this atom is connected to four Si – Si bridges. This principle extends to Si – Si bridges forming chains. The probability of encountering m Si – Si bridges connected to form a chain of length m is proportional to p^{m}.

Thus, p^{m}, where m is a natural number, serves as a measure of the abundance of various Si – Si cluster sizes present in the slag (Kim et al. 2012a). A critical cluster size can be defined to represent the formation of a percolating SiO_2 network. Once this cluster size is reached, the μ increases dramatically. Analysis of the viscosity data suggests that a cluster of 40 interconnected Si – Si pairs is an appropriate choice for the critical cluster size (Kim et al. 2012a).

7.1.4 Multicomponent Model Formulation

Systems Without Alumina

For the implemented model, both A and E are functions of slag composition, $\boldsymbol{x}$, and are expressed in terms of multiple additional contributing parameters shown in Equation (7.6) and Equation (7.7). These equations provide estimates for A and E for unary, binary, and multi-component systems, with the primary constraint of having the appropriate optimised binary parameters to describe the system of interest. As indicated by Equation (7.6) and Equation (7.7), each individual parameter within these equations are multiplied with ionic compositions of $x_{\mathrm{Si}}^{\$_0}$ or $x_{\mathrm{M}}^{\$_0}$ to account for their contributions to the overall viscosity of the slag.

Therefore, it is important to note that the input compositions that are generally expressed with the formulas of the oxide components, need to be converted to ionic compositions ($x_{\mathrm{SiO_2}}^{\$_\mathrm{f}} \rightarrow x_{\mathrm{Si}}^{\$_0}$) to be used in the model.

$$\begin{aligned} A = & \sum_{\mathrm{M=Na,Ca,Mg,...}} A_{\mathrm{M}} x_{\mathrm{M}}^{\$_0} + A_{\mathrm{Si}}^{*} x_{\mathrm{Si}}^{\$_0} + A_{\mathrm{Si}}^{E} x_{\mathrm{Si}}^{\$_0} p^{40} \\ & + \sum_{\mathrm{M}} A_{\mathrm{M-Si}} x_{\mathrm{M}}^{\$_0} x_{\mathrm{Si}}^{\$_0} + x_{\mathrm{Si}}^{\$_0} (p^4 - p^{40}) \times \sum_{\mathrm{M}} A_{\mathrm{M-Si}}^{R} \frac{x_{\mathrm{M}}^{\$_0}}{\sum_{\mathrm{M}} x_{\mathrm{M}}^{\$_0}} \end{aligned} \tag{7.6}$$

$$\begin{aligned} E = & \sum_{\mathrm{M=Na,Ca,Mg,...}} E_{\mathrm{M}} x_{\mathrm{M}}^{\$_0} + E_{\mathrm{Si}}^{*} x_{\mathrm{Si}}^{\$_0} + E_{\mathrm{Si}}^{E} x_{\mathrm{Si}}^{\$_0} p^{40} \\ & + \sum_{\mathrm{M}} E_{\mathrm{M-Si}} x_{\mathrm{M}}^{\$_0} x_{\mathrm{Si}}^{\$_0} + x_{\mathrm{Si}}^{\$_0} (p^4 - p^{40}) \times \sum_{\mathrm{M}} E_{\mathrm{M-Si}}^{R} \frac{x_{\mathrm{M}}^{\$_0}}{\sum_{\mathrm{M}} x_{\mathrm{M}}^{\$_0}} \end{aligned} \tag{7.7}$$

Background to these individual parameters is given as follows.

The parameters A_{M} and E_{M} are the contributions to the viscosity of the pure liquid oxides MO_x, Equation (7.8). These are non-network formers.

$$\ln \mu_{\mathrm{MO_x}} = A_{\mathrm{M}} + \frac{E_{\mathrm{M}}}{RT} \tag{7.8}$$

Similarly, Equation (7.9), describes the hypothetical viscosity of SiO_2 if it behaved as a basic oxide and did not form a network.

$$\ln \mu^*_{\mathrm{SiO}_2} = A^*_{\mathrm{Si}} + \frac{E^*_{\mathrm{Si}}}{RT} \tag{7.9}$$

The excess contribution per Si atom from large clusters of Q^4-species, where a silicon atom is at the center of a group containing at least 40 interconnected Si – Si pairs, is proportional to p^{40}. This contribution is expressed through $A^{\mathrm{E}}_{\mathrm{Si}}$ and $E^{\mathrm{E}}_{\mathrm{Si}}$. For a system with a composition of $x^{\$_0}_{\mathrm{Si}}$, the clustering effect is given by $x^{\$_0}_{\mathrm{Si}} \cdot p^{40}$, as shown in Equation (7.6) and Equation (7.7).

By combining the contributions of $A^{\mathrm{E}}_{\mathrm{Si}}$ and $E^{\mathrm{E}}_{\mathrm{Si}}$ with those of A^*_{Si} and E^*_{Si}, and assuming that the excess contributions of the silica network are independent of other cations M, the viscosity of pure SiO_2 can be calculated using Equation (7.10).

$$\ln \mu_{\mathrm{SiO}_2} = (A^*_{\mathrm{Si}} + A^E_{\mathrm{Si}}) + \frac{(E^*_{\mathrm{Si}} + E^E_{\mathrm{Si}})}{RT} \tag{7.10}$$

The excess contribution per Si atom from the remaining Q^4-species, particularly from smaller clusters with fewer than 40 interconnected Si – Si pairs, is proportional to (p^4 - p^{40}). These smaller clusters, containing less than 40 Si – Si pairs, also affect viscosity and interact more directly with other oxides in the slag. The M cations are positioned closer to a given Si atom, making their contribution to viscosity system-dependent, and are combined with the binary parameters $A^{\mathrm{R}}_{\mathrm{M-Si}}$ and $E^{\mathrm{R}}_{\mathrm{M-Si}}$.

Finally, the binary parameters $A_{\mathrm{M-Si}}$ and $E_{\mathrm{M-Si}}$, are cross-terms used to account for small nonlinearities of the viscosity, if any, for binary systems M – Si and are therefore multiplied by the concentrations of both respective ions, $x^{\$_0}_{\mathrm{M}}$ and $x^{\$_0}_{\mathrm{Si}}$, associated with a binary oxide system.

The parameters A^*_{Si}, $A^{\mathrm{E}}_{\mathrm{Si}}$, E^*_{Si} and $E^{\mathrm{E}}_{\mathrm{Si}}$ are properties of pure SiO_2 and so are common for all binary systems. $(A^*_{\mathrm{Si}} + A^{\mathrm{E}}_{\mathrm{Si}})$ and $(E^*_{\mathrm{Si}} + E^{\mathrm{E}}_{\mathrm{Si}})$ are equal to experimentally determined viscosity parameters A_{Si} and E_{Si} from pure SiO_2.

The parameters $A_{\mathrm{M-Si}}$, $E_{\mathrm{M-Si}}$, $A^{\mathrm{R}}_{\mathrm{M-Si}}$ and $E^{\mathrm{R}}_{\mathrm{M-Si}}$ are characteristic of each binary system and are the only true binary viscosity parameters. The values for these parameters were optimised using critically evaluated experimental viscosity data. For binary systems studied, except for the $AlO_{1.5}$ – SiO_2 system, the parameters $A_{\mathrm{M-Si}}$ and $A^{\mathrm{R}}_{\mathrm{M-Si}}$ were not required and are set to zero. The optimised parameters for the model are shown in Table 7.1 (Kim 2011; Kim et al. 2012b).

Systems Containing Al_2O_3 or Fe_2O_3

In the binary $AlO_{1.5}$ – SiO_2 system, Al^{3+} is assumed to be octahedrally coordinated by six oxygens, similar to its coordination in the aluminosilicate minerals mullite and sillimanite. In this state, Al^{3+} disrupts the silica network, forming non-bridging oxygens and acts as a network modifier, which lowers the viscosity of the silicate melt. However, in a melt containing both $AlO_{1.5}$ and MO_x, Al^{3+} can partially substitute for Si^{4+} in the silica network, acting as a network former. This substitution is possible as long as the network-forming Al^{3+} remains associated with the M^{1+} or M^{2+} ions that compensate for the missing charge. The same concept applies to Fe_2O_3, where Fe^{3+} will act as a network former. This concept is known as the charge-compensation effect, and has become generally accepted. Due to its ability to act both as a network former and a network modifier, $AlO_{1.5}$ and $FeO_{1.5}$ are termed "amphoteric" components.

The thermodynamic database of the MQM parameters, which the viscosity model is based on to determine $x_{\mathrm{Si-Si}}$, does not consider the different structural roles of Al^{3+} and Fe^{3+} because the thermodynamic properties do not strongly depend on the different structural states. Therefore, to model a viscosity maximum induced by the amount of network-forming Al^{3+} and Fe^{3+} in a slag, they have to be separately evaluated.

It is assumed that the charge-compensated Al^{3+} and Fe^{3+} in the silicate network have the same impact on viscosity as Si^{4+}. The quantity of network-forming associate species, in relation to temperature and composition, can be determined from the equilibrium constant (K) of the following equilibria, Equations (7.11) to (7.14).

$$2\,\mathrm{AlO_{1.5}} + \mathrm{CaO} \;\leftrightarrow\; \mathrm{CaAl_2O_4} \tag{7.11}$$
$$2\,\mathrm{AlO_{1.5}} + \mathrm{MgO} \;\leftrightarrow\; \mathrm{MgAl_2O_4} \tag{7.12}$$
$$2\,\mathrm{AlO_{1.5}} + \mathrm{FeO} \;\leftrightarrow\; \mathrm{FeAl_2O_4} \tag{7.13}$$
$$2\,\mathrm{FeO_{1.5}} + \mathrm{CaO} \;\leftrightarrow\; \mathrm{CaFe_2O_4} \tag{7.14}$$
$$\tag{7.15}$$

The concentrations of the associate species, $x^{\$_1}_{\mathrm{CaAl_2}}$, $x^{\$_1}_{\mathrm{MgAl_2}}$, $x^{\$_1}_{\mathrm{FeAl_2}}$ and $x^{\$_1}_{\mathrm{CaFe_2}}$ correspond to the concentration of network formers while the concentration of $x^{\$_1}_{\mathrm{Al_{15}}}$, $x^{\$_1}_{\mathrm{Fe}}$ and $x^{\$_1}_{\mathrm{Fe_{15}}}$ corresponds to the concentration of network modifiers. By increasing the Si content by the amount of the associate species calculated from Equations (7.11) to (7.14) it is possible to estimate values of A and E for Al-containing systems with Equation (7.6) and Equation (7.7).

Therefore, to accurately model the viscosity, equilibrium constants, Equations (7.16) to (7.19), of the reactions are required.

$$K_{\mathrm{CaAl_2}} = \frac{\gamma_{\mathrm{CaAl_2}}}{\gamma^2_{\mathrm{Al}} \cdot \gamma_{\mathrm{Ca}}} \tag{7.16}$$
$$K_{\mathrm{MgAl_2}} = \frac{\gamma_{\mathrm{MgAl_2}}}{\gamma^2_{\mathrm{Al}} \cdot \gamma_{\mathrm{Mg}}} \tag{7.17}$$
$$K_{\mathrm{FeAl_2}} = \frac{\gamma_{\mathrm{FeAl_2}}}{\gamma^2_{\mathrm{Al}} \cdot \gamma_{\mathrm{FeO}}} \tag{7.18}$$
$$K_{\mathrm{CaFe_2}} = \frac{\gamma_{\mathrm{CaFe_2}}}{\gamma^2_{\mathrm{FeO_{1.5}}} \cdot \gamma_{\mathrm{Ca}}} \tag{7.19}$$
$$\tag{7.20}$$

The activity coefficients γ_{i} of the species Al, Na, Ca, and Mg can be obtained from the implemented MQM model in FactSage. However, the activities of the associated species are not available, as they are not included in the thermodynamic database. Therefore, it is assumed that the activities of all species in Equations (7.16) to (7.19) can be approximated by their concentrations, i.e., $x^{\$_1}_{\mathrm{i}}$.

Using an equation for K, the concentration of an associate species can be determined by calculating the Gibbs free energy of the reaction, Equation (7.21), coupled with an optimised value for ΔG°, from Table 7.2.

$$\Delta G^\circ = -RT\ln K \tag{7.21}$$

An example case is provided for Equation (7.11) to determine the composition of the associate species $x^{\$_1}_{\mathrm{CaAl_2}}$, using the combined equations Equations (7.16) and (7.21) and the optimised value of $\Delta G^\circ_{\mathrm{CaAl_2}}$ from Table 7.2. The combined equation, Equation (7.22), is expressed in terms of compositions $x^{\$_1}_{\mathrm{i}}$, with the superscript $\$_1$ indicating compositions that now include the associate species.

$$5000 - 100000 x^{\$_0}_{\mathrm{Si}} = -RT\ln\frac{(x^{\$_1}_{\mathrm{CaAl_2}})}{(x^{\$_1}_{\mathrm{Al}})^2\cdot(x^{\$_1}_{\mathrm{Ca}})} \tag{7.22}$$

The compositions $x^{\$_1}_{\mathrm{CaAl_2}}$, $x^{\$_1}_{\mathrm{Ca}}$, and $x^{\$_1}_{\mathrm{Al}}$ can be expressed in terms of n_{i} with Equations (7.23) to (7.27).

$$x^{\$_1}_{\mathrm{CaAl_2}} = \frac{n^{\$_1}_{\mathrm{CaAl_2}}}{n^{\$_1}_{\mathrm{Total}}} = \frac{n^{\$_1}_{\mathrm{CaAl_2}}}{(n^{\$_1}_{\mathrm{CaAl_2}} + n^{\$_1}_{\mathrm{Al}} + n^{\$_1}_{\mathrm{Ca}})} \tag{7.23}$$

$$x^{\$_1}_{\mathrm{Ca}} = \frac{n^{\$_1}_{\mathrm{Ca}}}{n^{\$_1}_{\mathrm{Total}}} = \frac{n^{\$_1}_{\mathrm{Ca}}}{(n^{\$_1}_{\mathrm{CaAl_2}} + n^{\$_1}_{\mathrm{Al}} + n^{\$_1}_{\mathrm{Ca}})} \tag{7.24}$$

$$x^{\$_1}_{\mathrm{Al}} = \frac{n^{\$_1}_{\mathrm{Al}}}{n^{\$_1}_{\mathrm{Total}}} = \frac{n^{\$_1}_{\mathrm{Al}}}{(n^{\$_1}_{\mathrm{CaAl_2}} + n^{\$_1}_{\mathrm{Al}} + n^{\$_1}_{\mathrm{Ca}})} \tag{7.25}$$

$$n^{\$_1}_{\mathrm{Ca}} = n^{\$_0}_{\mathrm{Ca}} - n^{\$_1}_{\mathrm{CaAl_2}} \tag{7.26}$$

$$n^{\$_1}_{\mathrm{Al}} = n^{\$_0}_{\mathrm{Al}} - 2n^{\$_1}_{\mathrm{CaAl_2}} \tag{7.27}$$

A careful evaluation of Equations (7.22) to (7.27) reveals that $n^{\$_1}_{\mathrm{CaAl_2}}$ is the only unknown. This value can be determined through a root-finding procedure constrained by an elemental mass balance, ensuring the correct root is selected to satisfy mass conservation.

For MeO_x – $AlO_{1.5}$/$FeO_{1.5}$ – SiO_2 systems, ΔG° varies linearly as a function of SiO_2 content, with no temperature dependence. It becomes more negative with increasing SiO_2 concentration (Kim 2011).

Finally, calculating A and E using Equation (7.6) and Equation (7.7) requires updating the mole fractions to “equivalent” mole fractions $x^{\$_2}_{\mathrm{i}}$, as shown in Equations (7.28) to (7.31). This adjustment accounts for the network-forming effect of the associated species. In this approach, the slag is considered to have the same viscosity as an “equivalent” slag without network-forming Al^{3+}, which is compensated by $x^{\$_2}_{\mathrm{i}}$.

$$x_{\text{Si}}^{\$_2} = [x_{\text{Si}}^{\$_1} + 2x_{\text{CaAl}_2}^{\$_1} + 2x_{\text{MgAl}_2}^{\$_1} + 2x_{\text{FeAl}_2}^{\$_1} + 2x_{\text{CaFe}_2}^{\$_1}]/N_{tot} \tag{7.28}$$

$$x_{\text{Al}}^{\$_2} = [x_{\text{Al}}^{\$_1}]/N_{tot} \tag{7.29}$$

$$x_{\text{Ca}}^{\$_2} = [x_{\text{Ca}}^{\$_1}]/N_{tot} \tag{7.30}$$

$$x_{\text{Mg}}^{\$_2} = [x_{\text{Mg}}^{\$_1}]/N_{tot} \tag{7.31}$$

$$x_{\text{FeO}}^{\$_2} = [x_{\text{FeO}}^{\$_1}]/N_{tot} \tag{7.32}$$

$$x_{\text{FeO}_{1.5}}^{\$_2} = [x_{\text{FeO}_{1.5}}^{\$_1}]/N_{tot} \tag{7.33}$$

$$\tag{7.34}$$

with:

$$\begin{aligned} N_{tot} =& x_{\text{Si}}^{\$_1} + x_{\text{Al}}^{\$_1} + x_{\text{Ca}}^{\$_1} + x_{\text{Mg}}^{\$_1} + x_{\text{FeO}}^{\$_1} + x_{\text{FeO}_{1.5}}^{\$_1} \\ &+ 2x_{\text{CaAl}_2}^{\$_1} + 2x_{\text{MgAl}_2}^{\$_1} + 2x_{\text{FeAl}_2}^{\$_1} + 2x_{\text{CaFe}_2}^{\$_1} \end{aligned} \tag{7.35}$$

7.1.5 Variable Declarations

Table 7.1: Optimised viscosity parameters

System	A (Pa s)	E (J mol^{-1})
SiO_2	$A_{\text{Si}}^{*} = -10.56$	$E_{\text{SiO}_2}^{*} = 217200$
	$A_{\text{Si}}^{E} = -6.13$	$E_{\text{SiO}_2}^{E} = 298500$
$AlO_{1.5}$	$A_{\text{Al}_{15}} = -9.22$	$E_{\text{Al}} = 120400$
CaO	$A_{\text{Ca}} = -12.27$	$E_{\text{Ca}} = 137650$
MgO	$A_{\text{Mg}} = -10.58$	$E_{\text{Mg}} = 117160$
FeO	$A_{\text{Fe}} = -8.75$	$E_{\text{Fe}} = 52500$
$FeO_{1.5}$	$A_{\text{Fe}_{15}} = -8.63$	$E_{\text{Fe}_{15}} = 47250$
$SiO_2 - AlO_{1.5}$	$A_{\text{Al-Si}}^{R} = -12.30$	$E_{\text{Al-Si}} = -75000$
		$E_{\text{Al-Si}}^{R} = 303500$
$SiO_2 - CaO$	-	$E_{\text{Ca-Si}} = -101750$
		$E_{\text{Ca-Si}}^{R} = 81400$
$SiO_2 - MgO$	-	$E_{\text{Mg-Si}} = -86250$
		$E_{\text{Mg-Si}}^{R} = 72600$
$SiO_2 - FeO$	-	$E_{\text{Fe-Si}} = -115000$
		$E_{\text{Fe-Si}}^{R} = 87525$
$SiO_2 - FeO_{1.5}$	-	$E_{\text{Fe}_{15}\text{-Si}} = -107500$
		$E_{\text{Fe}_{15}\text{-Si}}^{R} = 88500$

Table 7.2: Optimised values of ΔG° for the associate species for slag systems containing $AlO_{1.5}$ (Grundy et al. 2008a).

System	
$CaO - AlO_{1.5} - SiO_2$	$\Delta G_{\text{CaAl}_2}^{\circ} = 5000 - 100000 x_{\text{Si}}^{\$_0}$
$MgO - AlO_{1.5} - SiO_2$	$\Delta G_{\text{MgAl}_2}^{\circ} = 13000 - 105000 x_{\text{Si}}^{\$_0}$
$FeO - AlO_{1.5} - SiO_2$	$\Delta G_{\text{FeAl}_2}^{\circ} = -66944 x_{\text{Si}}^{\$_0}$
$CaO - FeO_{1.5} - SiO_2$	$\Delta G_{\text{CaFe}_2}^{\circ} = 2092 - 5335 x_{\text{Si}}^{\$_0}$

7.1.6 Assumptions

The following assumptions was made to formulate this model.

1. Where no experimental data were available, viscosity parameters for unary systems are extrapolated from binary viscosity data.
2. For pure silica, two contributions to the viscosity are assumed. The first is that there is a contribution to viscosty that is independent on the formation of a polymer network. The second is that the silicate network itself contributes to the viscosity.
3. It is assumed that the effect of network-forming Al^{3+} and Fe^{3+} on the viscosity will be the same as that of Si^{4+}.
4. For solving the equilibrium equations of the associate species, the activities of all species are assumed to be accurately approximated by their concentrations.
5. For systems not containing Al_2O_3 or Fe_2O_3 it is assumed that $\ln(\mu)$ can be calculated from a linear combination of A and E of binary systems.

7.1.7 Simplifications

The following simplifications was made in this model. The critical group size for SiO_4 clusters is set to be $n = 40$ interconnected Si – Si pairs. Also, the interaction between MgO and Fe_2O_3 is not accounted for as it is for that between CaO and Fe_2O_3.

7.1.8 Literature Inaccuracies

Background

During development of the multicomponent model catered for systems containing Al_2O_3, we experienced significant difficulty to navigate uncertainties caused by literature inaccuracies. To ensure the user do not go through the same trouble, these are listed here.

Inaccuracies

1. Calculating ΔG

   Grundy et al. (2008a) reported that ΔG which dictates the equilibrium constant for the formation of $CaAl_2O_4$ and $MgAl_2O_4$ should be calculated as

   $\Delta G^{\circ}_{\mathrm{CaAl_2}} = 5000 - 100000 x^{\not S_0}_{\mathrm{Si}}$ and $\Delta G^{\circ}_{\mathrm{MgAl_2}} = 13000 - 105000 x^{\not S_0}_{\mathrm{Si}}$,

   while Kim et al. (2012a) reported

   $\Delta G^{\circ}_{\mathrm{CaAl_2}} = -5000 - 100000 x^{\not S_0}_{\mathrm{Si}}$ and $\Delta G^{\circ}_{\mathrm{MgAl_2}} = -13000 - 105000 x^{\not S_0}_{\mathrm{Si}}$.

   Grundy et al. (2008a) reported it correctly.

2. Calculating $x^{\not S_2}$

   Grundy et al. (2008a) reported the calculation of $x^{\not S_2}_{\mathrm{Si}}$ to be

$$x^{\not S_2}_{\mathrm{Si}} = [x^{\not S_1}_{\mathrm{Si}} + x^{\not S_1}_{\mathrm{NaAl}} + 2x^{\not S_1}_{\mathrm{CaAl_2}} + 2x^{\not S_1}_{\mathrm{MgAl_2}}]/N_{\mathrm{tot}} \tag{7.36}$$

where

$$N_{\text{tot}} = x_{\text{Si}}^{\$_1} + x_{\text{Al}}^{\$_1} + x_{\text{Na}}^{\$_1} + x_{\text{Ca}}^{\$_1} + x_{\text{Mg}}^{\$_1} - x_{\text{NaAl}}^{\$_1} - x_{\text{CaAl}_2}^{\$_1} - x_{\text{MgAl}_2}^{\$_1} \tag{7.37}$$

while Kim et al. (2012a) reported the same calculation for $x_{\text{Si}}^{\$_2}$ but with

$$N_{\text{tot}} = x_{\text{Si}}^{\$_1} + x_{\text{Al}}^{\$_1} + x_{\text{Na}}^{\$_1} + x_{\text{Ca}}^{\$_1} + x_{\text{Mg}}^{\$_1} + x_{\text{NaAl}}^{\$_1} + 2x_{\text{CaAl}_2}^{\$_1} + 2x_{\text{MgAl}_2}^{\$_1} \tag{7.38}$$

Here, Kim et al. (2012a) reported it correctly.

3. Incorrect plots presented in Grundy et al. (2008b) and Grundy et al. (2008a).

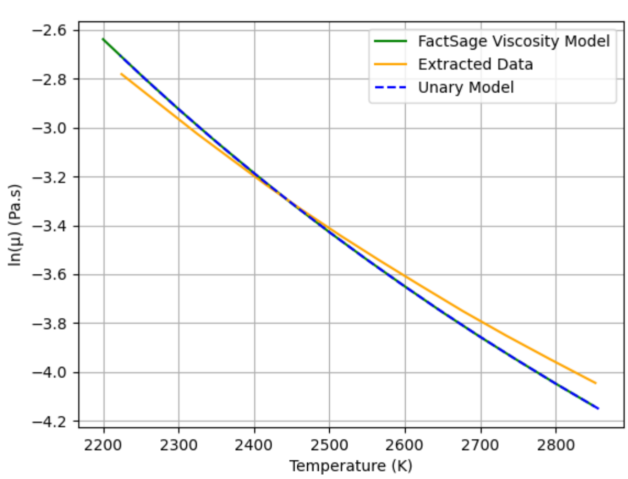

(a) Al_2O_3 – Grundy et al. (2008b) Fig. 7. 'Extracted Data' represents Grundy's model and 'Unary Model' represents auxi-mpp's model.

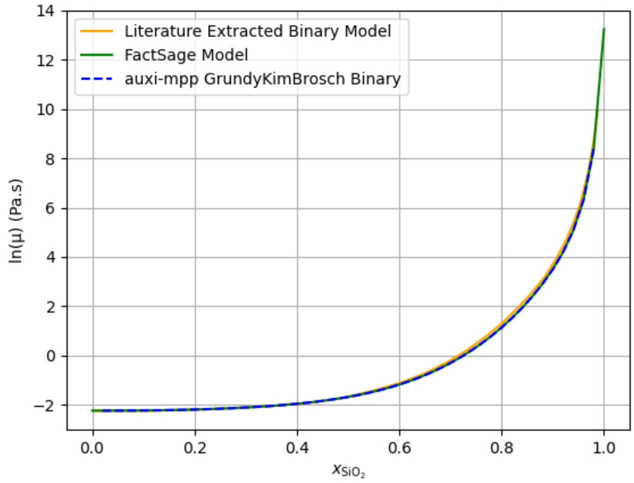

(b) $Al_2O_3 - SiO_2$ – Grundy et al. (2008b) Fig. 8. 'Literature Extracted Binary Model' represents Grundy's model.

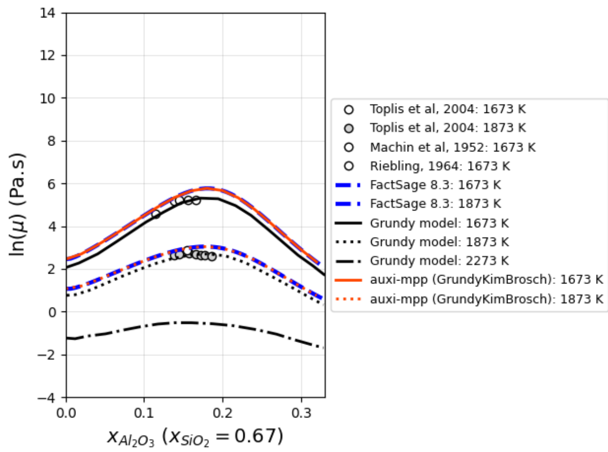

(c) $Al_2O_3 - MgO - SiO_2$ – Grundy et al. (2008a) Fig. 32

Figure 7.1: Inaccurate plots.

The seemingly small deviation present in Figure 7.1b at $x_{\text{SiO}_2} = 0.8$, was found to be double the deviation found in Figure 7.1a at $T = 2800$K. These deviations were confirmed not to be due to erroneous data extraction. The deviation in Figure 7.1c is also a definite inaccuracy since Fig. 31 and 33 matches correctly with auxi-mpp and FactSage's model, and Grundy's binary model agrees with the calculated viscosity at $x_{\mathrm{Al_2O_3}} = 0$. The same problem is present for Fig. 23 of Grundy et al. (2008a).

4. Incorrect plot presented in Kim et al. (2021a).

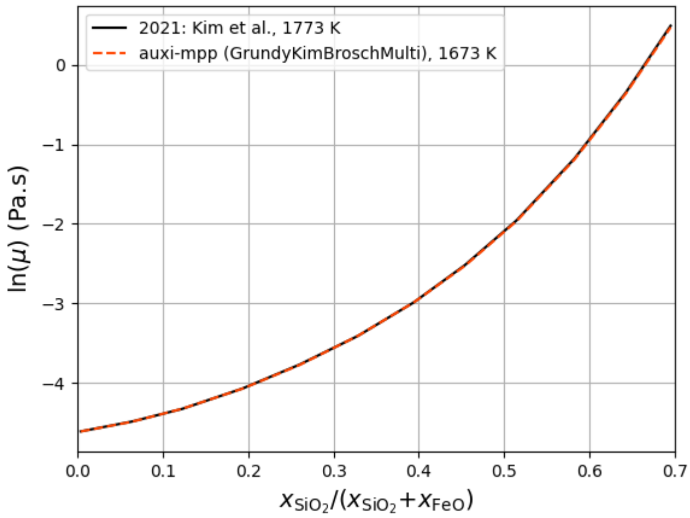

Figure 7.2: CaO – FeO – SiO_2

In Figure 7.2, auxi-mpp plotted the same compositions but 100 K lower than the literature plot at 1773 K. There is an exact match, implying that Kim et al. (2021a) provided the incorrect temperature label.

5. Incorrect plot section defined.

The original figure from which the literature data in Figure 7.2 were extracted is Figure 9 in Kim et al. (2021a). The section to plot is there defined as (81.24 mol % FeO, 13.76 mol % CaO) to (86.75 mol % SiO_2, 13.25 mol % CaO). The first endpoint does not border and is therefore incorrect. The correct endpoint is (**86.24** mol % FeO, 13.76 mol % CaO).

7.1.9 Model Validation

This section details the current status of the Grundy-Kim-Brosch viscosity model implementation in auxi-mpp and presents results for various slag systems. The auxi-mpp model results were compared against the literature model and experimental data extracted from Grundy et al. (2008b), Grundy et al. (2008a), Kim et al. (2021a), and Kim et al. (2021b). auxi-mpp were validated by means of literature figure reproduction as well as with a correlation plot. Validation by figure reproduction is summarised in Table 7.3, and those by correlation plot is listed thereafter.

Table 7.3: Viscosity Validation Ranges

Model	Systems	Composition ($mol\,mol^{-1}$)	Temperature (K)
Unary	SiO_2	pure substance	$1250 - 3250$
	FeO	pure substance	$1100 - 2100$
	Fe_2O_3	pure substance	$1100 - 1850$
Binary	$Al_2O_3 - SiO_2$	$x_{Al_2O_3} = 0 - 1$	$2073, 2173$
	$CaO - SiO_2$	$x_{CaO} = 0 - 1$	$1773, 1873, 2073$
	$MgO - SiO_2$	$x_{MgO} = 0 - 1$	$1773, 1873, 2073$
	$FeO - SiO_2$	$x_{FeO} = 0.3 - 1$	$1473, 1573, 1673, 1773$
Ternary	$CaO - MgO - SiO_2$	$y_{SiO_2} = 0.3 - 0.75, y_{SiO_2}/y_{MgO} = 1$	$1673, 1773, 1873$
	$CaO - MgO - SiO_2$	$y_{SiO_2} = 0.3 - 0.8, y_{MgO} = 0.2$	$1673, 1773, 1873$
	$Al_2O_3 - CaO - SiO_2$	$x_{Al_2O_3} = 0.0 - 0.33, x_{SiO_2} = 0.67$	$1673, 1873$
	$Al_2O_3 - CaO - SiO_2$	$x_{Al_2O_3} = 0.0 - 0.25, x_{SiO_2} = 0.75$	$1673, 1873$
	$Al_2O_3 - MgO - SiO_2$	$x_{Al_2O_3} = 0.0 - 0.50, x_{SiO_2} = 0.50$	$1673, 1873$
	$Al_2O_3 - MgO - SiO_2$	$x_{Al_2O_3} = 0.0 - 0.33, x_{SiO_2} = 0.67$	$1673, 1873$
	$Al_2O_3 - MgO - SiO_2$	$x_{Al_2O_3} = 0.0 - 0.25, x_{SiO_2} = 0.75$	$1673, 1873$
Quaternary	$Al_2O_3 - CaO - MgO - SiO_2$	$y_{Al_2O_3} = 0.0 - 0.45, y_{SiO_2} = 0.5, y_{MgO} = 0.05$	1773
	$Al_2O_3 - CaO - MgO - SiO_2$	$y_{Al_2O_3} = 0.0 - 0.35, y_{SiO_2} = 0.5, y_{MgO} = 0.15$	1773
	$Al_2O_3 - CaO - MgO - SiO_2$	$y_{Al_2O_3} = 0.0 - 0.25, y_{SiO_2} = 0.5, y_{MgO} = 0.25$	1773

Fe-bearing systems validated by means of correlation plots;

1. $Al_2O_3 - FeO - SiO_2$
2. $Fe_2O_3 - FeO - SiO_2$
3. $Al_2O_3 - CaO - FeO - SiO_2$
4. $FeO - MgO - SiO_2$
5. $CaO - Fe_2O_3 - FeO - SiO_2$
6. $CaO - FeO - MgO - SiO_2$
7. $Al_2O_3 - CaO - FeO - MgO - SiO_2$
8. $Al_2O_3 - FeO - MgO - SiO_2$

See Figure 7.8.

Unary Systems

Figure 7.3 demonstrates the agreement between auxi-mpp and the literature model for unary systems, plotting the natural logarithm of viscosity against temperature.

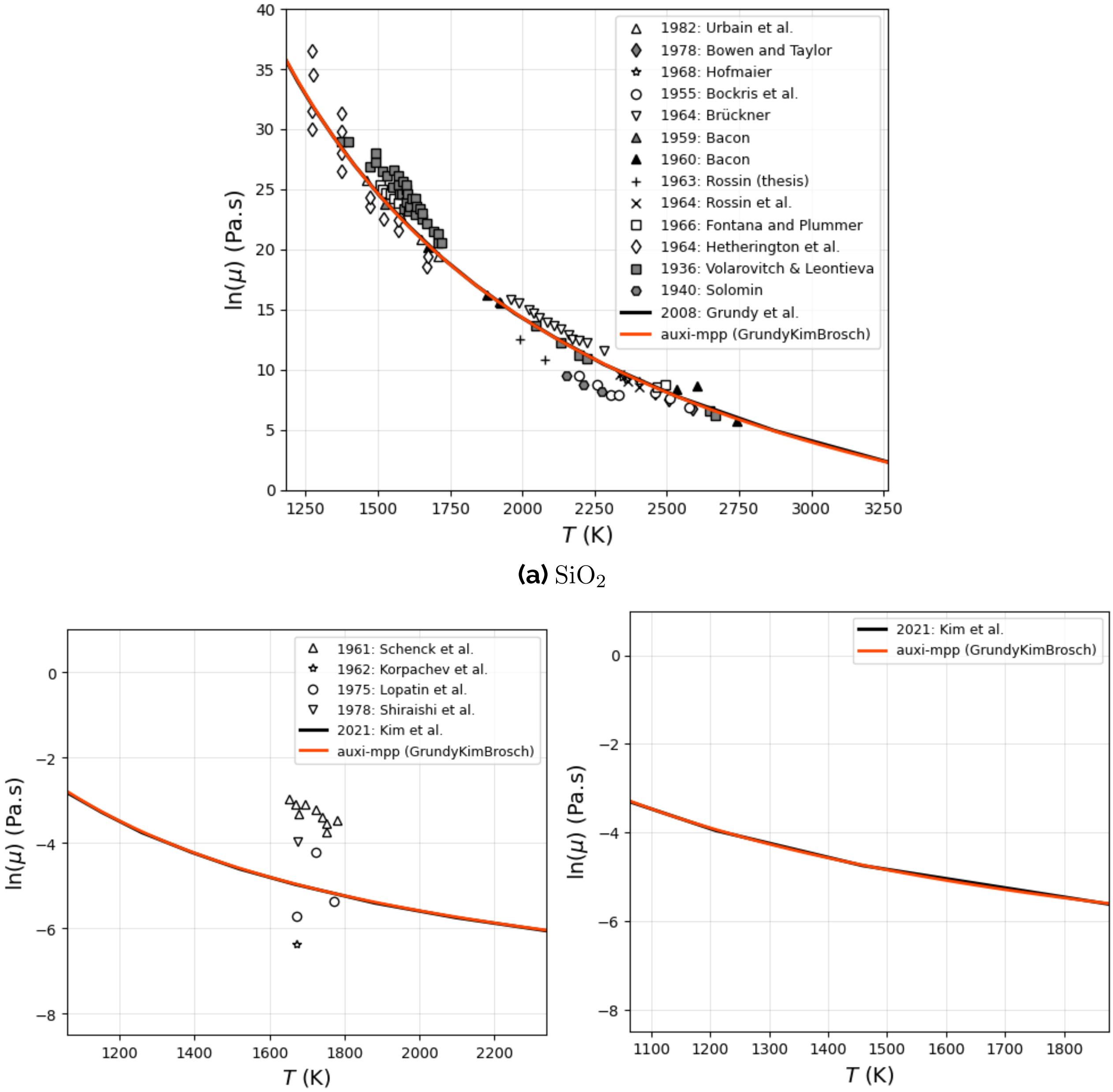

(a) SiO_2

(b) FeO **(c)** Fe_2O_3

Figure 7.3: Viscosity model estimates and comparison for pure SiO_2, FeO and Fe_2O_3.

Binary Systems

Figure 7.4 illustrates the accuracy of the Grundy-Kim-Brosch model ("auxi-mpp GrundyKimBrosch") for estimating viscosities in binary $Al_2O_3-SiO_2$, $CaO-SiO_2$, and $MgO-SiO_2$ systems. Note that validations above 2200 K were intentionally omitted.

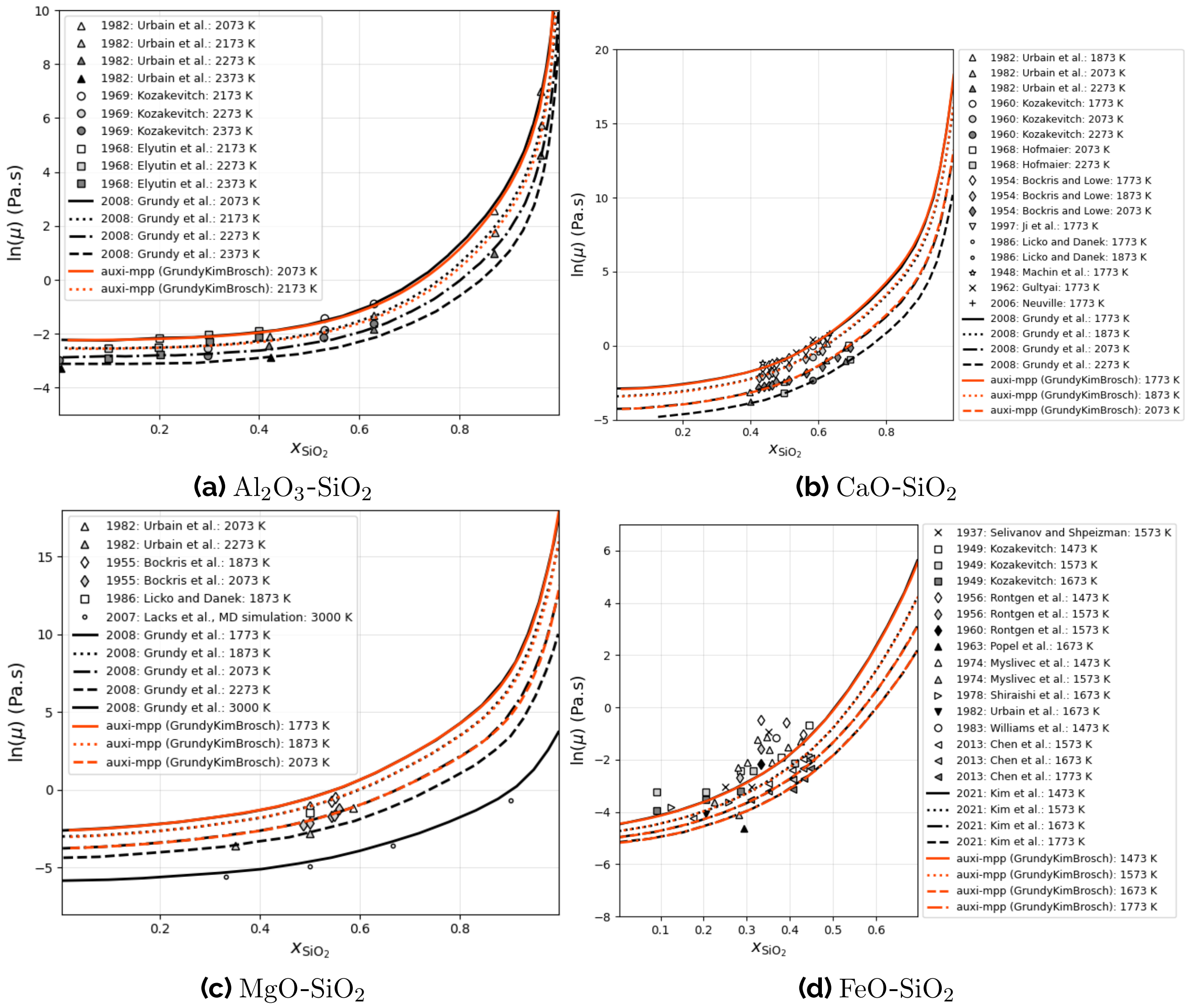

Figure 7.4: Viscosity model estimates and comparisons for binary slag systems.

Multicomponent Systems

Ternary systems without Al_2O_3 were validated initially, as the Grundy-Kim-Brosch model does not require consideration of the charge compensation effect of Al_2O_3 on slag viscosity (Kim 2011; Grundy et al. 2008a). Figure 7.5 demonstrates that viscosity estimates for systems of SiO_2 – MgO – CaO closely align with both model estimates and experimental data from the literature (Grundy et al. 2008a).

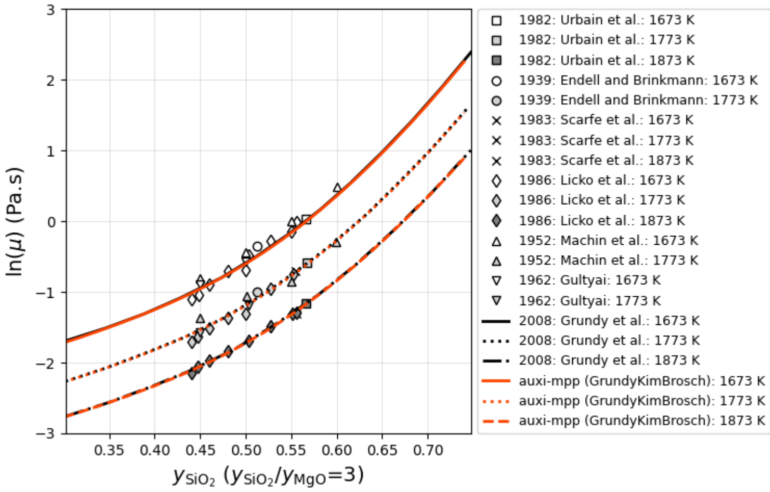

(a) $CaO - MgO - SiO_2$

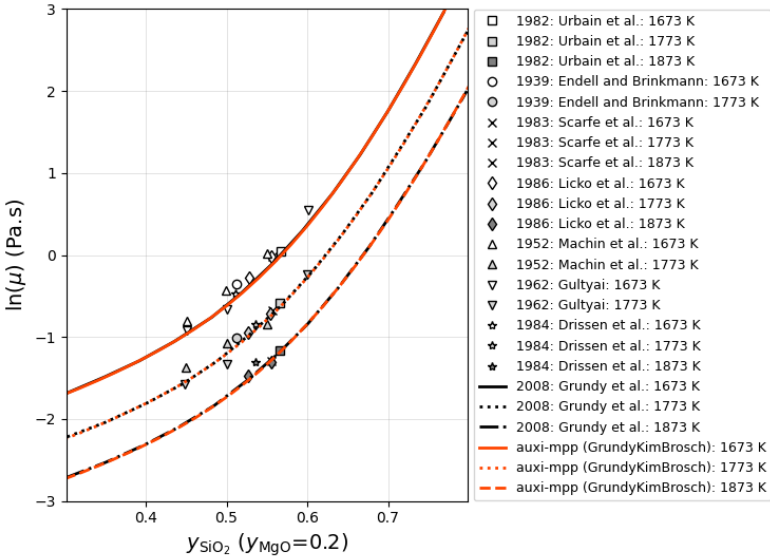

(b) $CaO - MgO - SiO_2$

Figure 7.5: Viscosity model estimates for ternary slag systems without alumina.

Some peculiar results were obtained when validating the model for systems containing Al_2O_3 as seen in Figure 7.6. In Figure 7.6a and Figure 7.6d we reason that the literature plots are incorrect. To support this, the results of FactSage 8.3 were added for comparison. In Figure 7.6d the auxi-mpp model follows the result of FactSage, confirming that the auxi-mpp implementation is correct. This was also applied to Figure 7.6a, however it seems like FactSage's model does not correctly estimate viscosity for systems containing CaO. At the extremes, the auxi-mpp model agrees with FactSage's model, however.

Another reason why these two literature figures are incorrect is that the auxi-mpp binary model, that were successfully validated for the relevant systems, agrees with the multi-component auxi-mpp model at $x_{\mathrm{Al_2O_3}} = 0.0$.

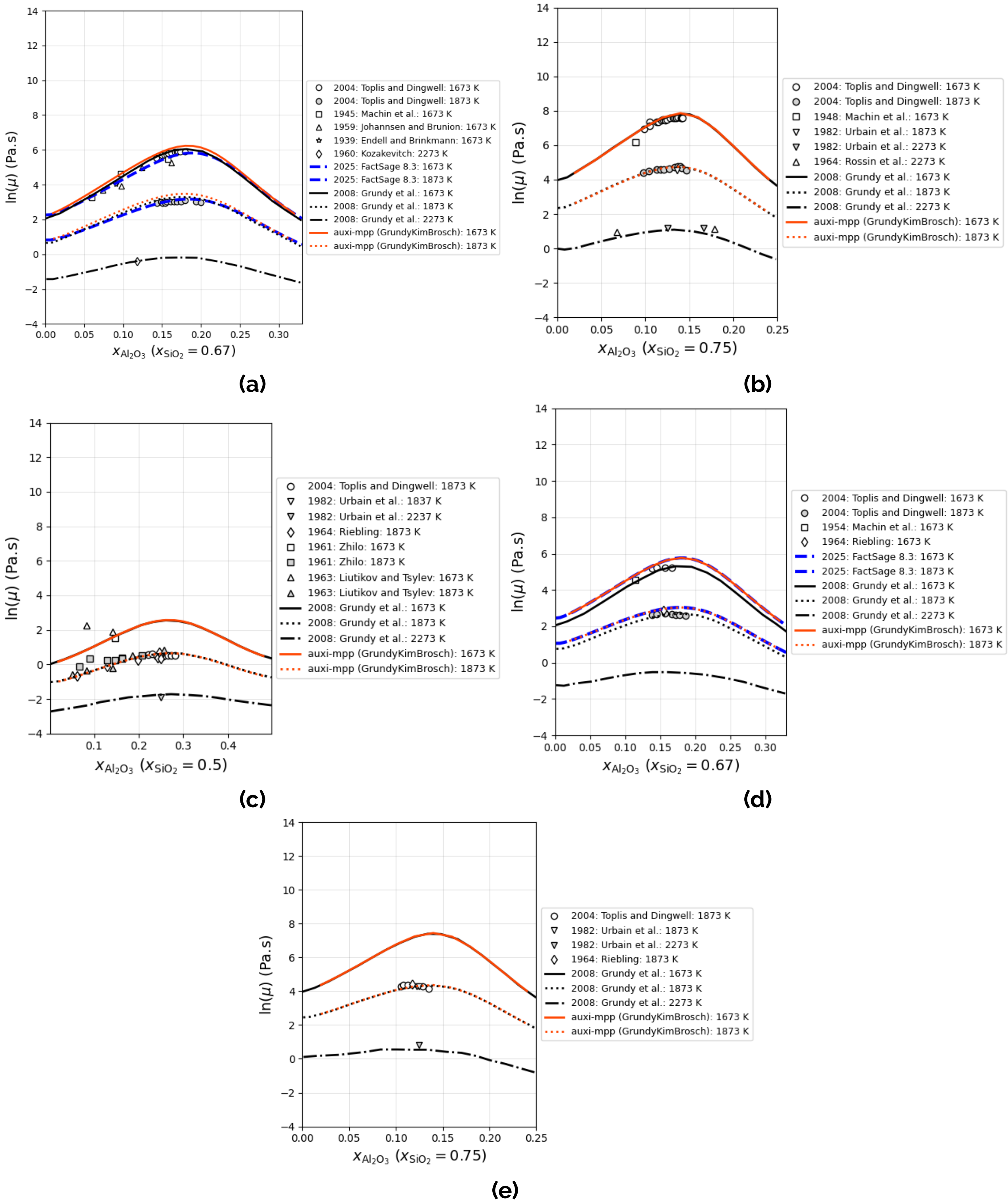

Figure 7.6: Viscosity model estimates for ternary slag systems containing alumina.

The multicomponent viscosity model was successfully validated for the $Al_2O_3-CaO-MgO-SiO_2$ system for a range of compositions at 1773 K as shown in Figure 7.7.

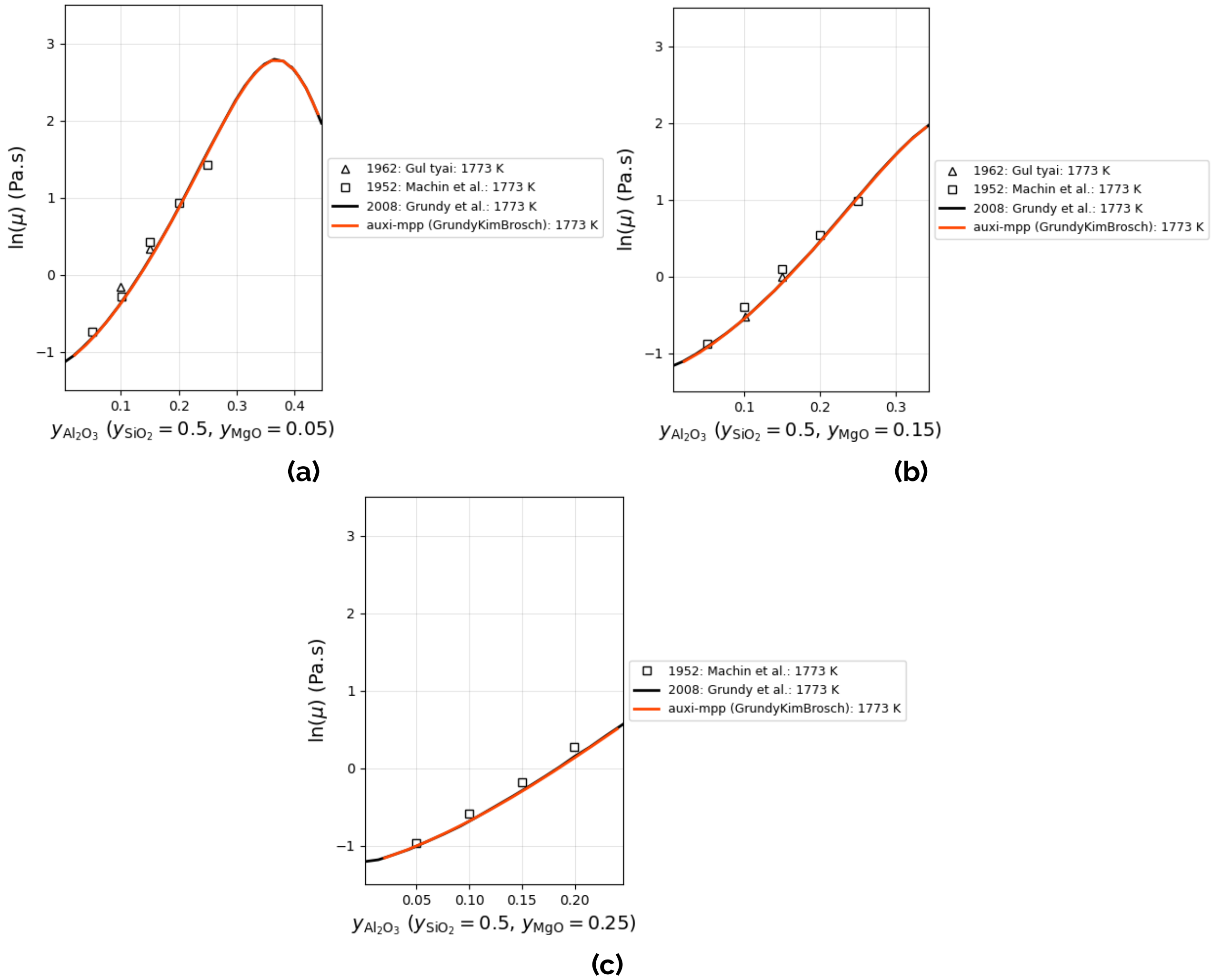

Figure 7.7: Viscosity model estimates for the $Al_2O_3 - CaO - MgO - SiO_2$ quaternary slag system at 1773 K.

Multicomponent Fe-bearing Systems

The available data for multi-component Fe-bearing systems often have abstract axes making it time-consuming to reproduce. These systems are therefore validated by means of correlation plots. Figure 7.8 shows how auxi-mpp performs, with systems containing either FeO or Fe_2O_3 or both, compared to Kim's model as presented in literature (Kim et al. 2021a; Kim et al. 2021b).

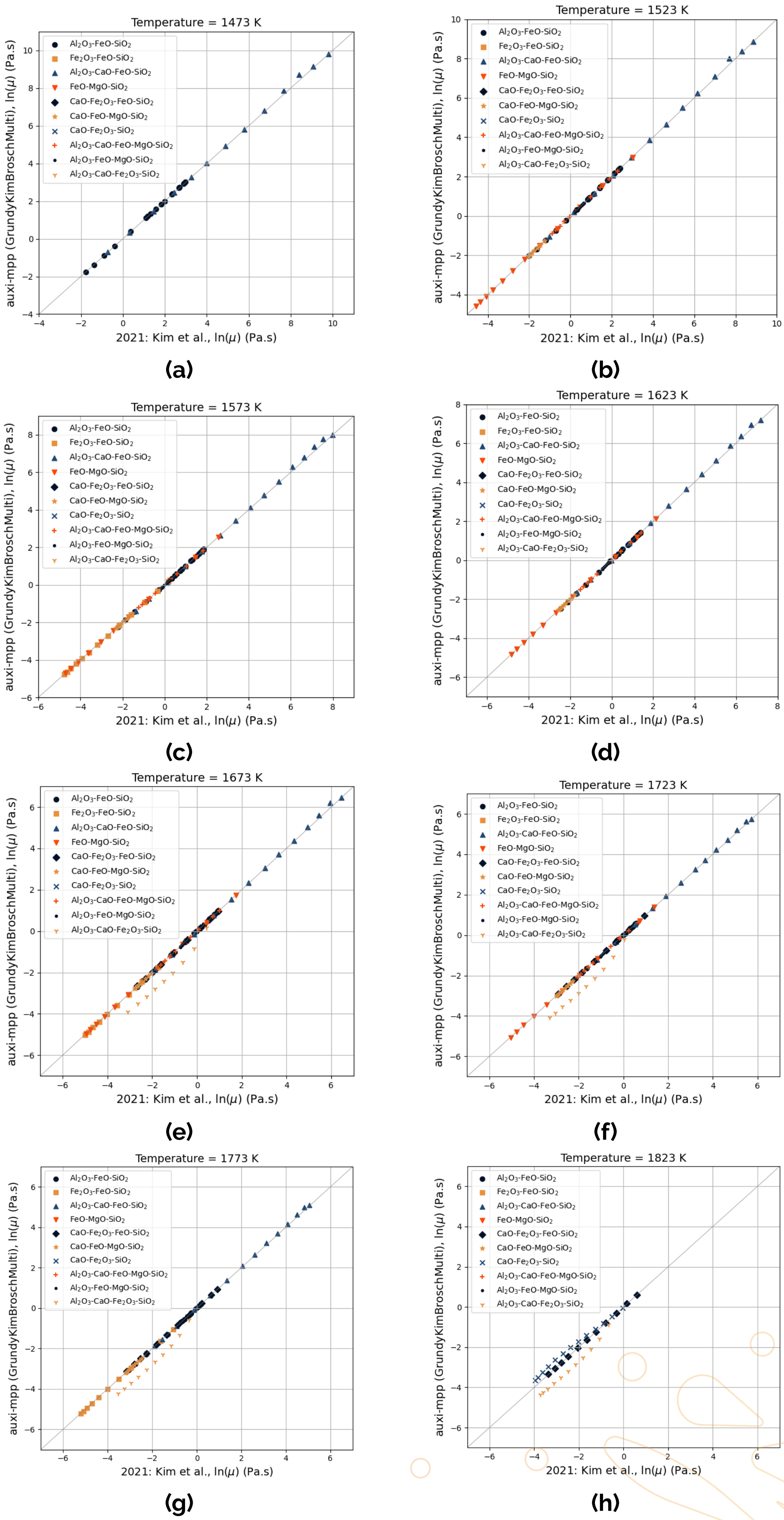

Figure 7.8: auxi-mpp vs Kim et al. (2021b) correlation plots.

For most systems auxi-mpp performs well. There are two systems for which there are visible deviation from literature, however. These are $CaO-Fe_2O_3-SiO_2$ and $Al_2O_3-CaO-Fe_2O_3-SiO_2$. For $CaO-Fe_2O_3-SiO_2$ the original figure were reproduced in Figure 7.9, adding the performance of FactSage 8.3's (2025) viscosity model. auxi-mpp plots close to but not exactly on top of FactSage, and both deviates significantly from literature. Whether this is an error in literature or if both auxi-mpp and FactSage are incorrect, is uncertain. It is also possible that this is caused by a parameter change in FactSage's FToxid database in the time period of 2021 to 2025.

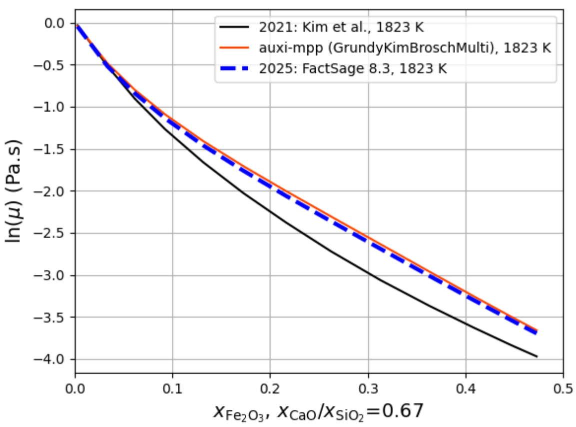

(a) $CaO-Fe_2O_3-SiO_2$

Figure 7.9: auxi-mpp vs FactSage 8.3 (2025) vs Kim et al. (2021b).

The issue with $Al_2O_3-CaO-Fe_2O_3-SiO_2$ is similar as auxi-mpp's results is close to FactSage 8.3, with both deviating significantly from literature.

Issues

Potential issue with the systems $CaO-Fe_2O_3-SiO_2$ and $Al_2O_3-CaO-Fe_2O_3-SiO_2$. See Figures 7.8 and 7.9.

Part III

Liquid Alloy Material Properties

Chapter 8

Background

In pyrometallurgical operations like the REF process, the formation of a liquid metal phase, or alloy, is the most important outcome. Liquid alloy is the primary product and a dynamic medium that interacts directly with the furnace lining and the overlying slag layer. Therefore, understanding the physical properties of molten alloy, not just the slag, is crucial for the successful and efficient operation of a REF process for the production of green steel.

The physical characteristics of the liquid alloy play a part in influencing process behaviour and outcomes. Density is fundamental to achieving effective gravitational separation between the valuable metal and the slag impurities. Viscosity governs the fluid dynamics within the furnace, influencing mixing, mass transfer rates within the alloy and at the interface between alloy and slag, and the ease of tapping the final product. Electrical and thermal conductivity are critical properties to understand in a furnace. Electrical conductivity directly impacts the energy efficiency of the furnace's heating systems, while thermal conductivity dictates heat distribution, which affects reaction kinetics and furnace wear.

Directly measuring these properties under the extreme temperatures and reactive conditions of a furnace is often impractical and expensive. Therefore, accurate and reliable physical property models are indispensable tools for process simulation, optimisation, and the development of new, more sustainable steelmaking technologies. This section of the manual details the theoretical foundations of the models implemented in auxi-mpp for estimating these key physical properties for liquid alloys, along with their validation against experimental data and literature models.

Chapter 9

Density

This chapter presents several models implemented in auxi-mpp to estimate the density of various liquid alloys. The models cover three distinct categories of alloy systems.

The primary approach, based on volumetric thermal expansion coefficients, is used to calculate the density of unary, binary, and multi-component liquid alloys that contain only metallic elements. For binary alloys that include non-metallic elements like carbon and sulfur, a set of distinct empirical models is provided. Lastly, the chapter details specific models for estimating the density of common multi-component commercial alloys, such as stainless steel and grey cast iron

9.1 Density by Volumetric Thermal Expansion

A density model based on volumetric thermal expansion coefficients.

9.1.1 Introduction

Extensive reference correlation data was discovered using the Nation Institute of Standards and Technology (NIST) Alloy Data web app to directly model density for a wide range of alloy systems ("Thermodynamics Research Center" 2009). Molar volume is then derived from the estimated densities.

9.1.2 Overview

Reference data for unary, binary and multi-component liquid alloy systems have been found in literature that employs volumetric thermal expansion coefficients to estimate the density of liquid alloys (Assael et al. 2006; Assael et al. 2010; Assael et al. 2012a; Assael et al. 2012b; Brillo et al. 2006; Brillo and Egry 2004; Brillo and Egry 2003). Density estimates for these unary, binary and multi-component systems only focus on alloys containing metallic elements. Systems containing non-metallic elements such as C, P and S are estimated with empirical models, which are described in Section 9.2.

9.1.3 Formulation

It is important to understand the relationship between molar volume and density. The following model formulation starts by first describing how molar volume can be determined followed by deriving density from it.

Molar volume for an ideal alloy system can be determined by applying Vegard's law, Equation (9.1), where x_i is the mole fraction of component i, V_i is the molar volume of component i, M_i is the molar mass of component i, and ρ_i is the density of component i.

$$V^{ideal} = \sum_i x_i V_i = \sum_i x_i \frac{M_i}{\rho_i} \tag{9.1}$$

For non-ideal systems where excess molar volume must be considered, Equation (9.2), the density of the system can be used to determine its molar volume, as shown in Equation (9.3). Here, $V^{non-ideal}$ is the non-ideal molar volume, M_i is the molar mass of component i, and ρ_{system} is the density of the system.

$$V^{non-ideal} = V_{ideal} + V_{excess} \tag{9.2}$$

$$V^{non-ideal} = \frac{\sum_i^{system} x_i M_i}{\rho_{system}} \tag{9.3}$$

The molar volume of molten alloy systems containing only metallic elements exhibits a linear temperature dependence that can be modelled using the volumetric thermal expansion coefficient, β, as shown in Equation (9.4), where $V_{T,melt}$ is the molar volume at the melting temperature and T is the temperature of the system.

$$V(T) = V_{T,melt}(1 + \beta(T - T_{melt})) \tag{9.4}$$

Similarly, this can be related to the density of pure liquid metals and alloys with Equation (9.5) and Equation (9.6) respectively, where $\rho_{T,melt}$ is the density at the melting temperature and $\rho_{T,liquidus}$ is the density at the liquidus temperature.

$$\rho(T) = \rho_{T,melt}(1 + \beta(T - T_{melt})) \tag{9.5}$$

$$\rho(T) = \rho_{T,liquidus}(1 + \beta(T - T_{liquidus})) \tag{9.6}$$

For modelling purposes using the density reference data found in literature, Equation (9.6) is rearranged to form Equation (9.7), where $\rho_T = \beta \cdot \rho_L$ is the thermal expansion coefficient, ρ_L is the density at the liquidus temperature, T_L is the liquidus temperature and T is the temperature of the system (Assael et al. 2006; Brillo and Egry 2004).

$$\rho(T) = \rho_L - \rho_T(T - T_L) \tag{9.7}$$

For each composition in a unary, binary, or multi-component system, the parameters ρ_L, ρ_T, and T_L are determined from experimental data and used in Equation (9.7) to estimate the density of the system at a given temperature. It is important to note that the parameters are only valid within a specific temperature range, which is also determined from the experimental data.

Unary Systems

For unary systems, the density of a pure liquid metal is estimated using Equation (9.7). The supported elements, along with their model parameters and valid temperature ranges, are listed in Table 9.1. It is important to note that the application of the model should be restricted to the temperature ranges for which the parameters have been validated. Using the model outside these ranges may lead to inaccurate density estimates.

Table 9.1: Supported elements, temperature limits and parameters for the unary density model.

Element	Symbol	Temp. Range (K)	ρ_L (kg/m^3)	ρ_T (kg/m^3· K)	T_{ref} (K)
Aluminum	Al	933 – 1190	2377.2	0.311	934
Antimony	Sb	900 – 1300	6467.0	0.608	899
Bismuth	Bi	545 – 1500	10028.0	1.213	545
Cadmium	Cd	594 – 833	8008.0	1.251	594
Chromium	Cr	2186 – 2503	6097.1	0.6536	2180
Cobalt	Co	1768 – 2500	7827.0	0.936	1768
Copper	Cu	1356 – 2500	7997.0	0.819	1358
Gallium	Ga	303 – 1500	6077.0	0.611	303
Hafnium	Hf	2500 – 4981	11902.6	0.6704	2500
Indium	In	430 – 1100	7022.0	0.762	430
Iron	Fe	1809 – 2480	7035.0	0.926	1811
Lead	Pb	601 – 2000	10656.0	1.239	601
Molybdenum	Mo	2896 – 5914	9062.6	0.3947	2896
Nickel	Ni	1728 – 2500	7861.0	0.988	1728
Niobium	Nb	2742 – 5848	7664.0	0.2943	2742
Silicon	Si	1687 – 2000	2550.0	0.264	1687
Silver	Ag	1235 – 1600	9294.0	0.877	1235
Tantalum	Ta	3293 – 7400	14977.5	0.6802	3293
Thallium	Tl	576 – 1200	11233.0	1.2	577
Tin	Sn	506 – 1950	6979.0	0.652	505
Titanium	Ti	1941 – 3520	4222.1	0.3952	1941
Tungsten	W	3695 – 5818	17146.4	0.6769	3695
Vanadium	V	2183 – 4500	5517.0	0.5895	2183
Zinc	Zn	692 – 910	6559.0	0.884	693
Zirconium	Zr	2128 – 4100	6100.0	0.242	2128

Binary Systems

Densities for binary alloy systems using Equation (9.7) can be estimated for the following compositions and temperature ranges found in Table 9.2. For compositions not explicitly listed, the required parameters (ρ_L, ρ_T, and T_L) are determined by linear interpolation between the two nearest compositions for which data is available. These interpolated parameters are then used in Equation (9.7). This approach is valid only for compositions that fall between the available data points and within their valid temperature ranges.

Table 9.2: Supported systems, compositions and parameters for the binary density model

System	Composition	Temp. Range (K)	ρ_L (kg/m^3)	ρ_T (kg/m$^3\cdot$ K)	T_{liquidus} (K)
Ag-Al	Ag0.10Al0.90	893 – 1193	2830.0	0.21	893
	Ag0.20Al0.80	864 – 1164	3830.0	0.42	864
	Ag0.40Al0.60	840 – 1140	5380.0	0.48	840
	Ag0.60Al0.40	979 – 1279	6810.0	1.05	979
	Ag0.79Al0.21	1049 – 1349	8070.0	0.68	1049
Ag-Au	Ag0.75Au0.25	1276 – 1576	11200.0	0.7	1276
	Ag0.50Au0.50	1306 – 1606	13300.0	0.6	1306
	Ag0.25Au0.75	1326 – 1626	15600.0	1.2	1326
Ag-Cu	Ag0.80Cu0.20	1135 – 1435	9000.0	0.6	1135
	Ag0.60Cu0.40	1053 – 1353	8900.0	0.7	1053
	Ag0.40Cu0.60	1132 – 1432	8600.0	0.6	1132
	Ag0.20Cu0.80	1225 – 1525	8400.0	1.2	1225
Al-Au	Al1.0Au0.0	934 – 1234	2291.0	0.251	934
	Al0.85Au0.15	835 – 1135	4425.0	0.327	835
	Al0.80Au0.20	847 – 1147	5275.0	0.59	847
	Al0.67Au0.33	895 – 1195	7231.0	0.685	895
	Al0.55Au0.45	1144 – 1444	9163.0	0.63	1144
	Al0.50Au0.50	1252 – 1552	10050.0	1.06	1252
	Al0.33Au0.67	1333 – 1633	12842.0	1.0	1333
	Al0.27Au0.73	1280 – 1580	13840.0	1.01	1280
	Al0.20Au0.80	1237 – 1537	15020.0	1.08	1237
	Al0.0Au1.0	1338 – 1638	17192.0	1.11	1338
Al-Cu	Al1.0Cu0.0	933 – 1233	2360.0	0.33	933
	Al0.80Cu0.20	835 – 1135	3320.0	0.53	835
	Al0.70Cu0.30	865 – 1165	3760.0	0.49	865
	Al0.60Cu0.40	900 – 1200	4440.0	0.54	900
	Al0.50Cu0.50	1087 – 1387	5050.0	0.61	1087
	Al0.40Cu0.60	1233 – 1533	5490.0	0.69	1233
	Al0.30Cu0.70	1314 – 1614	6170.0	0.85	1314
	Al0.20Cu0.80	1315 – 1615	6660.0	0.77	1315
	Al0.0Cu1.0	1358 – 1658	7920.0	0.76	1358
Al-Fe	Al0.90Fe0.10	1289 – 1589	950.0	0.48	1289
	Al0.80Fe0.20	1430 – 1730	1080.0	0.58	1430
	Al0.75Fe0.25	1433 – 1733	1080.0	0.37	1433
	Al0.71Fe0.29	1452 – 1752	1120.0	0.71	1452
	Al0.67Fe0.33	1457 – 1757	1160.0	0.44	1457
	Al0.60Fe0.40	1505 – 1805	1220.0	0.14	1505
Al-Ni	Al0.82Ni0.18	1221 – 1521	3310.0	0.48	1221
	Al0.75Ni0.25	1377 – 1677	3550.0	0.76	1377
	Al0.70Ni0.30	1565 – 1865	3800.0	0.94	1565
	Al0.60Ni0.40	1835 – 2135	4490.0	1.29	1835
	Al0.50Ni0.50	1913 – 2213	4460.0	1.92	1913
	Al0.25Ni0.75	1670 – 1970	6420.0	0.8	1670
Al-Si	Al0.8847Si0.1153	850 – 1700	2398.0	0.24	850
Al-Ti	Al0.90Ti0.10	843 – 1343	2500.0	0.306	843
	Al0.80Ti0.20	835 – 1335	2760.0	0.353	835
	Al0.70Ti0.30	1063 – 1563	3040.0	0.33	1063
	Al0.60Ti0.40	1410 – 1910	3300.0	0.401	1410
	Al0.50Ti0.50	1643 – 2143	3580.0	0.45	1643
	Al0.40Ti0.60	1750 – 2250	3740.0	0.42	1750
	Al0.30Ti0.70	1808 – 2308	3900.0	0.377	1808
	Al0.20Ti0.80	1883 – 2383	4000.0	0.368	1883
	Al0.10Ti0.90	1910 – 2410	4090.0	0.33	1910
Co-Cu	Co1.0Cu0.0	1768 – 2068	7810.0	0.885	1768
	Co0.85Cu0.15	1713 – 2013	7740.0	1.16	1713
	Co0.75Cu0.25	1687 – 1987	7750.0	0.94	1687

Table 9.2 continued from previous page

System	Composition	Temp. Range (K)	ρ_L (kg/m^3)	ρ_T (kg/m^3· K)	T_{liquidus} (K)
	Co0.50Cu0.50	1652 – 1952	7660.0	0.72	1652
	Co0.25Cu0.75	1628 – 1928	7690.0	0.72	1628
Co-Fe	Co1.0Fe0.0	1768 – 2068	7810.0	0.885	1768
	Co0.75Fe0.25	1752 – 2052	7580.0	0.954	1752
	Co0.50Fe0.50	1752 – 2052	7430.0	0.748	1752
	Co0.25Fe0.75	1767 – 2067	7210.0	0.332	1767
	Co0.0Fe1.0	1811 – 2111	7040.0	1.08	1811
Cr-Fe	Cr0.10Fe0.90	1805 – 2105	6980.0	0.54	1805
	Cr0.20Fe0.80	1800 – 2100	6900.0	0.862	1800
	Cr0.40Fe0.60	1798 – 2098	7911.0	0.792	1798
Cr-Ni	Cr0.10Ni0.90	1710 – 2010	7690.0	0.79	1710
	Cr0.20Ni0.80	1700 – 2000	7410.0	0.792	1700
	Cr0.40Ni0.60	1648 – 1948	8111.0	0.608	1648
	Cr0.0Ni1.0	1728 – 2028	7820.0	0.856	1728
Cu-Au	Cu1.0Au0.0	1357 – 1673	7900.0	0.77	1357
	Cu0.75Au0.25	1243 – 1673	11390.0	1.95	1243
	Cu0.50Au0.50	1193 – 1673	13500.0	1.26	1193
	Cu0.25Au0.75	1215 – 1673	15670.0	1.76	1215
	Cu0.0Au1.0	1337 – 1673	17390.0	1.1	1337
Cu-Fe	Cu0.0Fe1.0	1811 – 2111	7040.0	1.08	1811
	Cu0.70Fe0.30	1693 – 1993	7370.0	0.79	1693
	Cu0.80Fe0.20	1673 – 1973	7480.0	0.813	1673
	Cu0.90Fe0.10	1578 – 1878	7670.0	0.857	1578
	Cu1.0Fe0.0	1357 – 1657	7900.0	0.765	1357
Cu-Ni	Cu1.0Ni0.0	1357 – 1657	7900.0	0.765	1357
	Cu0.90Ni0.10	1409 – 1709	7970.0	0.795	1409
	Cu0.80Ni0.20	1473 – 1773	8090.0	0.957	1473
	Cu0.60Ni0.40	1553 – 1853	8130.0	1.03	1553
	Cu0.50Ni0.50	1593 – 1893	8100.0	0.772	1593
	Cu0.30Ni0.70	1653 – 1953	8060.0	0.911	1653
	Cu0.10Ni0.90	1706 – 2006	7960.0	0.926	1706
	Cu0.0Ni1.0	1727 – 2027	7920.0	1.01	1727
Cu-Si	Cu0.95Si0.05	1311 – 1611	7790.0	0.701	1311
	Cu0.90Si0.10	1246 – 1546	7590.0	0.631	1246
	Cu0.851Si0.149	1159 – 1459	7470.0	0.673	1159
	Cu0.84Si0.16	1125 – 1425	7380.0	0.673	1125
	Cu0.854Si0.166	1118 – 1418	7400.0	0.704	1118
	Cu0.80Si0.20	1094 – 1394	7210.0	0.695	1094
	Cu0.775Si0.225	1131 – 1431	7090.0	0.681	1131
	Cu0.76Si0.24	1132 – 1432	6800.0	0.573	1132
	Cu0.75Si0.25	1131 – 1431	6830.0	0.627	1131
	Cu0.725Si0.275	1114 – 1414	6700.0	0.514	1114
	Cu0.70Si0.30	1075 – 1375	6510.0	0.592	1075
	Cu0.65Si0.35	1164 – 1464	6070.0	0.55	1164
	Cu0.60Si0.40	1235 – 1535	5740.0	0.567	1235
	Cu0.50Si0.50	1363 – 1663	5260.0	0.54	1363
Cu-Ti	Cu1.0Ti0.0	1358 – 1758	7900.0	0.76	1358
	Cu0.9Ti0.1	1380 – 1850	7300.0	0.32	1293
	Cu0.8Ti0.2	1320 – 1850	6900.0	0.87	1204
	Cu0.7Ti0.3	1260 – 1633	6300.0	0.58	1190
	Cu0.6Ti0.4	1360 – 1576	6100.0	1.23	1238
	Cu0.5Ti0.5	1260 – 1510	5300.0	0.55	1254
	Cu0.4Ti0.6	1327 – 1516	5000.0	0.62	1253
	Cu0.3Ti0.7	1326 – 1492	4600.0	0.13	1415
	Cu0.2Ti0.8	1545 – 1766	4600.0	0.1	1641
	Cu0.1Ti0.9	1659 – 1805	4300.0	0.46	1807
	Cu0.0Ti1.0	1858 – 1982	4100.0	0.33	1941
Fe-Cr	Fe1.0Cr0.0	1808 – 2108	6990.0	0.555	1808
	Fe0.90Cr0.10	1748 – 2048	7090.0	0.604	1748
	Fe0.80Cr0.20	1710 – 2010	6890.0	0.939	1710
	Fe0.70Cr0.30	1723 – 2023	7882.0	0.627	1723
	Fe0.60Cr0.40	1635 – 1935	8064.0	0.747	1635
	Fe0.50Cr0.50	1640 – 1940	8011.0	0.634	1640
Fe-Ni	Fe1.0Ni0.0	1811 – 2111	7040.0	1.08	1811

Table 9.2 continued from previous page

System	Composition	Temp. Range (K)	ρ_L (kg/m^3)	ρ_T (kg/m$^3\cdot$ K)	T_{liquidus} (K)
	Fe0.80Ni0.20	1753 – 2053	7320.0	1.0	1753
	Fe0.60Ni0.40	1725 – 2025	7430.0	1.15	1725
	Fe0.50Ni0.50	1716 – 2016	7500.0	1.02	1716
	Fe0.40Ni0.60	1713 – 2013	7510.0	1.06	1713
	Fe0.20Ni0.80	1713 – 2013	7870.0	1.23	1713
	Fe0.0Ni1.0	1727 – 2027	7930.0	1.01	1727
Pb-Bi	Pb0.4375Bi0.5625	400 – 1200	10484.0	1.1	400
Pb-Sn	Pb0.261Sn0.739	400 – 1000	8148.0	0.81	400

Multi-Component Systems

The density of multi-component (specifically ternary) liquid alloys is estimated using the same linear temperature-dependent equation, Equation (9.7), as for unary and binary systems. The supported systems are listed in Table 9.3.

For compositions not explicitly listed, the required parameters (ρ_L, ρ_T, and T_L) are estimated via barycentric interpolation from known compositions within the ternary system. Barycentric interpolation is a method of estimating values between known data points by weighting the contributions of each point based on its distance to the target point. These parameters are then used in Equation (9.7) to calculate the density at a given temperature. To ensure accuracy, and prevent extrapolation errors, calculations must be performed within the composition and temperature ranges for which the parameters have been experimentally determined.

Table 9.3: Supported systems, compositions, and parameters for the multi-component density model.

System	Composition	Temp. Range (K)	ρ_L (kg/m^3)	ρ_T (kg/m$^3\cdot$ K)	T_{liquidus} (K)
Ag-Al-Cu	Ag0.10Al0.90Cu0.0	920 – 1220	2820.0	0.21	920
	Ag0.10Al0.80Cu0.10	890 – 1190	3480.0	0.54	890
	Ag0.10Al0.60Cu0.30	810 – 1110	4490.0	0.64	810
	Ag0.10Al0.50Cu0.40	840 – 1140	5480.0	0.98	840
	Ag0.10Al0.40Cu0.50	880 – 1180	6030.0	1.01	880
	Ag0.10Al0.20Cu0.70	1190 – 1490	6900.0	0.646	1190
	Ag0.10Al0.0Cu0.90	1310 – 1610	8120.0	1.05	1310
Al-Cu-Si	Al1.0Cu0.00Si0.00	933 – 1233	2420.0	0.3	933
	Al0.90Cu0.05Si0.05	870 – 1170	2690.0	0.48	870
	Al0.80Cu0.10Si0.10	837 – 1137	3070.0	0.55	837
	Al0.60Cu0.20Si0.20	1035 – 1335	3230.0	0.24	1035
	Al0.33Cu0.33Si0.33	1270 – 1570	3890.0	0.26	1270
	Al0.0Cu0.50Si0.50	1363 – 1663	5260.0	0.54	1363
	Al0.30Cu0.40Si0.30	1245 – 1545	4360.0	0.37	1245
	Al0.40Cu0.20Si0.40	1302 – 1602	3330.0	0.25	1302
Co-Cu-Fe	Co0.50Cu0.0Fe0.50	1752 – 2052	7430.0	0.748	1752
	Co0.40Cu0.20Fe0.40	1696 – 1996	7470.0	1.37	1696
	Co0.30Cu0.40Fe0.30	1675 – 1975	7480.0	1.03	1675
	Co0.20Cu0.60Fe0.20	1662 – 1962	7530.0	1.17	1662
	Co0.15Cu0.70Fe0.15	1656 – 1956	7570.0	1.15	1656
	Co0.10Cu0.80Fe0.10	1639 – 1939	7630.0	0.779	1639
	Co0.05Cu0.90Fe0.05	1558 – 1858	7710.0	0.499	1558
	Co0.0Cu1.0Fe0.0	1357 – 1657	7900.0	0.765	1357
	Co0.20Cu0.20Fe0.60	1711 – 2011	7260.0	0.839	1711
	Co0.20Cu0.40Fe0.40	1696 – 1996	7470.0	1.37	1696
	Co0.20Cu0.60Fe0.20	1693 – 1993	7610.0	1.05	1693
Co-Cu-Ni	Co0.80Cu0.0Ni0.20	1758 – 2058	8100.0	0.76	1758
	Co0.70Cu0.10Ni0.20	1721 – 2021	8250.0	1.17	1721
	Co0.50Cu0.30Ni0.20	1654 – 1954	8170.0	1.26	1654

Table 9.3 continued from previous page

System	Composition	Temp. Range (K)	ρ_L (kg/m^3)	ρ_T (kg/m^3· K)	T_{liquidus} (K)
	Co0.40Cu0.40Ni0.20	1621 – 1921	8220.0	0.81	1621
	Co0.30Cu0.50Ni0.20	1590 – 1890	8190.0	1.09	1590
	Co0.10Cu0.70Ni0.20	1508 – 1808	8210.0	0.8	1508
	Co0.0Cu0.80Ni0.20	1473 – 1773	8130.0	0.96	1473
	Co0.50Cu0.50Ni0.0	1650 – 1950	7660.0	0.72	1650
	Co0.35Cu0.35Ni0.30	1641 – 1941	8400.0	0.91	1641
	Co0.30Cu0.30Ni0.40	1642 – 1942	8220.0	1.67	1642
	Co0.20Cu0.20Ni0.60	1643 – 1943	8240.0	1.46	1643
	Co0.15Cu0.15Ni0.70	1685 – 1985	8130.0	0.87	1685
	Co0.10Cu0.10Ni0.80	1685 – 1985	8250.0	1.21	1685
	Co0.0Cu0.0Ni1.0	1728 – 2028	7930.0	1.01	1728
Cr-Fe-Ni	Cr0.10Fe0.18Ni0.72	1724 – 2024	7500.0	0.376	1724
	Cr0.10Fe0.36Ni0.54	1724 – 2024	7330.0	0.41	1724
	Cr0.10Fe0.54Ni0.36	1722 – 2022	7180.0	0.572	1722
	Cr0.10Fe0.63Ni0.27	1734 – 2034	7100.0	0.613	1734
	Cr0.10Fe0.72Ni0.18	1748 – 2048	7090.0	0.604	1748
	Cr0.20Fe0.16Ni0.64	1690 – 1990	7160.0	0.687	1690
	Cr0.20Fe0.32Ni0.48	1690 – 1990	7050.0	0.558	1690
	Cr0.20Fe0.48Ni0.32	1698 – 1998	6950.0	0.636	1698
	Cr0.20Fe0.56Ni0.24	1710 – 2010	6930.0	0.703	1710
	Cr0.20Fe0.64Ni0.16	1710 – 2010	6890.0	0.939	1710
	Cr0.40Fe0.12Ni0.48	1640 – 1940	8011.0	0.634	1640
Cu-Fe-Ni	Cu0.13Fe0.54Ni0.33	1692 – 1992	7110.0	0.28	1692
	Cu0.40Fe0.35Ni0.25	1610 – 1910	7140.0	0.79	1610
	Cu0.50Fe0.30Ni0.20	1591 – 1891	7200.0	0.36	1591
	Cu0.60Fe0.24Ni0.16	1580 – 1880	7530.0	1.96	1580
	Cu0.70Fe0.13Ni0.17	1546 – 1846	7760.0	1.16	1546
	Cu0.20Fe0.65Ni0.15	1701 – 2001	7160.0	1.43	1701
	Cu0.20Fe0.48Ni0.32	1669 – 1969	7400.0	1.7	1669
	Cu0.20Fe0.35Ni0.45	1663 – 1963	7420.0	1.04	1663
	Cu0.20Fe0.20Ni0.60	1668 – 1968	7560.0	0.83	1668
	Cu0.20Fe0.10Ni0.70	1673 – 1973	7790.0	0.86	1673

9.1.4 Model Validation

Due to time constraints and the extensive amount of data available for unary, binary, and multi-component liquid alloy systems, only a selection of the validation plots are presented. Additional validation plots will be made available in future releases of the manual as more systems with their respective parameters are validated against experimental data. **Therefore, users are cautioned that not all the model estimates may be accurate, especially those not explicitly validated here.**

Unary Systems

For the unary systems shown Figure 9.1, density estimates from auxi-mpp's EmpiricalUnary model are validated against recommended referenced data (Assael et al. 2006; Assael et al. 2010; Assael et al. 2012a; Assael et al. 2012b; Ntonti et al. 2024). Model estimates for each supported element show good agreement with the reference data over the recommended temperature ranges.

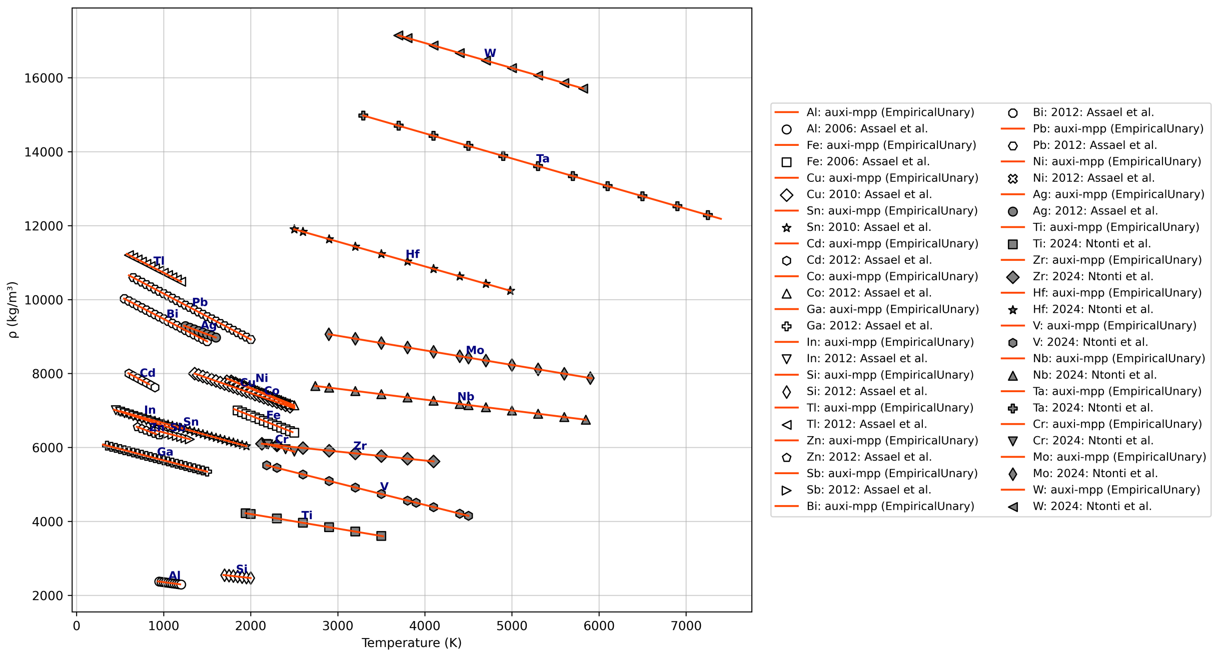

Figure 9.1: EmpiricalUnary model estimates versus recommended values for all supported liquid metals.

Binary Systems

For the binary systems, only the Fe – Ni system has been validated against experimental data, as shown in Figure 9.2. The model estimates from auxi-mpp's EmpiricalBinary model are plotted over the recommended temperature range where the alloy is fully liquid and show good agreement with the experimental data (Brillo and Egry 2004). It is evident in Figure 9.2 that some of the model estimate lines do not extend over the entire range of available experimental data. This is because some of these experimental data points are below the liquidus temperature and, therefore, fall outside the model's valid temperature range, making them invalid for comparison.

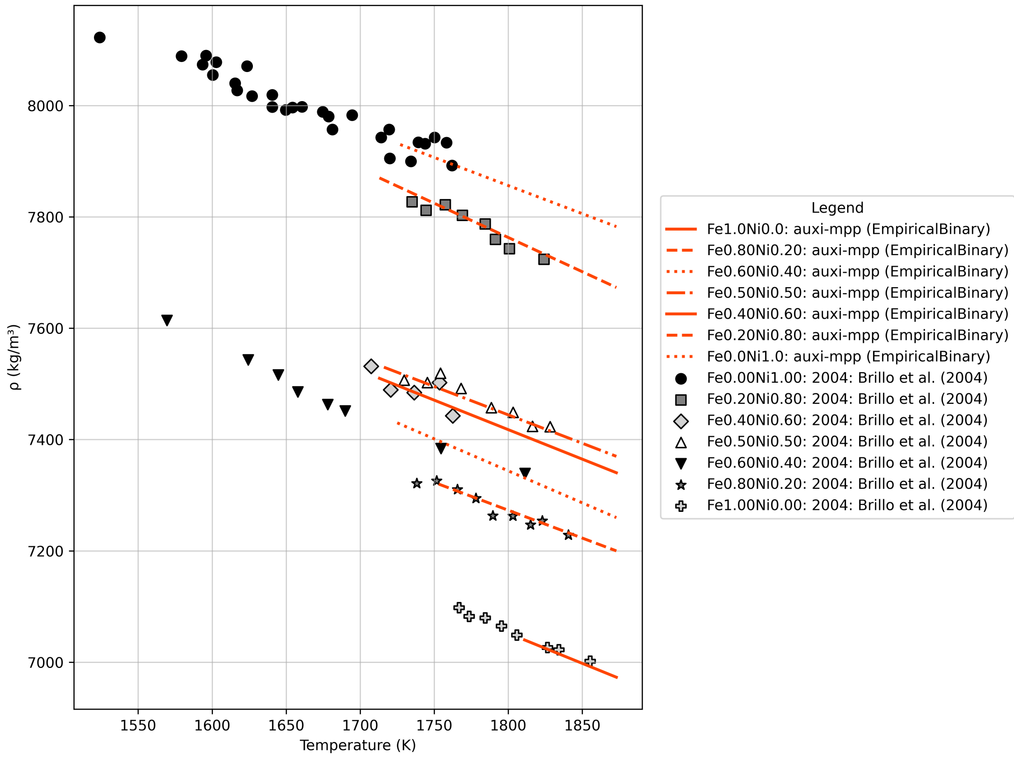

Figure 9.2: EmpiricalBinary model estimates for Fe – Ni at various compositions compared to experimental data (Brillo and Egry 2004).

Multi-Component Systems

Lastly, for the multi-component systems, only the Cu – Fe – Ni system has been validated against experimental data, as shown in Figure 9.3. Again, the model estimates from auxi-mpp's EmpiricalMultitiComponent model are plotted only over the recommended temperature range where the alloy is fully liquid and shows good agreement with the experimental data (Brillo et al. 2006).

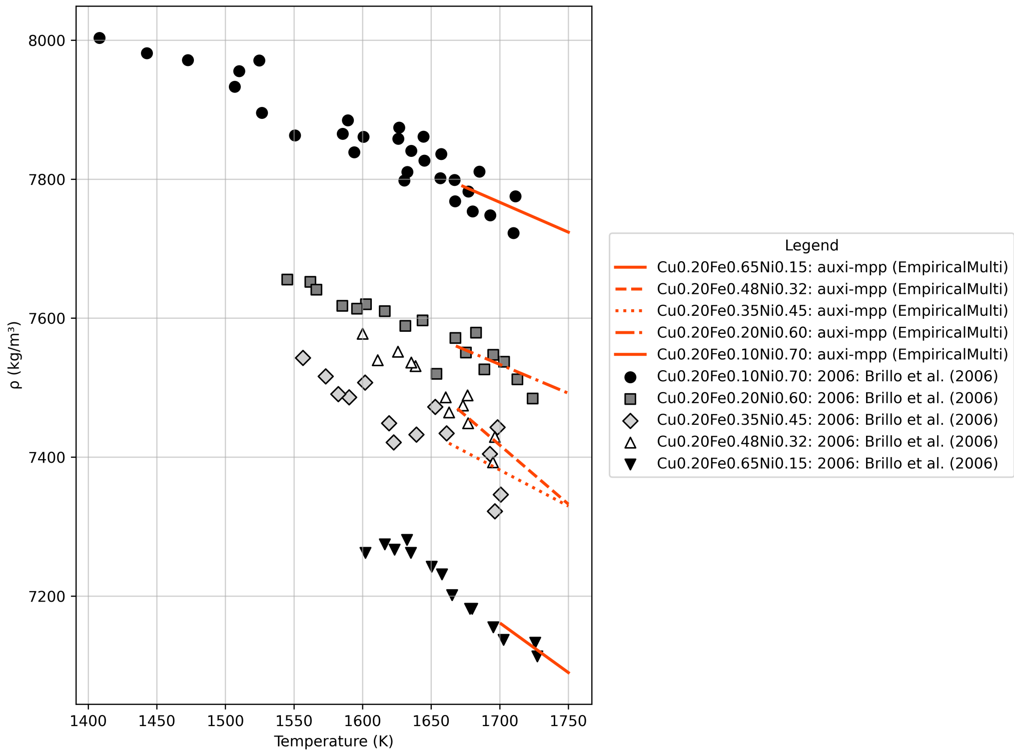

Figure 9.3: EmpiricalMulti model estimates for the Cu – Fe – Ni system at various compositions compared to experimental data (Brillo et al. 2006).

9.1.5 Issues

There are no known issues.

9.2 Binary Metallic Alloys with Non-Metallics

Simple empirical models have been implemented in auxi-mpp to help estimate the density of binary alloys containing non-metallic elements such as C and S.

9.2.1 Introduction

Empirical models for estimating the density for system of Fe – C, Fe – S, Cu – S and Ni – S have been found in literature (Tesfaye and Taskinen 2010). These models serve as a first approximation for estimating the density of binary alloys containing non-metallic elements.

9.2.2 Formulation

Fe-S System (Nagamori, 1968)

The density of a liquid Fe-S alloy system is estimated using an empirical model developed by Nagamori, which is based on experimental data at high temperatures. This model describes the properties as a function of sulfur content (Tesfaye and Taskinen 2010).

The density, ρ, of Fe-S melts at 1200°C is given by a quadratic function of the weight percent of sulfur (C_S) as shown in Equation (9.8):

$$\rho(C_S) = 6.957 - 7.523 \times 10^{-2} C_S - 2.997 \times 10^{-4} C_S^2 \tag{9.8}$$

The density composition range for which the model is valid is: 28-37 wt% S.

Ni-S System (Nagamori, 1969)

The density of Ni-S melts is calculated based on the density at a reference temperature of 1200 °C and a linear temperature correction as shown in Equation (9.9) (Tesfaye and Taskinen 2010).

$$\rho(T, C_S) = \rho_{1200} + \frac{d\rho}{dT}(T_C - 1200) \tag{9.9}$$

Here, ρ_{1200} is the density at 1200 °C and $\frac{d\rho}{dT}$ is the temperature coefficient. As shown in Equations (9.10) and (9.11), both are dependent on the weight percent of sulfur, C_S.

$$\rho_{1200} = c_0 - c_1 C_S - c_2 C_S^2 \tag{9.10}$$

$$\frac{d\rho}{dT} = d_0 + d_1 C_S \tag{9.11}$$

The resulting density is in g/cm^3 and is converted to kg/m^3 by multiplying by 1000.

Table 9.4: Parameters for the Ni-S Density Model

Parameter	**Value**	**Unit**
c_0	7.24	g/cm^3
c_1	2.254e-2	g/(cm^3 · wt%)
c_2	1.795e-3	g/(cm^3 · wt%^{2})
d_0	-2.4e-3	g/(cm^3·°C)
d_1	8.0e-5	g/(cm^3·°C · wt%)

The model is valid within the following ranges temperature range of 1000-1200 °C and a composition of 18-30 wt% S.

Cu-S System (Nagamori, 1969)

The density of molten Cu-S at a fixed temperature of 1200 °C (1473.15 K) is estimated using Equation (9.12). The model describes density as a linear function of the sulfur weight percent, C_S (Tesfaye and Taskinen 2010).

$$\rho(C_S) = c_0 - c_1 C_S \tag{9.12}$$

The resulting density is in g/cm^3 and is converted to kg/m^3 by multiplying by 1000.

The model is valid only within the composition range of 19.6-20.6 wt% S.

Table 9.5: Parameters for the Cu-S Density Model

Parameter	Value	Unit
c_0	7.9	g/cm^3
c_1	1.348e-1	g/(cm$^3 \cdot$ wt%)

Fe-C System (Jimbo and Cramb, 1993)

The density of liquid Fe-C alloys is modelled as a function of temperature and the weight percent of carbon, as shown in Equation (9.13), where T_K is the temperature in Kelvin and C_C is the weight percent of carbon (Jimbo and Cramb 1993).

$$\rho(T, C_C) = (a_0 - a_1 C_C) - (b_0 - b_1 C_C) \times 10^{-4}(T_K - 1823) \tag{9.13}$$

The resulting density is in g/cm^3 and is converted to kg/m^3 by multiplying by 1000.

Table 9.6: Parameters for the Fe-C Density Model

Parameter	Value	Unit
a_0	7.10	g/cm^3
a_1	0.0732	g/(cm$^3 \cdot$ wt%)
b_0	8.28	g·K/(cm^3)
b_1	0.874	g·K/(cm$^3 \cdot$ wt%)

The model is valid within the temperature range of 1550-1900 °C and a composition range of 0-4 wt% C.

9.2.3 Model Validation

Due to time constraints, model validation for binary alloys with non-metallics was limited to the Fe-S and Fe-C systems. Estimates from the EmpiricalBinaryWithNonMetallics model in auxi-mpp, which incorporates the Fe-S and Fe-C submodels, show good agreement with experimental data (Tesfaye and Taskinen 2010; Jimbo and Cramb 1993). Validation for the Cu-S and Ni-S systems is planned for a future release.

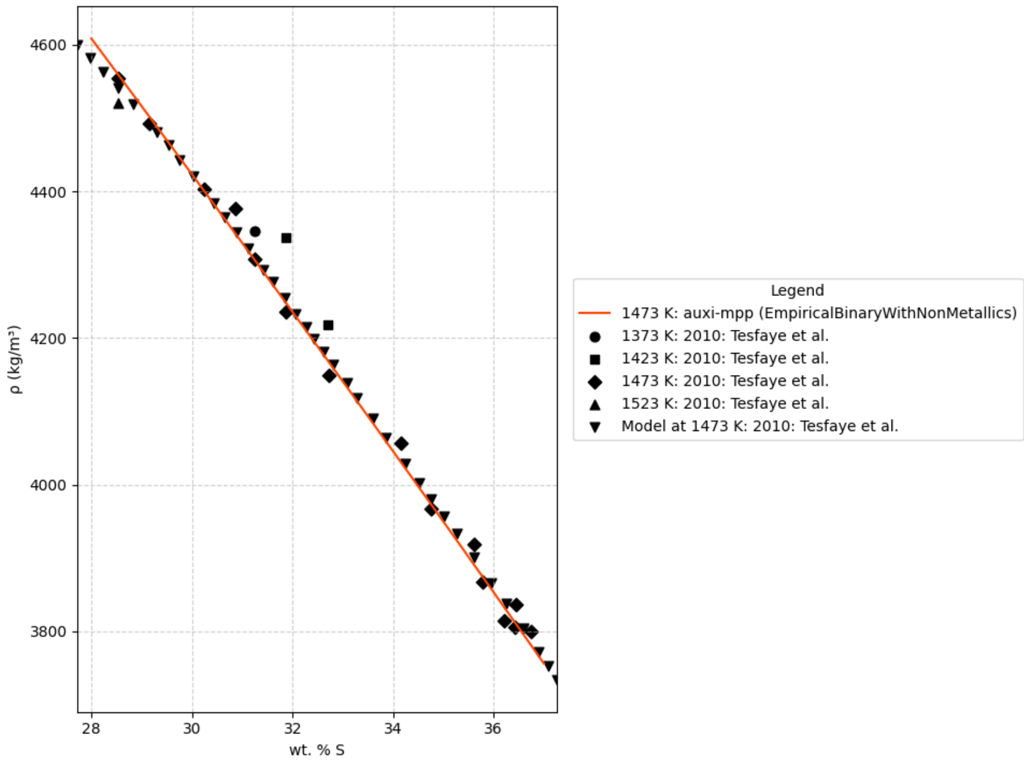

(a) Binary Fe – S system (Tesfaye and Taskinen 2010).

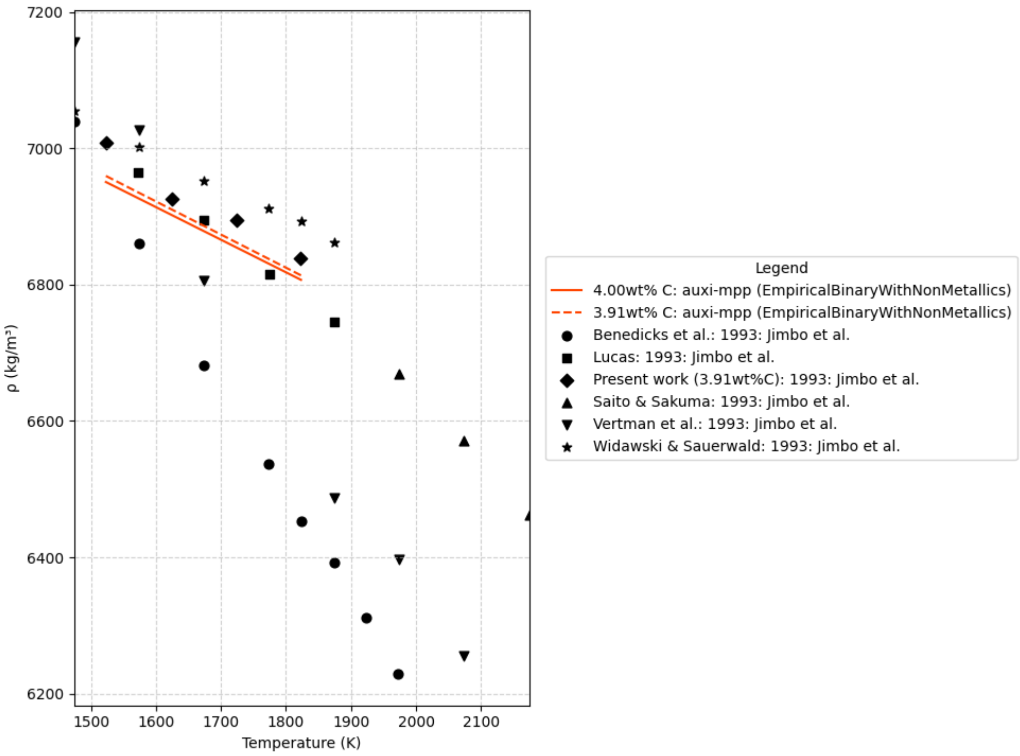

(b) Binary Fe – C system (Jimbo and Cramb 1993).

Figure 9.4: EmpiricalBinaryWithNonMetallics model estimates for binary alloys with non-metallic elements versus experimental data.

9.2.4 Issues

There are no known issues.

9.3 Density for Multi-Component Commercial Alloys

Liquid alloy density models for estimating the density of various commercial liquid alloys have been implemented in auxi-mpp.

9.3.1 Introduction

The work of Mills (2002) contains various commercial alloys of Al, Co, Cu, Fe, Mg, Ni, Si, Ti, and Zn with associated material property data and estimates. These alloys consist of unique multi-component compositions that include both metallic and non-metallic elements. As first an implementation into auxi-mpp, the liquid alloy density models for Fe based commercial alloys have been implemented.

9.3.2 Formulation

The density, ρ, of a commercial alloy is calculated as a function of temperature in Celsius (T_C). For some alloys, the density is also dependent on the weight percent of silicon (wt% Si). The general form of the equation is given by Equation (9.14).

$$\rho(T) = A - B(T_C - T_{\text{ref,C}}) - C_{\text{Si}}(\text{wt\% Si}) \tag{9.14}$$

where:

1. $\rho(T)$ is the density of the alloy in kg/m^3.
2. T_C is the temperature in degrees Celsius (°C).
3. A is an empirical density parameter in kg/m^3.
4. B is the empirical temperature coefficient of density in kg/m$^3 \cdot^\circ$ C.
5. $T_{\text{ref,C}}$ is a reference temperature in degrees Celsius (°C).
6. C_{Si} is the coefficient for the silicon content adjustment, in kg/m$^3 \cdot$ wt%. This term is only applicable for certain alloys, such as cast irons.
7. wt% Si is the weight percent of silicon in the alloy.

The model calculates the density for a specific set of supported commercial alloys based on fixed compositions and parameters. Table 9.7 details the supported alloys, their compositions, valid temperature ranges, and the specific parameters used in Equation (9.14).

Table 9.7: Supported Commercial Alloys and Model Parameters

Alloy Name	Parameter	Value	Unit
Grey Cast Iron	Temp. Range	1463 – 1773	K
	Composition	C: 3.72, Fe: 91.9, Si: 1.89, Cr: 0.95, Mn: 0.66, Mg: 0.002, Mo: 0.59, Ni: 0.19, P: 0.09, S: 0.03	wt%
	A	6829.0	kg/m^3
	B	0.50	kg/(m^3·°C)

Table 9.7 continued from previous page

Alloy Name	Parameter	Value	Unit
	$T_{\text{ref,C}}$	1550.0	°C
	C_{Si}	130.0	kg/(m³· wt%)
Ductile Iron	Temp. Range	1451 – 1773	K
	Composition	C: 3.61, Fe: 92.4, Si: 2.91, Mn: 0.65, Mg: 0.002, Ni: 0.13, P: 0.12, Cr: 0.08, S: 0.076	wt%
	A	6836.0	kg/m³
	B	0.513	kg/(m³·°C)
	$T_{\text{ref,C}}$	1550.0	°C
	C_{Si}	130.0	kg/(m³· wt%)
304 Stainless Steel	Temp. Range	1727 – 1873	K
	Composition	C: 0.08, Cr: 19.0, Fe: 69, Ni: 9.5, Mn: 2.0, Cu: 0.3	wt%
	A	6900.0	kg/m³
	B	0.80	kg/(m³·°C)
	$T_{\text{ref,C}}$	1454.0	°C
316 Stainless Steel	Temp. Range	1723 – 1873	K
	Composition	C: 0.08, Cr: 17.0, Fe: 65, Ni: 12.0, Mn: 2.0, Mo: 2.5, Si: 1.0, Cu: 0.3	wt%
	A	6881.0	kg/m³
	B	0.77	kg/(m³·°C)
	$T_{\text{ref,C}}$	1450.0	°C

9.3.3 Model Validation

Due to time constraints, this initial validation is limited to the liquid density of stainless steel 304. The model estimates from MillsCommericalhows good agreement with the experimental data, as shown in Figure 9.5 (Mills 2002). The other commercial alloys listed in Table 9.7 will be validated in future releases of the manual.

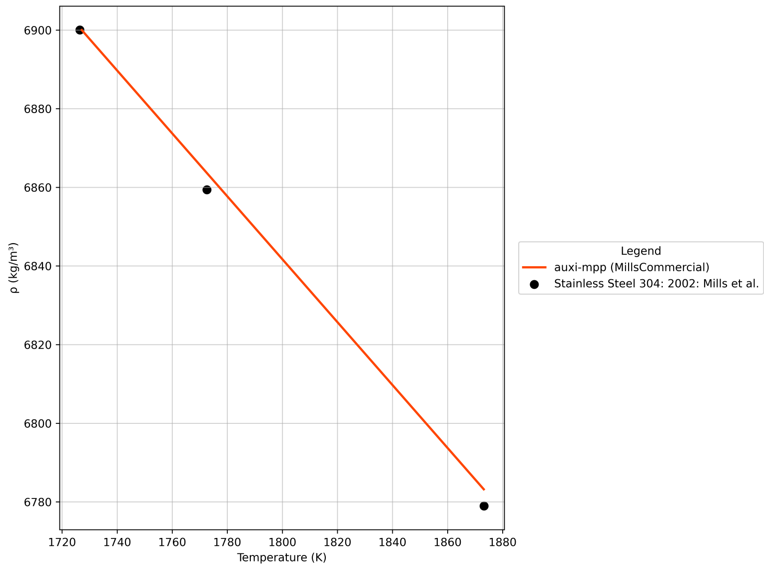

Figure 9.5: MillsCommerical model estimates over recommended temperature range for stainless steel 304 compared to experimental data points (Mills 2002).

9.3.4 Issues

There are no known issues.

9.3.5 Molar Volume

Once the density is known, the molar volume can be calculated. The molar volume can be calculated from density with Equation (9.15).

$$\bar{V}_{\text{alloy}} = \frac{\sum_i \bar{m}_{\text{i}} x_{\text{i}}}{\rho_{\text{alloy}}} \tag{9.15}$$

If the density model proofs to be accurate, accurate molar volume values can be calculated from it.

Chapter 10

Electrical Conductivity

Charge in liquids is transported in two ways – the movement of electrons and that of ions. The dominant mechanism for electrical conductivity in liquid alloys is the movement of electrons. While the ions in liquid metals are mobile and do diffuse, their contribution to electrical current is completely overshadowed by the flow of electrons.

The reason for this is the staggering difference in mass. An ion consists of a nucleus (protons and neutrons) and core electrons, making it thousands of times more massive than a single free electron. Under the influence of an electric field, electrons will accelerate orders of magnitudes faster than ions, establishing a current long before the ions have had a chance to diffuse in any meaningful way. Any model, attempting to estimate the electrical conductivity of liquid alloys from fundamental principles, will therefore have to describe the movement of electrons.

The Kubo-Greenwood formalism stands out as the most successful at this, deriving conductivity from fundamental quantum mechanics without empirical inputs. However, its reliance on computationally intensive ab initio molecular dynamics (MD) and density functional theory (DFT) calculations makes it prohibitively expensive for routine use. It is best employed as a computational experiment to generate high-fidelity benchmark data for validating more practical models.

As the more popular alternative, Ziman theory is a semi-empirical model that still offers valuable physical insights by linking resistivity to atomic structure and electron scattering. While effective for simple metals, it critically fails for alloys containing transition metals like iron, whose strong electron scattering violates the theory's core assumptions, leading to significant errors. Proposed enhancements involve using structural data from large-scale MD simulations and employing advanced scattering potentials (t-matrix formalism) for such elements. Finally, it should also be noted that Ziman theory is formally documented only up to binary alloys.

Besides these two techniques of estimating electrical conductivity, there are no physically rigorous ones available in literature.

10.1 Electrical Conductivity Polynomial Fit

Polynomial fits to measured liquid alloy electrical resistivity data.

10.1.1 Introduction

Due to the lack of readily available models to estimate electrical conductivity for liquid metals, polynomials were fitted to experimental measurements instead. The technicalities of the polynomials available in auxi-mpp are documented here.

10.1.2 Overview

Polynomials have been fitted to electrical resistivity measurements of liquid Fe, Fe – C, Fe – Si, Fe – Mn, Fe – Ni and Fe – C – Si. Electrical resistivity data was used instead of conductivity data for two reasons. Firstly, in literature almost exclusively resistivity measurement data are found and therefore there are no actual conductivity data available. This is likely because of the conductivity being very high for liquid alloys, and therefore difficult to measure accurately. Secondly, the fits have a slightly better R^2 value for resistivity data as these tend to scale linearly with temperature.

Before using these polynomial fits, the user is encouraged to first evaluate the range of data used to fit them before using. For this, see Section 10.1.4. This is because these are polynomial fits and are therefore not based on any physical principle. Their extrapolation accuracy should thus be assumed to be low, and it is recommended to use them within the range of the experimental measurements.

The alloy systems chosen are aimed at representing pig iron which roughly has a composition of 92% Fe, 4% C, 2% Si, 1% Mn, 0.3% P and 0.1% S. Unfortunately, no measurement data could be obtained for Fe – S and Fe – P liquid alloys.

The reason Fe – Ni was included, is that it is the only binary system for which thermal conductivity data was also found. We could therefore use this system to test first-hand how well the Wiedemann-Franz law can estimate the thermal conductivity from electrical conductivity values. See Chapter 12 for the comparison.

Finally, it should be noted that occasionally, conductivity and resistivity is used interchangably. If the performance of auxi-mpp is shown as resistivity, it simply means that the reciprocal of the output from auxi-mpp was taken.

10.1.3 Formulation

For pure Fe, a first and second degree polynomial was fitted, for the binaries a first, second and third degree and for Fe – C – Si a second, third and fourth degree polynomial was fitted. The polynomials were set up to take temperature and composition as inputs, assuming Fe will always be present in the binary and ternary systems. Below, the fitted polynomials are presented for each system. To see the R^2 values, see Section 10.1.4.

Unary Fe System

Equations (10.1) and (10.2) presents the first and second degree polynomial fitted to pure Fe resistivity measurements.

$$\rho_{\text{first}} = 93.6919 + 0.0240T \tag{10.1}$$

$$\rho_{\text{second}} = 72.2778 + 0.0410T - 3.1276 \times 10^{-6}T^2 \tag{10.2}$$

Unary Ni System

Equations (10.3) and (10.4) presents the first and second degree polynomial fitted to pure Ni resistivity measurements.

$$\rho_{\text{first}} = 59.36181 + 0.01575T \tag{10.3}$$

$$\rho_{\text{second}} = 63.73571 + 0.01203T + 7.3751 \times 10^{-7}T^2 \tag{10.4}$$

Unary Si System

Equations (10.5) and (10.6) presents the first and second degree polynomial fitted to pure Si resistivity measurements.

$$\rho_{\text{first}} = 72.92953 - 0.00069T \tag{10.5}$$

$$\rho_{\text{second}} = 146.44446 - 0.08317T + 2.3098 \times 10^{-5}T^2 \tag{10.6}$$

Binary Fe – C System

Equations (10.7) to (10.9) presents the first, second and third degree polynomial fitted to the Fe – C resistivity measurements. Assuming that Fe makes up the rest of the composition, only the mole fraction of the second component should be provided.

$$\rho_{\text{first}} = 92.9871 + 0.0243T + 112.5398x_{\text{C}} \tag{10.7}$$

$$\rho_{\text{second}} = 75.3933 + 0.0387T + 8.2111x_{\text{C}} - 2.7378 \times 10^{-6}T^2 + 0.0435Tx_{\text{C}} + 264.2014x_{\text{C}}^2 \tag{10.8}$$

$$\begin{aligned}\rho_{\text{third}} = {} & 133.9585 - 0.0295T + 297.2871x_{\text{C}} + 2.2889 \times 10^{-5}T^2 - 0.3647Tx_{\text{C}} \\ & + 92.7134x_{\text{C}}^2 - 3.0932 \times 10^{-5}T^3 + 0.0001T^2x_{\text{C}} + 0.1280Tx_{\text{C}}^2 + 31.8100x_{\text{C}}^3\end{aligned} \tag{10.9}$$

Binary Fe – Si System

Equations (10.10) to (10.12) presents the first, second and third degree polynomial fitted to the Fe – Si resistivity measurements.

$$\rho_{\text{first}} = 145.16895 + 0.00355T - 52.44309x_{\text{Si}} \tag{10.10}$$

$$\begin{aligned}\rho_{\text{second}} = {} & 1.07524 + 0.09575T + 419.23624x_{\text{Si}} \\ & - 1.2854 \times 10^{-5}T^2 - 0.13748Tx_{\text{Si}} - 231.77971x_{\text{Si}}^2\end{aligned} \tag{10.11}$$

$$\begin{aligned}\rho_{\text{third}} = {} & 201.38264 - 0.10332T + 864.82400x_{\text{Si}} \\ & + 4.8753 \times 10^{-5}T^2 - 1.16402Tx_{\text{Si}} + 653.88877x_{\text{Si}}^2 \\ & - 6.0184 \times 10^{-9}T^3 + 0.00040T^2x_{\text{Si}} - 0.28473Tx_{\text{Si}}^2 - 263.35838x_{\text{Si}}^3\end{aligned} \tag{10.12}$$

Binary Fe – Mn System

Equations (10.13) to (10.15) presents the first, second and third degree polynomial fitted to the Fe – Mn resistivity measurements.

$$\rho_{\text{first}} = 94.4813 + 0.0238T + 227.6563x_{\text{Mn}} \tag{10.13}$$

$$\rho_{\text{second}} = 74.6696 + 0.0393T + 177.9867x_{\text{Mn}} - 2.8329 \times 10^{-6}T^2 + 0.0667Tx_{\text{Mn}} - 660.5977x_{\text{Mn}}^2 \tag{10.14}$$

$$\begin{aligned}\rho_{\text{third}} &= 133.3610 - 0.0289T + 0.0002x_{\text{Mn}} + 2.2645 \times 10^{-5}T^2 + 0.1703Tx_{\text{Mn}} \\ &- 0.0002x_{\text{Mn}}^2 - 3.0650 \times 10^{-9}T^3 - 6.5907 \times 10^{-6}T^2x_{\text{Mn}} - 0.3341Tx_{\text{Mn}}^2 - 3.3852 \times 10^{-5}x_{\text{Mn}}^3\end{aligned} \tag{10.15}$$

Binary Fe – Ni System

Equations (10.16) to (10.18) presents the first, second and third degree polynomial fitted to the Fe – Ni resistivity measurements.

$$\rho_{\text{first}} = 132.32556 + 0.00816T - 41.28897x_{\text{Ni}} \tag{10.16}$$

$$\begin{aligned}\rho_{\text{second}} &= 93.20065 + 0.02342T + 116.51028x_{\text{Ni}} \\ &+ 2.3049 \times 10^{-7}T^2 - 0.01233Tx_{\text{Ni}} - 138.91424x_{\text{Ni}}^2\end{aligned} \tag{10.17}$$

$$\begin{aligned}\rho_{\text{third}} &= 142.95516 - 0.03978T - 189.69026x_{\text{Ni}} \\ &+ 2.6654 \times 10^{-5}T^2 + 0.05863Tx_{\text{Ni}} + 421.13095x_{\text{Ni}}^2 \\ &- 3.5400 \times 10^{-9}T^3 + 4.6242 \times 10^{-6}T^2x_{\text{Ni}} - 0.09280Tx_{\text{Ni}}^2 - 231.85544x_{\text{Ni}}^3\end{aligned} \tag{10.18}$$

Ternary Fe – C – Si System

Equations (10.19) and (10.20) presents the second and third degree polynomial fitted to the Fe – C – Si resistivity measurements. For this ternary system, a fourth degree polynomial have also been fitted, however due to its complexity, it is not shown here. The coefficients for its terms can be found in the source code of auxi-mpp, however.

$$\begin{aligned}\rho_{\text{second}} &= 13.12644 + 0.08669T + 315.76813x_{\text{C}} + 408.54928x_{\text{Si}} \\ &- 1.1268 \times 10^{-5}T^2 - 0.08207Tx_{\text{C}} - 0.13297Tx_{\text{Si}} - 158.67827x_{\text{C}}^2 \\ &- 745.16858x_{\text{C}}x_{\text{Si}} - 230.08561x_{\text{Si}}^2\end{aligned} \tag{10.19}$$

$$\begin{aligned}\rho_{\text{third}} = 251.74375 - 0.15978T - 3.09670x_{\text{C}} + 779.52392x_{\text{Si}} \\ + 6.9083 \times 10^{-5}T^2 - 0.18232Tx_{\text{C}} - 1.08060Tx_{\text{Si}} + 5.30280x_{\text{C}}^2 \\ - 7.68851x_{\text{C}}x_{\text{Si}} + 660.19505x_{\text{Si}}^2 - 8.3788 \times 10^{-9}T^3 + 0.00011T^2x_{\text{C}} \\ + 0.00038T^2x_{\text{Si}} + 0.25701Tx_{\text{C}}^2 + 0.36579Tx_{\text{C}}x_{\text{Si}} - 0.29099Tx_{\text{Si}}^2 \\ + 0.25065x_{\text{C}}^3 + 1.70881x_{\text{C}}^2x_{\text{Si}} - 5.66292x_{\text{C}}x_{\text{Si}}^2 - 258.92131x_{\text{Si}}^3 \end{aligned} \quad (10.20)$$

10.1.4 Model Validation

Table 10.1 summarises the temperature and composition ranges for which liquid alloy electrical resistivity data could be collected. These data points was used to fit the polynomials to. Note that when fitting a polynomial to the binary system data, the unary Fe data was included. Similarly, fitting a polynomial to the Fe – C – Si data, the relevant binary and unary data were also included to make the fit.

Table 10.1: Temperature and composition ranges for which liquid metal or alloy electrical resistivity data was captured.

System (c1-c2-c3)	T (K)	x_{c1} (mol mol^{-1})	x_{c2} (mol mol^{-1})	x_{c3} (mol mol^{-1})	# of data points
Fe	$1824 - 3950$	1.0	-	-	96
Ni	$1722 - 3704$	1.0	-	-	91
Si	$1685 - 1899$	1.0	-	-	31
Fe – C	$1448 - 1873$	$0.830 - 0.999$	$0.001 - 0.170$	-	53
Fe – Si	$1473 - 1849$	$0.197 - 0.911$	$0.089 - 0.803$	-	67
Fe – Mn	$1753 - 2053$	$0.867 - 0.961$	$0.039 - 0.133$	-	50
Fe – Ni	$1714 - 1908$	$0.000 - 0.988$	$0.012 - 1.000$	-	163
Fe – C – Si	$1497 - 1846$	$0.784 - 0.918$	$0.041 - 0.124$	$0.035 - 0.175$	41

Below the polynomials are validated by plotting them against the experimental data.

Unary Model Validation

In Figure 10.1, the performance of auxi-mpp is compared to measured data for pure iron. The data points were obtained from Ono et al. (1976), Zytveld (1980), and Hixson et al. (1990).

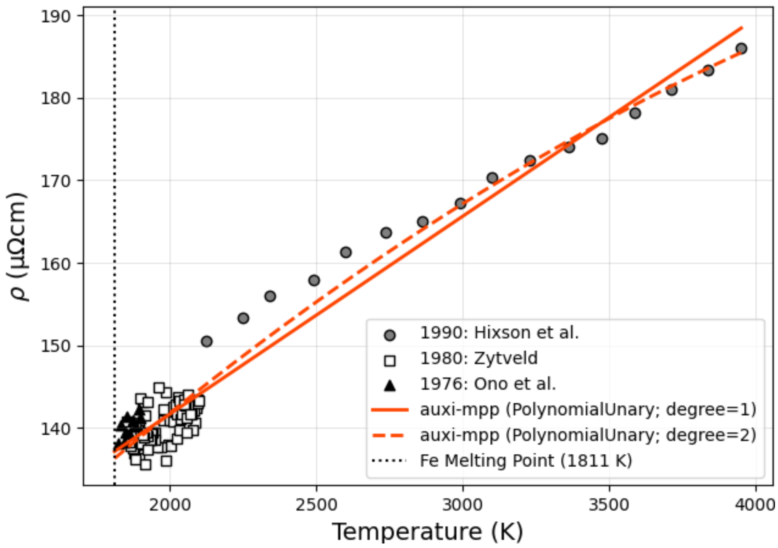

Figure 10.1: Validating auxi-mpp PolynomialUnary for pure Fe. Degree $= 1$ R^2 : 0.957. Degree $= 2$ R^2 : 0.960.

In Figure 10.2, the performance of auxi-mpp is compared to measured data for pure nickel. The data points were obtained from Kita et al. (1978), Seydel and Fucke (1977), Hixson et al. (1990), and Cagran et al. (2007). Surprisingly, the second degree fit has an R^2 of only 0.0005

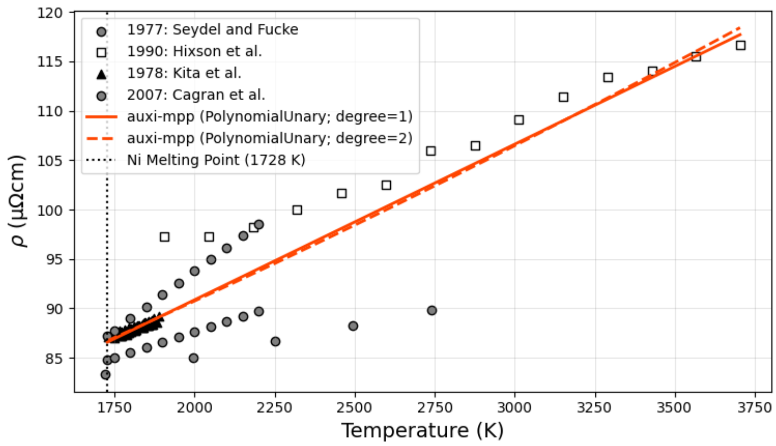

Figure 10.2: Validating auxi-mpp PolynomialUnary for pure Ni. Degree $= 1$ R^2 : 0.846. Degree $= 2$ R^2 : 0.846.

In Figure 10.3, the performance of auxi-mpp is compared to measured data for pure silicon. The data points were obtained from Sasaki et al. (1995).

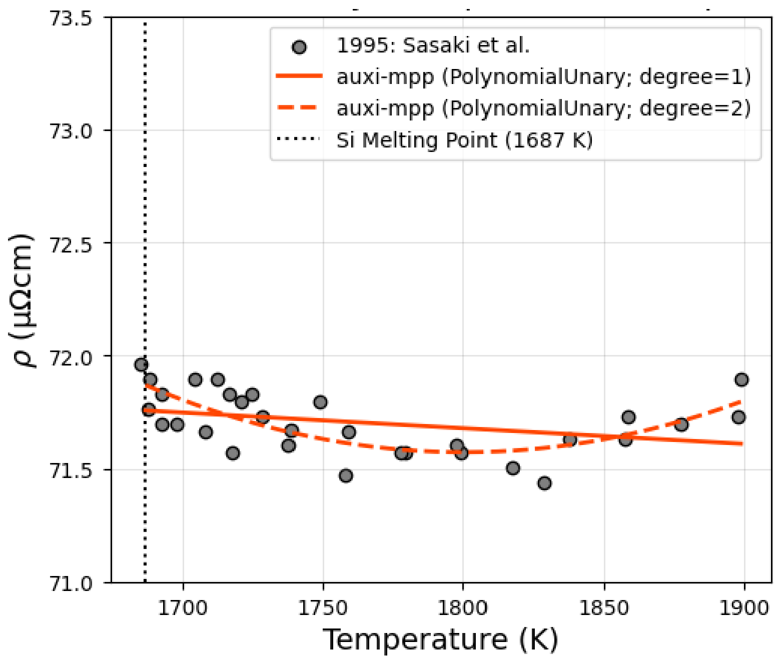

Figure 10.3: Validating auxi-mpp PolynomialUnary for pure Si. Degree $= 1$ R^2 : 0.117. Degree $= 2$ R^2 : 0.530.

For these we regard the second degree fit to be the best.

Binary Model Validation

In Figures 10.4, 10.5, 10.7 and 10.8, the performance of the first, second and third degree polynomials are presented with experimental data of the Fe – C, Fe – Si, Fe – Mn and Fe – Ni systems, respectively. In all cases, we regard the second degree fit to be the best, despite higher R^2 values for third degree fits. The apparent better fits to the data by third degree polynomials, brings about unnecessary complexities and extremities (see Figures 10.5c and 10.8c), rendering them not suitable for reliable interpolations. The first degree fits are also not suitable as the linear dependence of resistivity on temperature changes with composition.

The data points were obtained from Baum et al. (1971), Ono and Yagi (1972), Ono et al. (1976), Zytveld (1980), Kita and Morita (1984), Hixson et al. (1990), and Chikova et al. (2021).

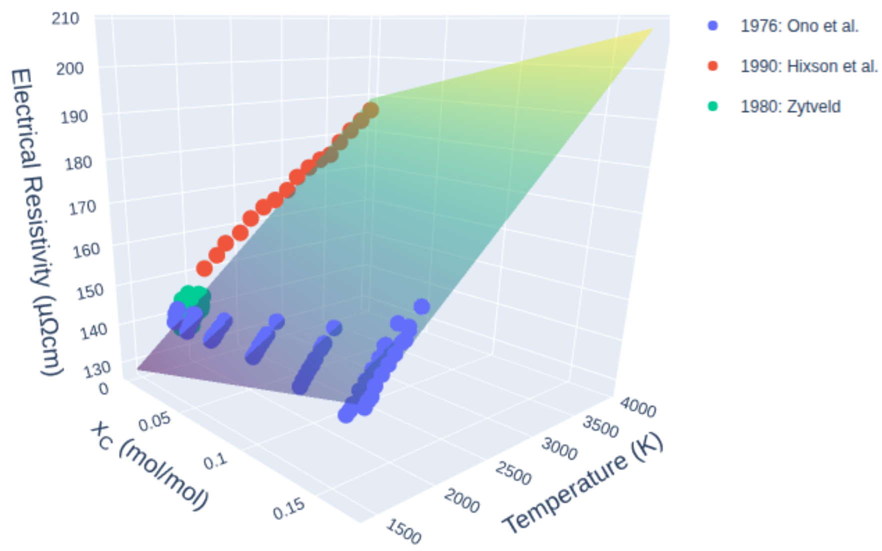

(a) Degree $= 1$. $R^2 = 0.950$

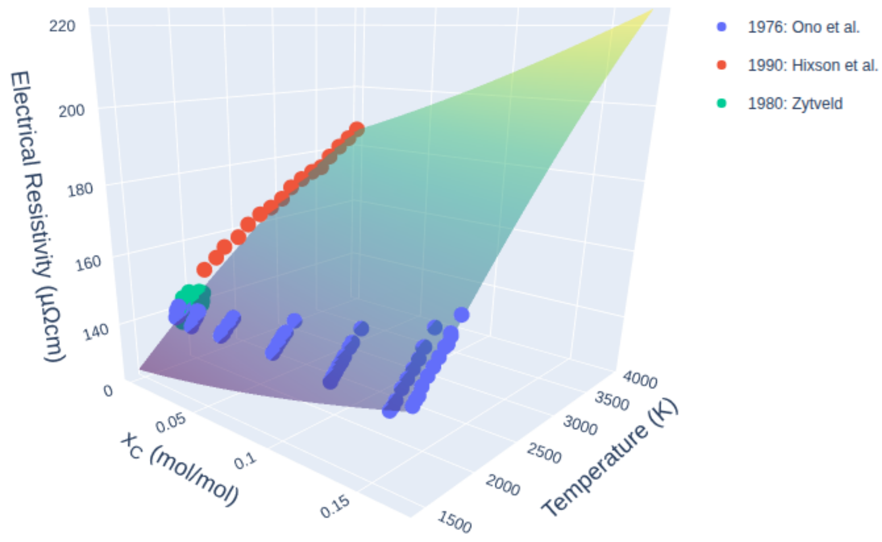

(b) Degree $= 2$. $R^2 = 0.959$

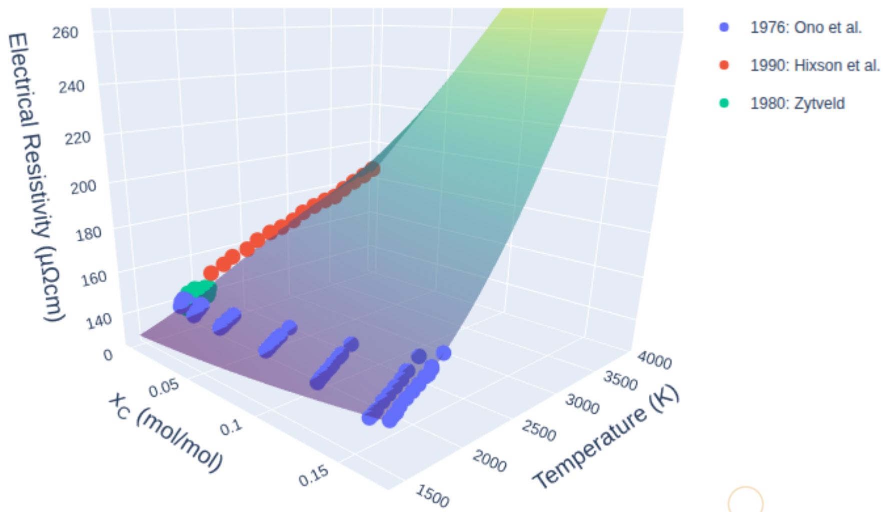

(c) Degree $= 3$. $R^2 = 0.961$

Figure 10.4: Polynomial fits to Fe – C electrical resistivity measurement data.

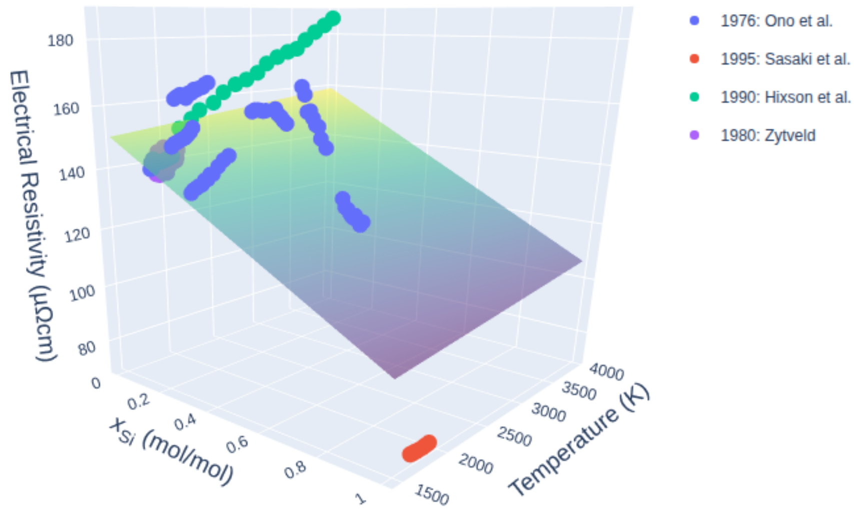

(a) Degree $= 1$. $R^2 = 0.474$

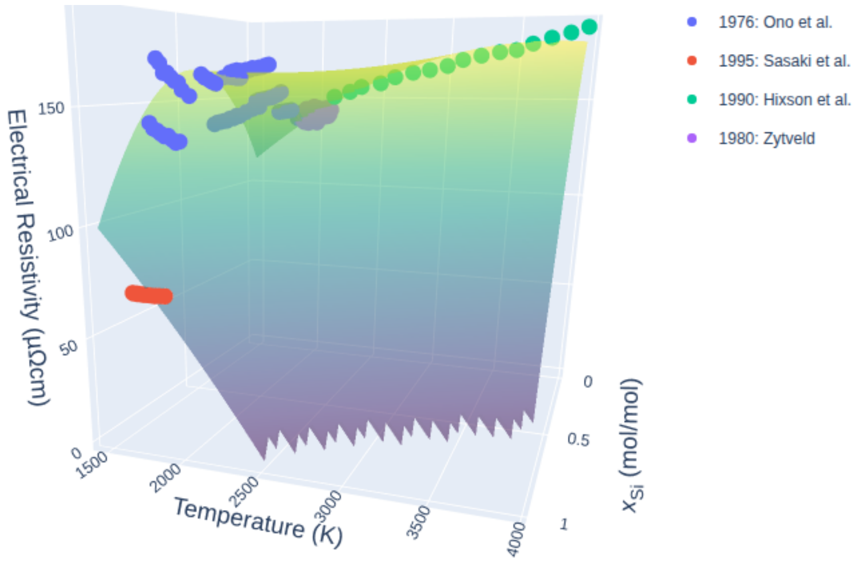

(b) Degree $= 2$. $R^2 = 0.935$

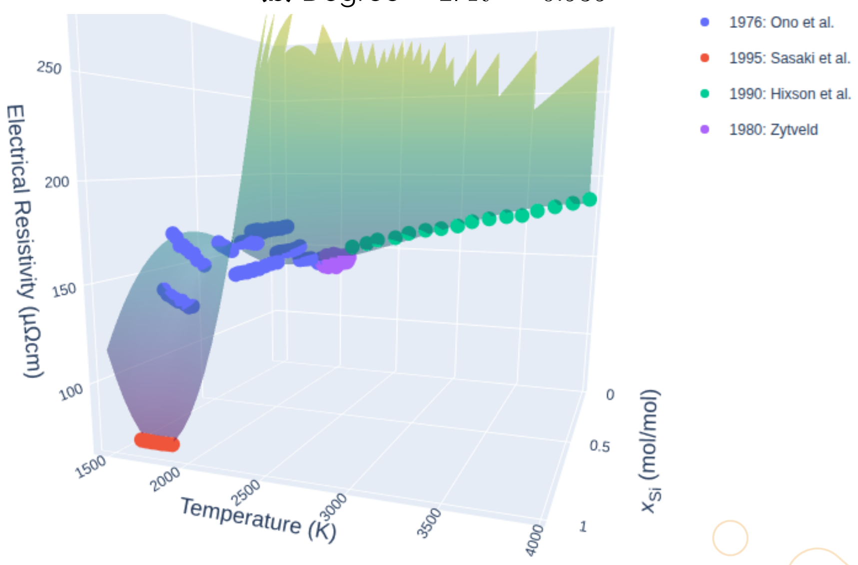

(c) Degree $= 3$. $R^2 = 0.964$

Figure 10.5: Polynomial fits to Fe – Si electrical resistivity measurement data.

To have a better view of the data in Figure 10.5, the second and third degree plots were plotted in 2D in Figure 10.6.

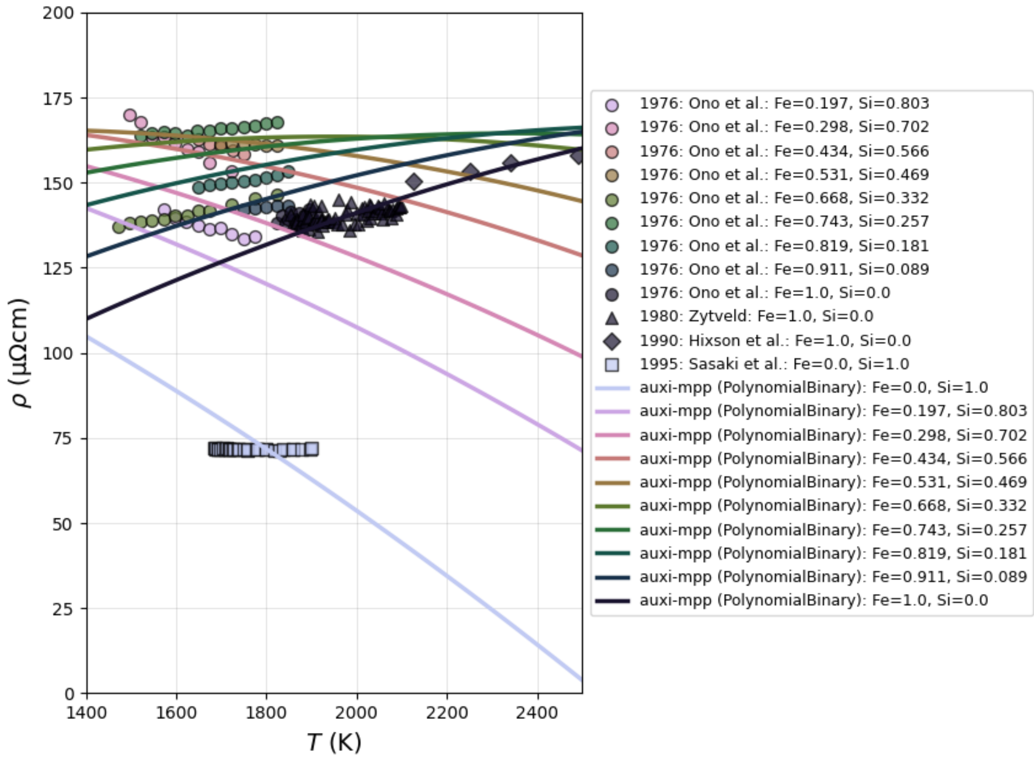

(a) Degree $= 2$. $R^2 = 0.935$

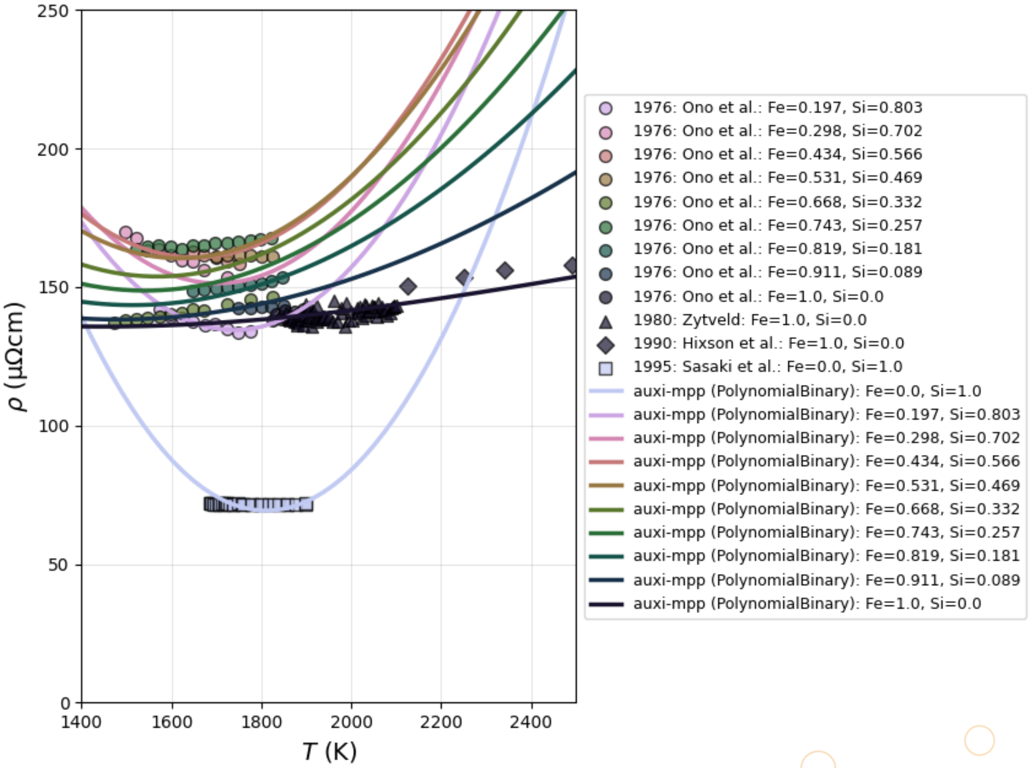

(b) Degree $= 3$. $R^2 = 0.964$

Figure 10.6: A 2D view of the second and third order polynomial fits to Fe – Si electrical resistivity measurement data.

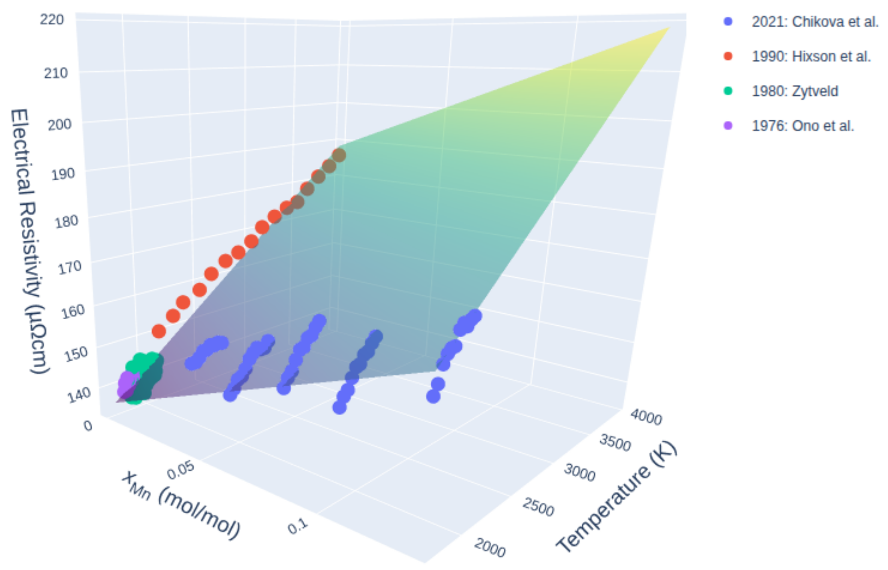

(a) Degree $= 1.\ R^2 = 0.957$

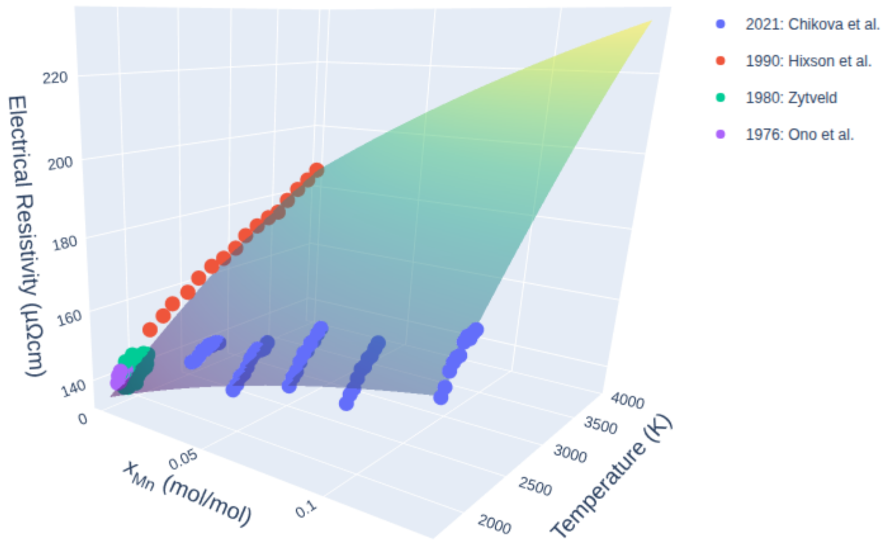

(b) Degree $= 2.\ R^2 = 0.966$

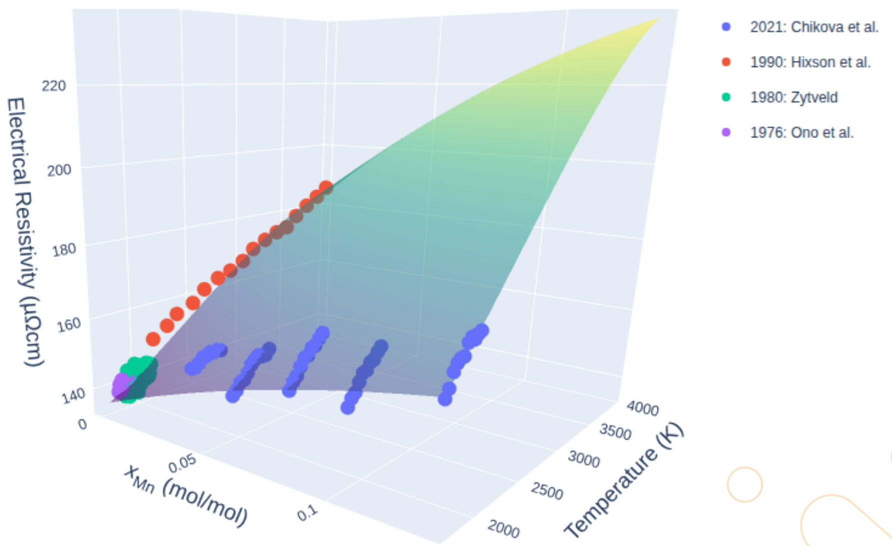

(c) Degree $= 3.\ R^2 = 0.967$

Figure 10.7: Polynomial fits to Fe – Mn electrical resistivity measurement data.

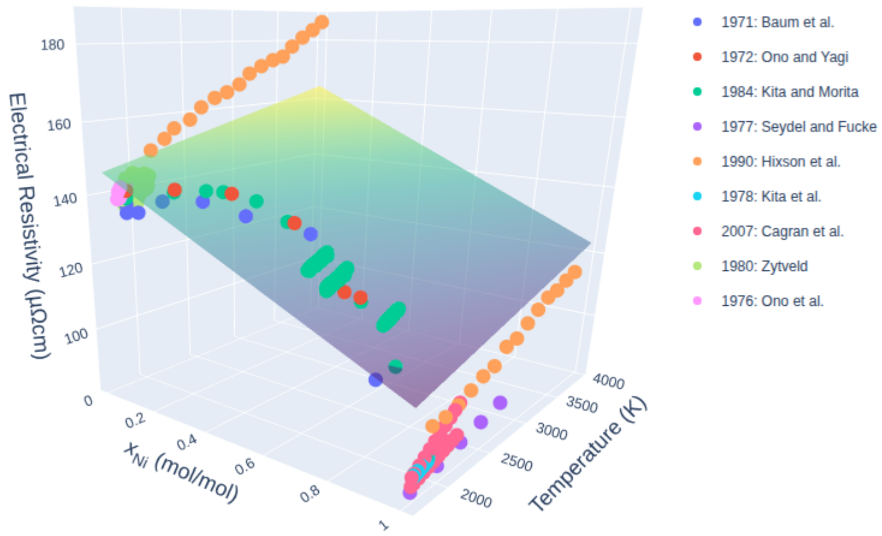

(a) Degree $= 1$. $R^2 = 0.634$

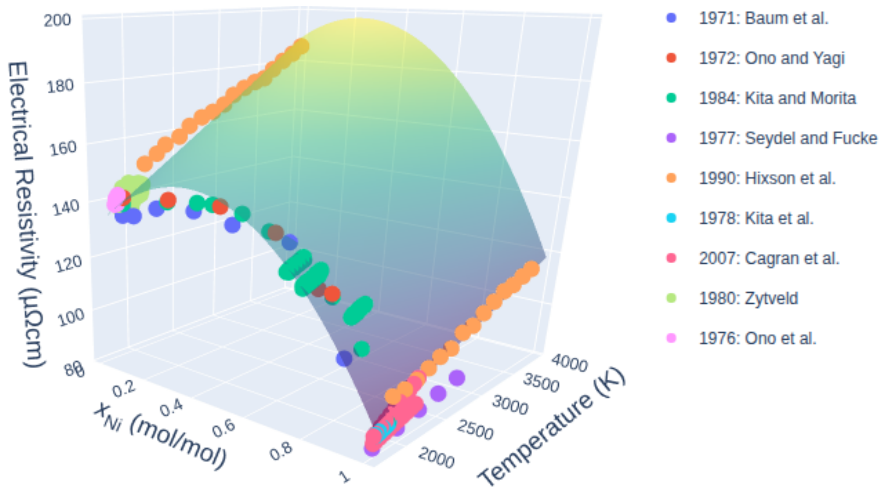

(b) Degree $= 2$. $R^2 = 0.943$

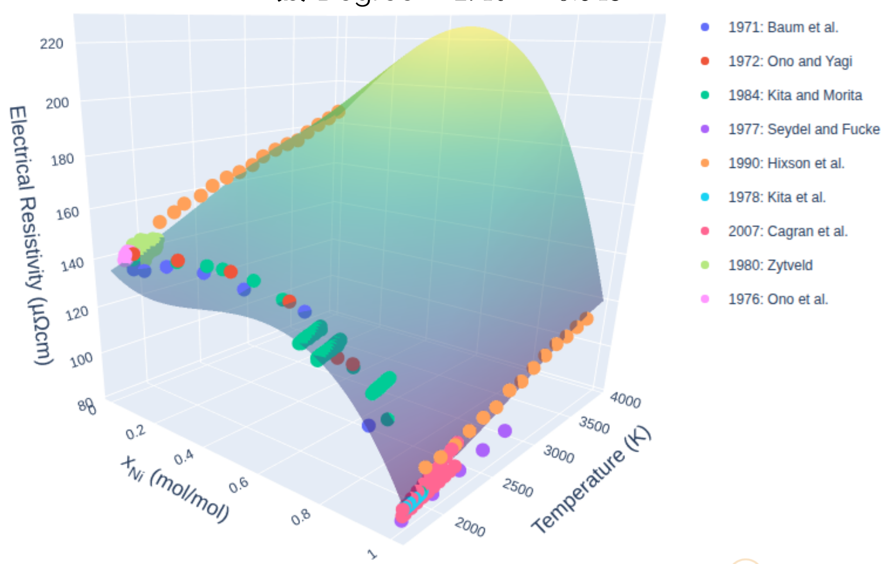

(c) Degree $= 3$. $R^2 = 0.963$

Figure 10.8: Polynomial fits to Fe – Ni electrical resistivity measurement data.

Multi-Component Model Validation

Currently, Fe – C – Si is the only multi-component system available for liquid alloys in auxi-mpp. To the available experimental data, a second, third and fourth degree polynomial have been fitted. The data used is the combination of pure Fe, Fe – C, Fe – Si and Fe – C – Si data. The performance of these polynomials can be analysed in Table 10.2 and Figure 10.9.

Table 10.2: Comparing the electrical conductivity calculated from second, third, and fourth-degree polynomial fits, with the measured values (Ono et al. 1976).

T (K)	x_{Fe}	x_C	x_{Si}	$\sigma_{measured}$ (S m^{-1})	$\Delta\sigma_{second}$	$\Delta\sigma_{third}$	$\Delta\sigma_{fourth}$
1473	0.78	0.04	0.18	660455	-10969	-10585	-6686
1497	0.78	0.04	0.18	660290	-8288	-11136	-7751
1522	0.78	0.04	0.18	655547	-10140	-15725	-12919
1548	0.78	0.04	0.18	651666	-11020	-18812	-16652
1573	0.84	0.12	0.04	725003	38954	40502	40884
1574	0.79	0.12	0.09	684150	15368	21154	21529
1574	0.78	0.04	0.18	649225	-10696	-19901	-18355
1598	0.78	0.04	0.18	644122	-13221	-23165	-22190
1598	0.84	0.12	0.04	717683	35855	36220	36420
1599	0.79	0.12	0.09	677723	12238	18165	18143
1623	0.79	0.12	0.09	670854	8444	14936	14585
1623	0.78	0.04	0.18	641651	-13171	-23260	-22818
1623	0.84	0.12	0.04	710613	32850	32446	32500
1646	0.87	0.04	0.09	670124	-18297	-21213	-21821
1647	0.84	0.12	0.04	702655	28645	27869	27819
1647	0.79	0.12	0.09	666879	7486	14959	14333
1647	0.78	0.04	0.18	638014	-14438	-24106	-24124
1671	0.84	0.12	0.04	699716	29548	28741	28622
1671	0.87	0.04	0.09	667820	-16613	-20774	-21569
1671	0.78	0.04	0.18	635338	-14768	-23455	-23866
1671	0.79	0.12	0.09	661587	5159	14026	13189
1696	0.87	0.04	0.09	662969	-17699	-22604	-23525
1696	0.84	0.12	0.04	691602	25223	24745	24603
1696	0.79	0.12	0.09	655041	1556	12246	11271
1697	0.78	0.04	0.18	631608	-16106	-23178	-23901
1723	0.78	0.04	0.18	631293	-14115	-19004	-19918
1723	0.84	0.12	0.04	687283	24802	25052	24936
1723	0.79	0.12	0.09	652310	1849	14885	13856
1723	0.87	0.04	0.09	661078	-15519	-20734	-21717
1723	0.92	0.04	0.04	702816	-3350	1406	139
1748	0.92	0.04	0.04	702324	1057	3695	2643
1749	0.87	0.04	0.09	657667	-15198	-20224	-21183
1749	0.84	0.12	0.04	687400	28621	29940	29908
1749	0.78	0.04	0.18	624358	-18766	-20854	-21822
1773	0.92	0.04	0.04	699997	3401	4342	3534
1774	0.87	0.04	0.09	654469	-14880	-19293	-20145
1774	0.84	0.12	0.04	679760	24490	27174	27278
1774	0.78	0.04	0.18	625914	-15084	-13957	-14827
1797	0.92	0.04	0.04	700524	8278	7935	7394
1821	0.92	0.04	0.04	695689	7739	6420	6183
1846	0.92	0.04	0.04	695206	11600	9600	9721
				Standard Deviation	**17943**	**21232**	**21162**

Considering only the Fe – C – Si data, the second degree polynomial results in a standard deviation of about 2.5% of the average of the measured data.

A correlation plot of the performance of auxi-mpp are presented in Figure 10.9.

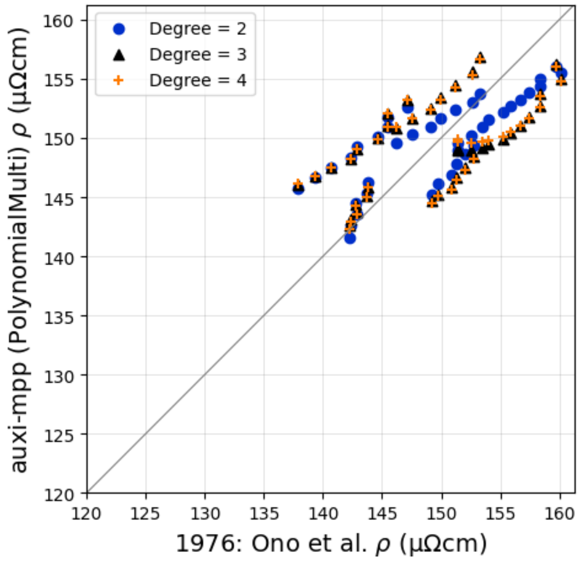

Figure 10.9: Correlation plot for the Fe – C – Si data of auxi-mpp vs experimental data measured by Ono et al. (1976). Degree $= 2$ R^2 : 0.935. Degree $= 3$ R^2 : 0.960. Degree $= 4$ R^2 : 0.959.

The reason for the larger standard deviation for the third and fourth degree polynomial, compared to the second degree, is likely because the data shown in Table 10.2 is only the Fe – C – Si data and thus not all data points used to fit the polynomials.

10.1.5 Issues

There are no known issues.

Chapter 11

Viscosity

This chapter details the models implemented in auxi-mpp for estimating the viscosity of different liquid alloy systems. This chapter details the models implemented in the auxi-mpp for estimating the viscosity of different liquid alloy systems. Two primary approaches are presented.

The first is a model for unary liquid alloys, which estimates viscosity as a function of temperature using an Andrade-type equation. The second approach is an empirical, linear model developed by (Deng et al. 2018) for calculating the viscosity of binary and multi-component iron-based alloys.

11.1 Viscosity with Andrade Type Equation

A viscosity model to estimate the viscosity of unary liquid alloys is described in this section.

11.1.1 Introduction

The viscosity of pure liquid metals is modelled as a function of temperature using an Andrade-type equation, shown in Equation (11.1). The parameters of this equation were fitted to reference experimental data for various elements (Assael et al. 2006; Assael et al. 2010; Assael et al. 2012a; Assael et al. 2012b). The resulting models for each element are implemented in auxi-mpp to provide viscosity estimates for unary liquid systems.

$$\log(\mu(T)) = -a_1 + \frac{a_2}{T} \tag{11.1}$$

11.1.2 Formulation

The viscosity of a unary liquid metal system, μ, is estimated as a function of the absolute temperature, T, using the further developed Andrade-type equation shown in Equation (11.2).

$$\mu(T) = \frac{10^{(-a_1+a_2/T)}}{1000} \tag{11.2}$$

where:

1. $\mu(T)$ is the dynamic viscosity of the liquid metal in Pascal-seconds (Pa·s).
2. T is the absolute temperature of the system in Kelvin (K).
3. a_1 is a dimensionless empirical parameter.
4. a_2 is an empirical parameter related to the activation energy for viscous flow, in Kelvin (K).

The parameters a_1 and a_2 are specific to each element. The equation is formulated to calculate viscosity in millipascal-seconds (mPa·s), which is then divided by 1000 to convert to the standard SI unit of Pa·s.

This model is applicable to a specific set of elements, each within a defined temperature range. Table 11.1 lists the supported elements, their valid temperature ranges, and the corresponding model parameters derived from experimental data. Using the model outside of the recommended temperature limits may result in inaccuracies.

Table 11.1: Supported Elements, Temperature Limits, and Parameters for the Unary Viscosity Model

Element Name	Symbol	Temp. Range (K)	a_1 (dimensionless)	a_2 (K)
Aluminum	Al	933 – 1270	0.7324	803.49
Antimony	Sb	900 – 1300	0.637	712.5
Bismuth	Bi	545 – 1000	0.345	321.4
Cadmium	Cd	600 – 900	0.4239	513.89
Cobalt	Co	1768 – 2100	0.9030	2808.7
Copper	Cu	1356 – 1970	0.4220	1393.4
Gallium	Ga	304 – 800	0.4465	204.03
Indium	In	429 – 1000	0.3621	272.06
Iron	Fe	1809 – 2480	0.7209	2694.95
Lead	Pb	601 – 1400	0.295	427.1
Mercury	Hg	234 – 600	0.2561	132.29
Nickel	Ni	1728 – 2100	0.505	2108.2
Silicon	Si	1685 – 1900	1.0881	1478.7
Silver	Ag	1235 – 1500	0.258	1081.8
Thallium	Tl	577 – 800	0.3017	412.84
Tin	Sn	506 – 1280	0.408	343.4
Zinc	Zn	695 – 1100	0.3291	631.12

11.1.3 Model Validation

The unary viscosity model implemented in auxi-mpp is validated against recommended reference viscosity data for various pure liquid metals (Assael et al. 2010; Assael et al. 2012a; Assael et al. 2012b). The MillsCommercial model implemented in auxi-mpp is validated against recommended reference viscosity data for various pure liquid metals (Assael et al. 2010; Assael et al. 2012a; Assael et al. 2012b).

All supported unary liquid metal systems show good agreement between the model estimates and the reference data, as illustrated in Figure 11.1.

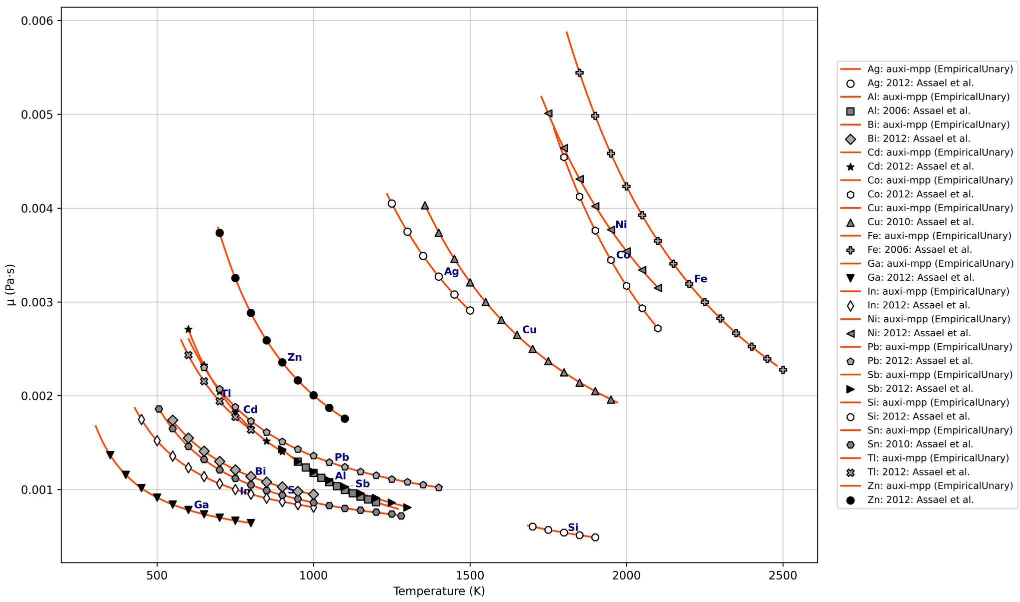

Figure 11.1: MillsCommercial model estimates for unary liquid metals versus recommended reference data (Assael et al. 2010; Assael et al. 2012a; Assael et al. 2012b).

11.1.4 Issues

There are no known issues.

11.2 Deng Viscosity Model

A viscosity model based on the work by Deng et al. (2018) is implemented for binary and multi-component liquid alloys of iron.

11.2.1 Introduction

Based on experimental data, Deng et al. (2018) developed a quantitative, linear model for estimating the viscosity of multi-component liquid iron-based alloys. This empirical equation calculates the alloy's viscosity by considering its temperature and the weight percentage of several alloying elements.

11.2.2 Formulation

The model calculates the viscosity of liquid ferrous alloys by starting with a temperature-dependent base viscosity for pure iron and then adding the contributions from various alloying elements. This approach is applicable to binary Fe – C and multi-component Fe – C – X systems, where X can be Si, Mn, P, S, or Ti. The model is valid for a temperature range of 1463 K to 1723 K and requires a carbon content between 3.0 and 4.5 wt%.

Fe-C System

The viscosity of the Fe-C system, μ, is calculated based on the contributions of the base element (Fe) and the alloying element (C) of the system, as shown in Equation (11.3). Table 11.2 lists the parameters used in the model for the Fe-C system.

$$\mu(T, \text{wt\%}_C) = \frac{(\text{A}_\text{Fe} + k_T T) + (k_C \cdot \text{wt\%}_C)}{1000} \tag{11.3}$$

where:

1. $\mu(T, \text{wt\%}_C)$ is the dynamic viscosity in Pascal-seconds (Pa·s).
2. T is the absolute temperature in Kelvin (K).
3. $\text{wt\%}_C$ is the weight percent of carbon in the alloy.
4. A_Fe is the constant term for pure iron's viscosity.
5. k_T is the temperature coefficient for iron's viscosity.
6. k_C is the coefficient for the effect of carbon on viscosity.

The calculation is performed in millipascal-seconds (mPa·s) and then converted to Pa·s.

Table 11.2: Parameters for the Fe-C Viscosity Model

Component	Parameter	Value	Unit
Fe	A_Fe	34.42973	mPa·s
	k_T	-0.01514	mPa·s/K
C	k_C	-0.00349	mPa·s / wt%

Multi-Component

For multi-component systems, the viscosity is calculated by summing the contributions from all alloying elements present in the alloy, as shown in Equation (11.4).

$$\mu(T, \text{wt\%}_i) = \frac{(\text{A}_\text{Fe} + k_T T) + \sum_i (k_i \cdot \text{wt\%}_i)}{1000} \tag{11.4}$$

where the additional terms are defined as:

1. k_i is the coefficient for the effect of alloying element i on viscosity.
2. $\text{wt\%}_i$ is the weight percent of the alloying element i.

The summation is performed over all alloying elements present in the system (excluding Fe). The calculation gives a result in millipascal-seconds (mPa·s), which is then converted to Pa·s.

The model is validated for several Fe-based ternary systems (Deng et al. 2018). Each alloying element has a specific coefficient and a valid composition range.

Table 11.3: Parameters for the Multi-Component Viscosity Model

Component	Parameter	Value	Composition Range (wt%)
Fe	A_{Fe}	34.42973	-
	k_T	-0.01514	-
C	k_C	-0.00349	3.0 – 4.5
Si	k_{Si}	0.76756	0.2 – 0.6
Mn	k_{Mn}	-2.35139	0.1 – 0.5
P	k_P	-3.63856	0.1 – 0.3
S	k_S	-6.91921	0.02 – 0.08
Ti	k_{Ti}	5.91118	0.05 – 0.2

11.2.3 Model Validation

The DengBinary and DengMulti models, implemented in auxi-mpp, show good agreement with experimental data for the Fe – C and multi-component liquid iron-based alloy systems, as illustrated in Figures 11.2 to 11.7.

Fe-C System

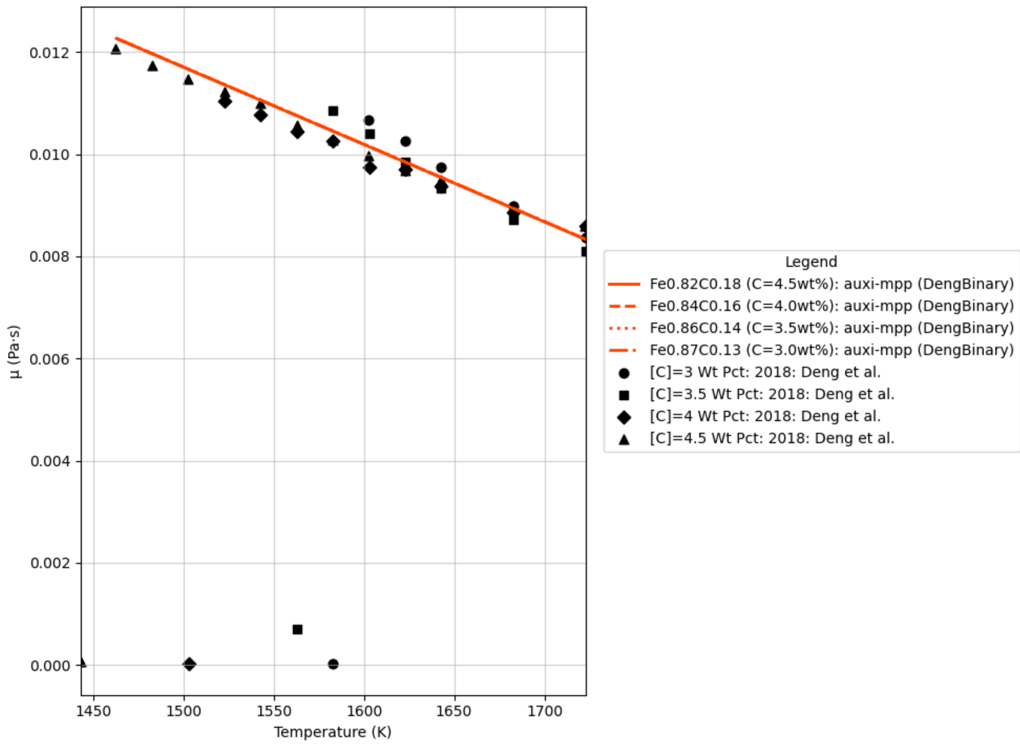

Figure 11.2: DengBinary model estimates for the binary Fe – C system versus experimental data (Deng et al. 2018).

Multi-Component Systems

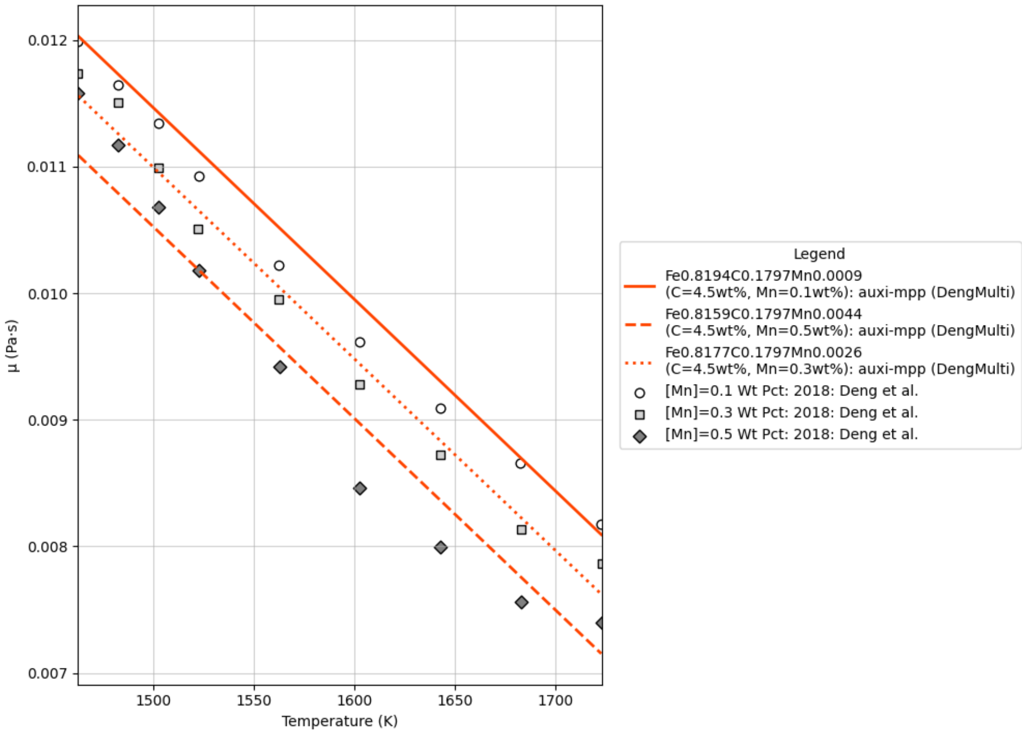

Figure 11.3: DengMulti model estimates for Fe – C – Mn system versus experimental data (Deng et al. 2018).

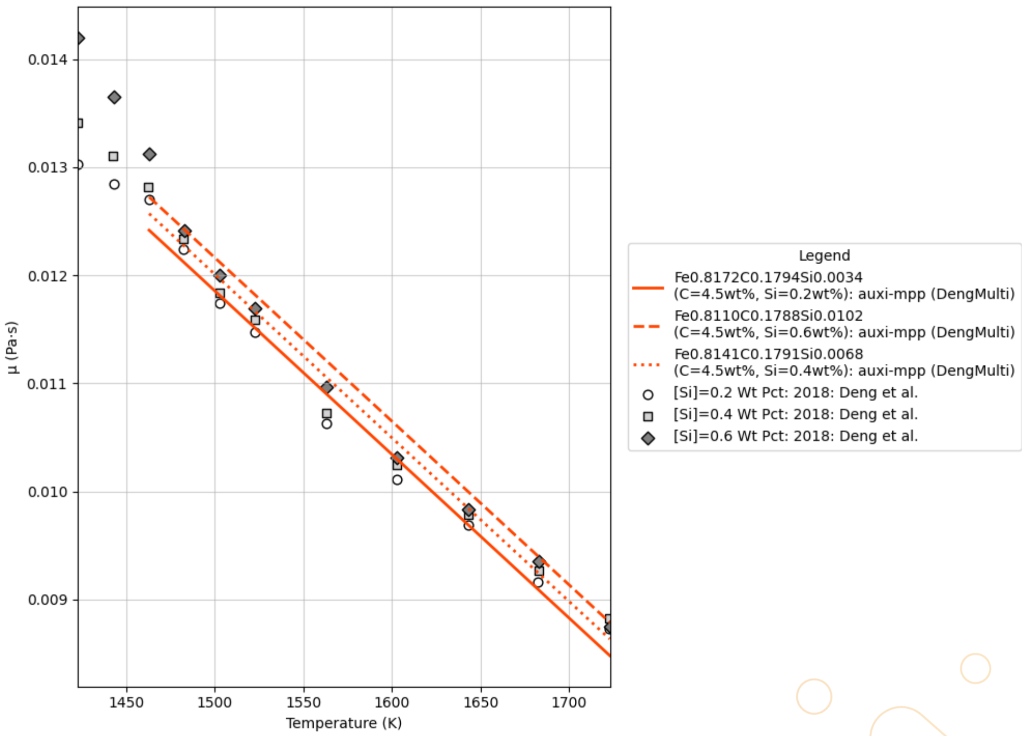

Figure 11.4: DengMulti model estimates for Fe – C – Si system versus experimental data (Deng et al. 2018).

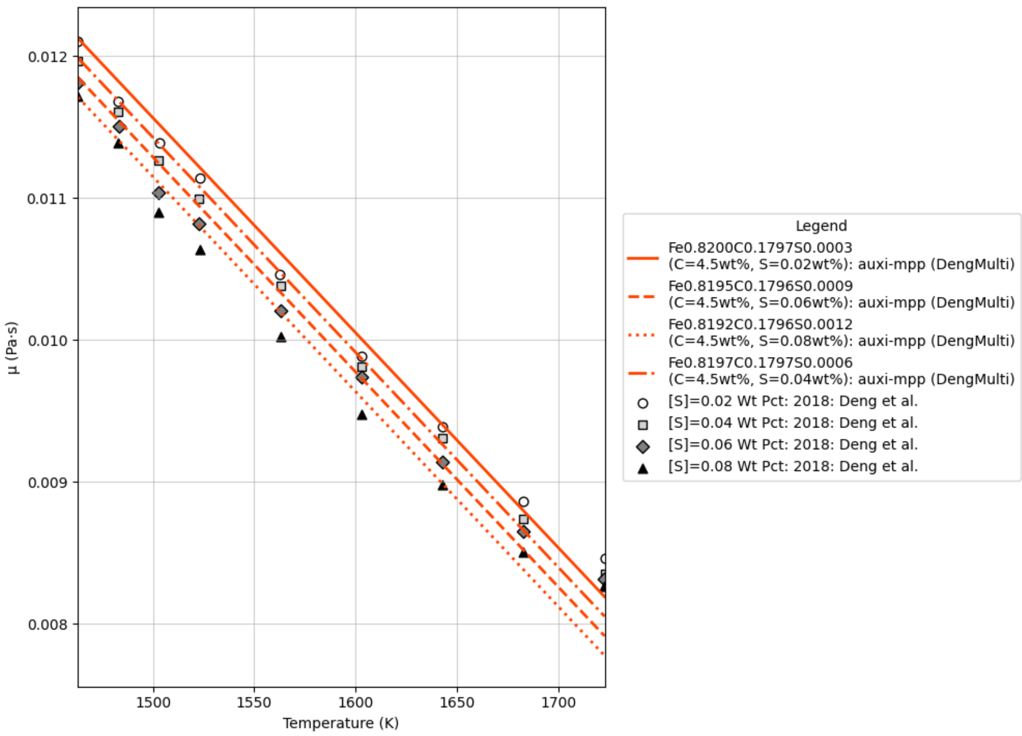

Figure 11.5: DengMulti model estimates for Fe – C – S system versus experimental data (Deng et al. 2018).

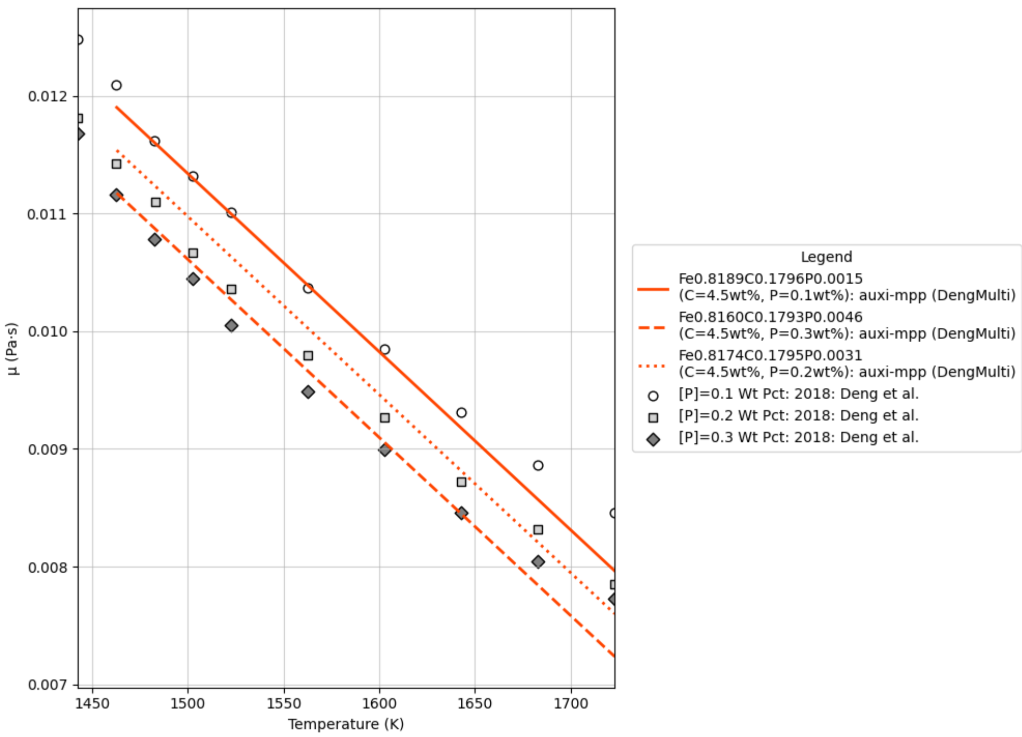

Figure 11.6: DengMulti model estimates for Fe – C – P system versus experimental data (Deng et al. 2018).

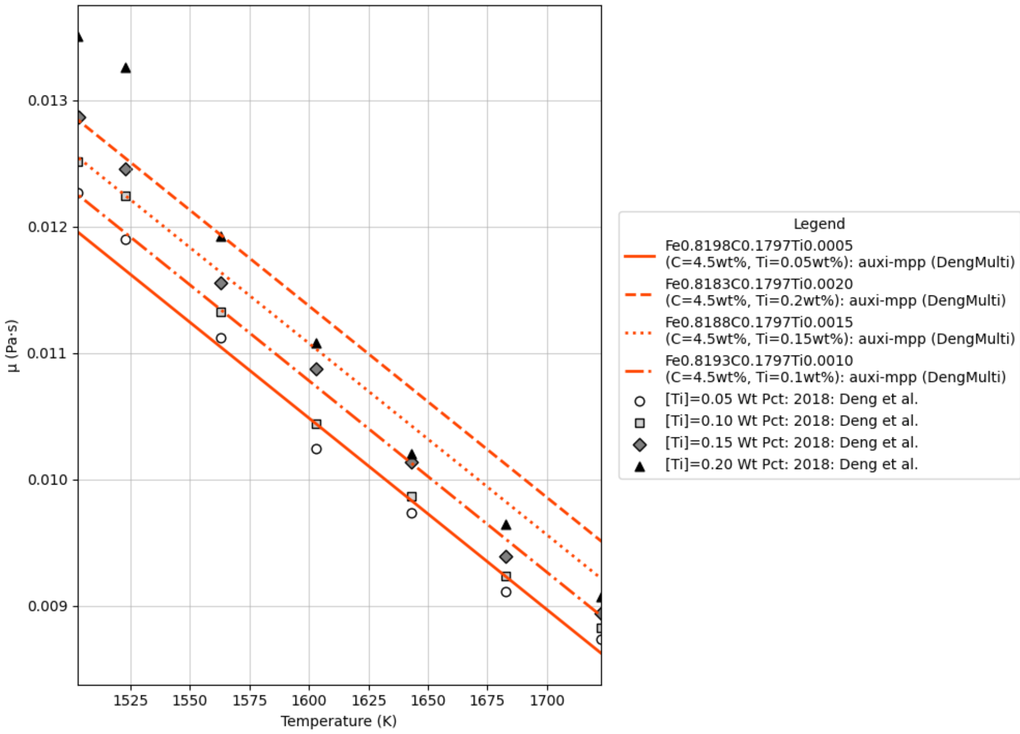

Figure 11.7: DengMulti model estimates for Fe – C – Ti system versus experimental data (Deng et al. 2018).

11.2.4 Issues

There are no known issues.

Chapter 12

Thermal Conductivity

There are two mechanisms for transferring thermal energy in liquid alloys. These are transfer by phonons, which are quantized lattice vibrations, and transfer by free electons. The dominant mechanism in liquid alloys is the transfer of thermal energy by the movement of free electrons. In high temperature liquids, phonons are scattered significantly more than in crystalline solids. Consequently, the phonon contribution to thermal conductivity becomes minor – about 1 % of total heat transfer (Ziman 2001).

The state-of-the-art ab initio workflow for calculating the transport properties, including thermal conductivity, of liquid metals involves a multi-step computational process that combines quantum molecular dynamics with the Kubo-Greenwood linear response theory. The major drawback for this method is its prohibitive computational cost.

The dominance of electrons in both thermal and electrical conduction in metals leads to a powerful and elegant relationship between the two properties known as the Wiedemann-Franz (W-F) Law. First proposed empirically by Gustav Wiedemann and Rudolph Franz in 1853 and later given a theoretical basis by Ludvig Lorenz, the law states that the ratio of the electronic thermal conductivity (κ_e) to the electrical conductivity (σ) for a metal is directly proportional to the absolute temperature (T). Note that the W-F law only accounts for the electronic contribution to the thermal conductivity of the melt.

The W-F law effectively transforms the problem of estimating the thermal conductivity of a liquid alloy – a property that is extremely difficult to measure directly – into the much more manageable problem of estimating its electrical conductivity. We can therefore invest in a proper description of the electrical conductivity and simply derive the thermal conductivity from that using the W-F law.

The scarcity of experimental data for the thermal conductivity of liquid metals and alloys remains a critical challenge for validating the W-F law, however.

12.1 Thermal Conductivity by Wiedemann-Franz

A thermal conductivity model by applying the Wiedemann-Franz law to electrical conductivity estimations.

12.1.1 Introduction

Due to the lack of readily available models to estimate thermal conductivity for liquid metals, the W-F law were applied to the available electrical conductivity models instead. Applying the W-F law is documented here.

12.1.2 Overview

To estimate thermal conductivity, the W-F law is applied to all models available to estimate electrical conductivity. For an overview of the electrical conductivity polynomials, see Section 10.1.2.

It should be noted that the W-F law makes assumptions that, strictly speaking, disqualify using it on pig iron melts. The models available should therefore be used with caution, and the user is encouraged to ponder the listed assumptions and the presented validation before using them.

The validation of the W-F law was performed on the Fe – Ni system, as this is the only one for which data on both thermal and electrical conductivity could be obtained. To give the user a general idea of the performance of the W-F law, we cite a few use cases found in the literature.

Literature on Applying the W-F Law

Mills et al. (1996) and Giordanengo et al. (1999) reported that the W-F law is valid for most pure metals at their melting points.

According to Zhao and Garay (2023), the Lorenz number varies with pressure, temperature and metal composition. They state that the real L does not exactly equal L_0 for liquid metals, so the W-F law has to be applied with caution when measuring thermal conductivity directly from electrical conductivity measurements. Nevertheless, they do report that the law provides a reasonable approximation of thermal conductivity from electron transport.

Watanabe et al. (2019) reported a higher measured thermal conductivity than that estimated by the W-F law for Fe and Ni systems. From this, they deduced that atomic thermal vibration (phonons) also contributes significantly to the thermal conductivity in Fe and Ni and their alloys.

Secco (2017) have shown that the Lorenz number can vary between $1L_0$ and $3L_0$ for Fe – Si alloys in the solid state. That leaves the question of whether this is also the case for liquid Fe – Si melts.

Yamasue et al. (2003) have shown that around the melting point, the measured thermal conductivity values for liquid Sn and Pb are in good agreement with the values obtained using the W-F law. They put this forward as evidence that liquid metals indeed have a free-electron structure.

Another study indicates that Sn-based alloys deviate from the W-F law (Mizuno et al. 2020) – one of the few studies not confirming the W-F law.

To conclude, the majority of the literature confirms the validity of the W-F law; however, it should indeed be applied with caution.

12.1.3 Formulation

Applying the Wiedemann-Franz law is straight forward and is captured in Equation (12.1).

$$\kappa_e = \sigma L_0 T \tag{12.1}$$

Here, $L_0 = 2.445 \times 10^{-8}$, and σ is the electrical conductivity of the system at the particular temperature. Equation (12.1) was applied to all electrical conductivity estimations of the unary, binary and multi-component polynomial fits described in Section 10.1.3.

12.1.4 Assumptions

To apply the universal Lorenz number (see Equation (12.1)), which gives the W-F law its estimating power, the following assumptions are made.

1. **Electron scattering is elastic scattering**. Inelastic scattering events can transport charge without proportional transport of heat and will therefore deviate from the W-F law.
2. **The alloy's electronic structure has a low complexity.** Significant deviation can be expected for complex alloys.
3. **No transition metals are present.** The d-orbitals of transition metals can lead to different scattering behaviour for electrons. First principles calculations have shown that for binary iron-based alloys, the Lorenz number can deviate by more than 25%.
4. **The alloy is made up of only metal atoms.** There is evidence that alloys containing semi-metals like Sn, Bi and Si exhibit complex eletronic interactions, causing significant deviations from the W-F law.

The last two assumptions are particularly problematic for the pig iron alloys we are interested in. Pig iron contain substantian amounts of Fe, a transition metal, as well as small amounts of C and Si, which are not metals. The user should therefore be aware that some of the core assumptions of the W-F law are violated when applying it to pig iron melts.

12.1.5 Model Validation

To validate the W-F law we test its performance against experimental measurements. We therefore require the systems to have measurements for both electrical resistivity and thermal conductivity. We then need to fit polynomials to the measured resistivity data, apply the W-F to the polynomials to get thermal conductivity, and then finally plot the resulting functions against measured thermal conductivity data. Due to the scarcity of measured thermal conductivity data, the only binary system for which we could find both electrical resistivity and thermal conductivity measurements is the Fe – Ni system. This system is therefore the only one we can use to validate the W-F law.

The Fe – Ni System

In Figure 12.1, a surface of the W-F law, applied to the second degree polynomial fit for electrical resistivity data, were plotted against measured thermal conductivity data.

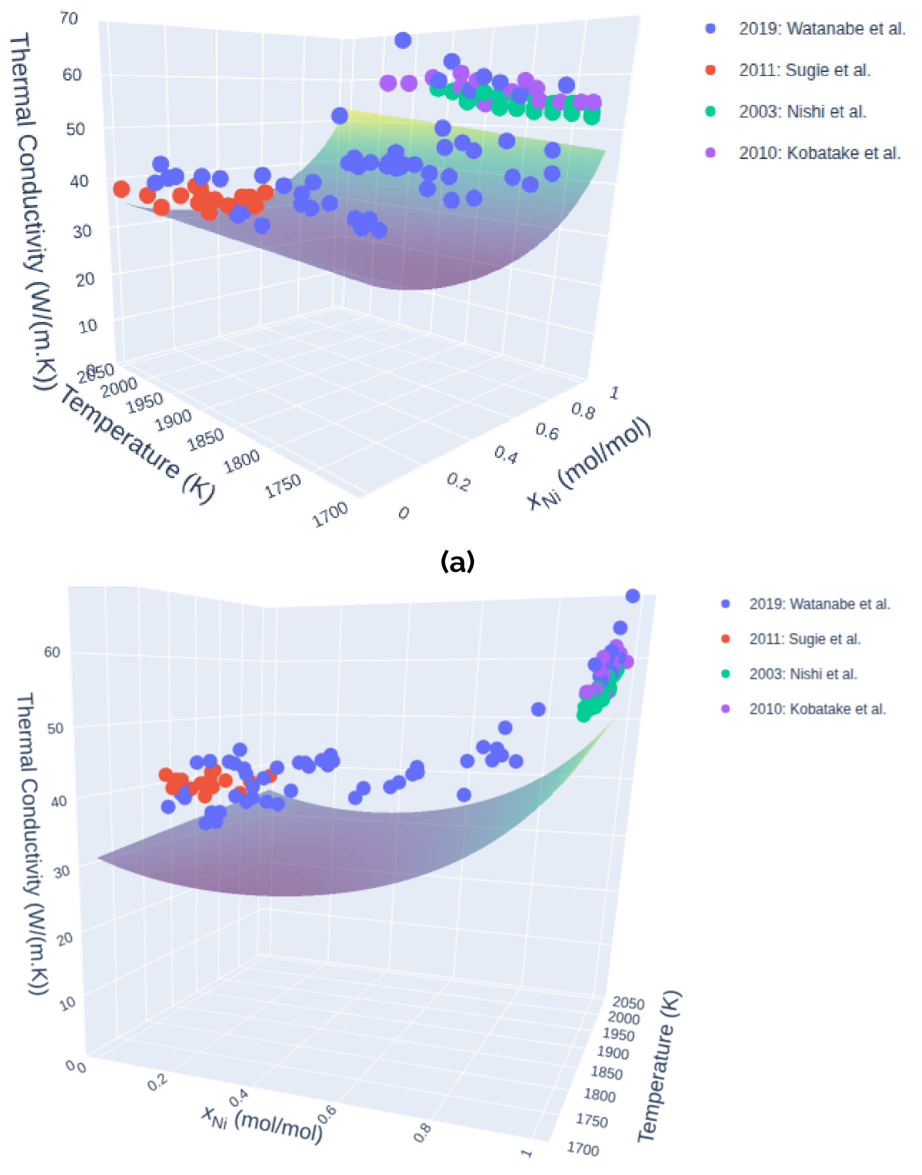

(a)

(b)

Figure 12.1: Testing the performance of the Wiedemann-Franz law against experimental measurements. Surface: auxi-mpp (WiedemannFranzBinary, degree=2).

Figure 12.2 shows Figure 12.1 in 2D slices.

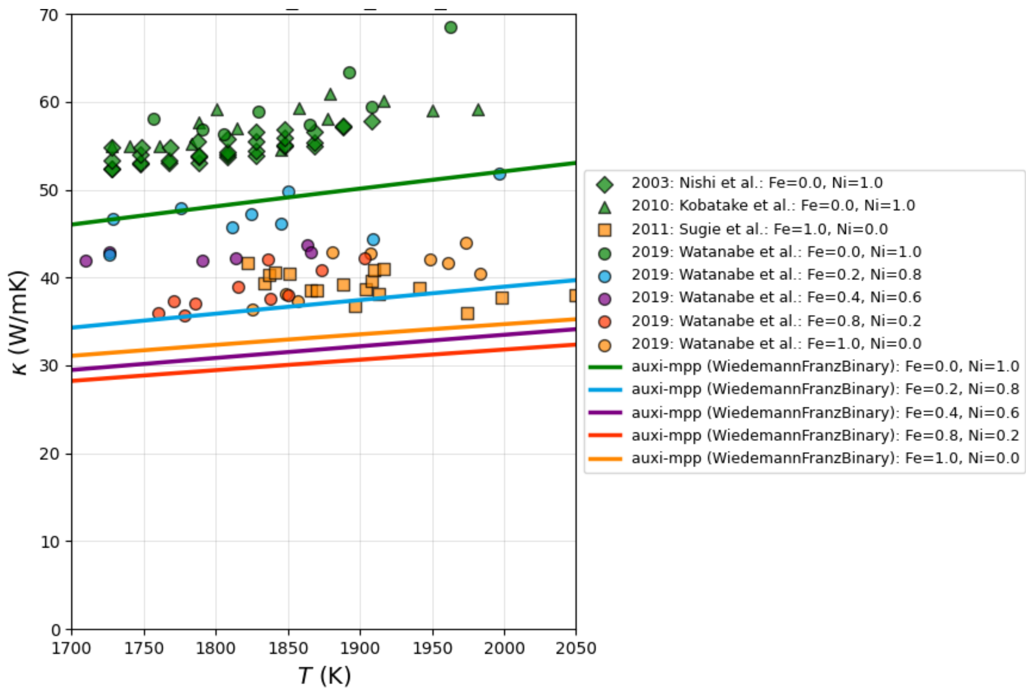

Figure 12.2: Testing auxi-mpp (WiedemannFranzBinary, degree=2) against experimental measurements.

As confirmed by Watanabe et al. (2019), the W-F law underestimates the thermal conductivity by roughly 10 $W\,m^{-1}\,K^{-1}$ for the pure substances and roughly 15 $W\,m^{-1}\,K^{-1}$ for a 1:1 Fe – Ni ratio. This amounts to an underestimation of roughly 20% to 38%. Interestingly, Watanabe et al. (2019) comments on this underestimation and suggests that thermal vibration of atoms contributed to the thermal conductivities of Fe – Ni alloys, not attributing it to violating the core assumptions of the W-F law.

Performance for Pig Iron Binaries

For reference, in Figure 12.3 we present the performance of the W-F law over realistic composition ranges for binary systems representing pig iron melts over the temperature range 1000 to 2500 K.

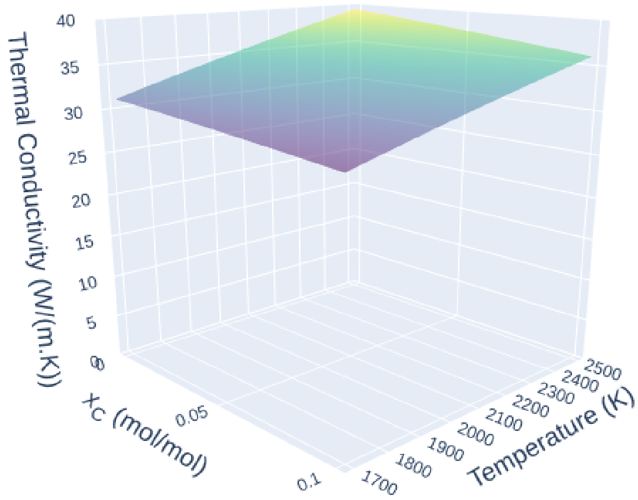

(a) Fe – C

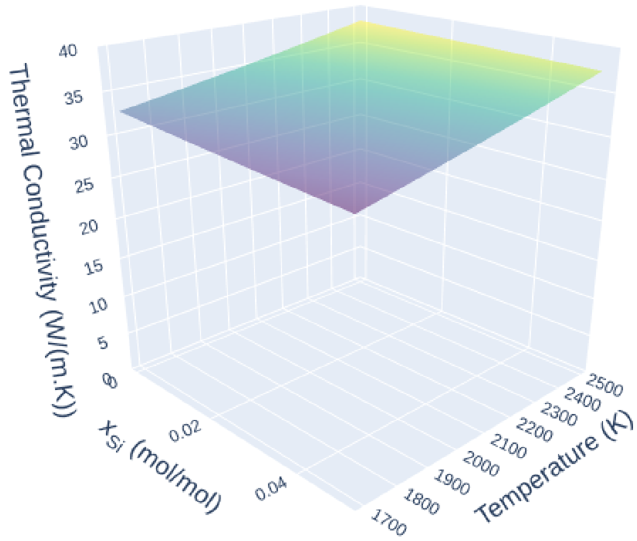

(b) Fe – Si

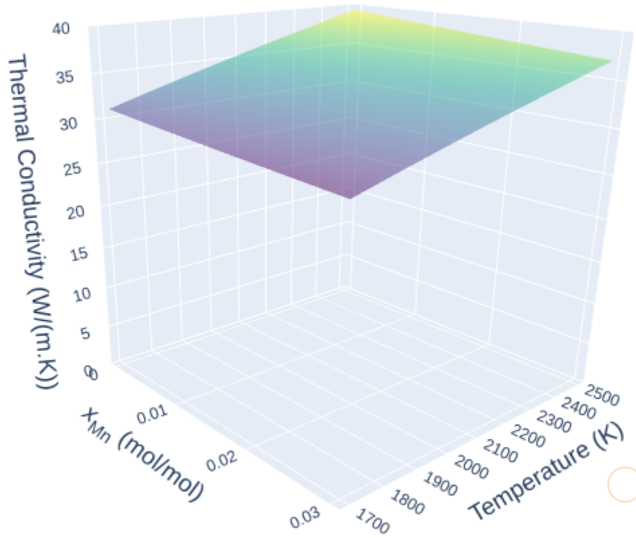

(c) Fe – Mn

Figure 12.3: Thermal conductivity estimates by auxi-mpp (WiedemannFranzBinary; degree=2) for pig iron representing binaries.

Figure 12.4 compares the sensitivity of thermal conductivity to either carbon, silicon or manganese.

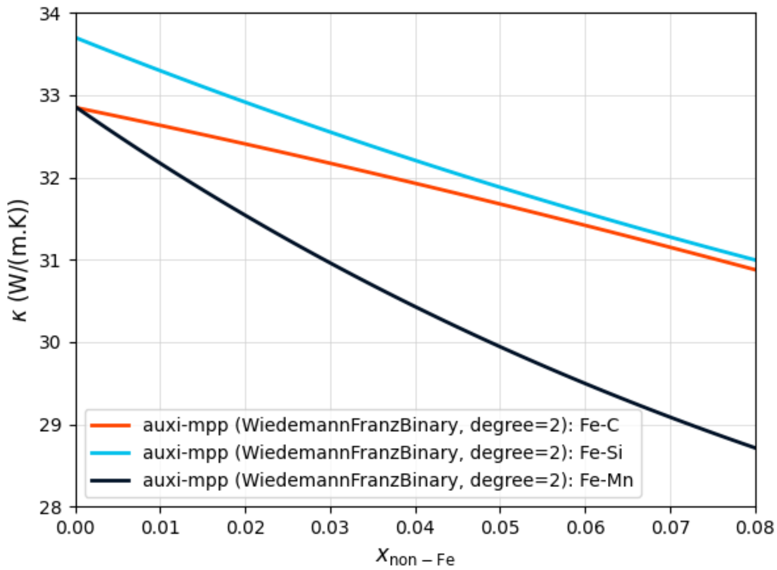

Figure 12.4: Sensitivity of thermal conductivity to carbon, silicon or manganese at the 1850 K isotherm.

Here, the effect of the rapidly changing electrical resistivity data for the Fe – Si system, as seen in Figure 10.5b, can be seen as the polynomial used for the W-F law deviates from pure iron thermal conductivity compared to Fe – C and Fe – Mn.

12.1.6 Issues

The performance of the W-F law could not be validated against experimental measurements for pig iron related melts, due to a lack of data. The models should therefore be used with caution.

Part IV

Appendices

Appendix A

Definitions

The following definitions apply to manual.

EM-MPPF means the Ex Mente Material Physical Property Framework.

EM-MPP-STK means the Ex Mente Material Physical Property Simulation Toolkit, which is a Python package.

EM-AMDF refers to the Ex Mente Accelerated Material Description Framework.

The Slag Sub-package means a sub-package of EM-MPP-STK that contains slag physical property models and their parameters and the necessary documentation.

REF processes means Reducing Electric Furnace processes.

REF-MPP means Reducing Electric Furnace Material Physical Property.

MQM means Modified Quasichemical Model

ChemApp for Python means the ChemApp for Python package for computational thermochemistry owned by GTT-Technologies.

FactSage means the FactSage suite for computational thermochemistry owned by GTT-Technologies.

auxi-mpp is the python package containing all material pysical property models, where 'auxi' means help, and 'mpp' means material physical properties.

References

Assael, M. J., I. J. Armyra, J. Brillo, S. V. Stankus, J. Wu, and W. A. Wakeham (July 2012a). "Reference Data for the Density and Viscosity of Liquid Cadmium, Cobalt, Gallium, Indium, Mercury, Silicon, Thallium, and Zinc". In: *Journal of Physical and Chemical Reference Data* 41.3, p. 033101. ISSN: 0047-2689. DOI: 10.1063/1.4729873. (Visited on 08/05/2025).

Assael, M. J., K. Kakosimos, R. M. Banish, J. Brillo, I. Egry, R. Brooks, P. N. Quested, K. C. Mills, A. Nagashima, Y. Sato, and W. A. Wakeham (Mar. 2006). "Reference Data for the Density and Viscosity of Liquid Aluminum and Liquid Iron". In: *Journal of Physical and Chemical Reference Data* 35.1, pp. 285–300. ISSN: 0047-2689, 1529-7845. DOI: 10.1063/1.2149380. (Visited on 07/30/2025).

Assael, M. J., A. E. Kalyva, K. D. Antonia, R. M. Banish, I. Egry, J. Wu, E. Kaschnitz, and W. A. Wakeham (Aug. 2012b). "Reference Data for the Density and Viscosity of Liquid Antimony, Bismuth, Lead, Nickel and Silver." In: *High Temperatures - High Pressures* 41.3, pp. 161–184. ISSN: 0018-1544. (Visited on 08/05/2025).

Assael, M. J., A. E. Kalyva, K. D. Antoniadis, R. Michael Banish, I. Egry, J. Wu, E. Kaschnitz, and W. A. Wakeham (Sept. 2010). "Reference Data for the Density and Viscosity of Liquid Copper and Liquid Tin". In: *Journal of Physical and Chemical Reference Data* 39.3, p. 033105. ISSN: 0047-2689, 1529-7845. DOI: 10.1063/1.3467496. (Visited on 08/05/2025).

Brillo, J. and I. Egry (July 2003). "Density Determination of Liquid Copper, Nickel, and Their Alloys". In: *International Journal of Thermophysics* 24.4, pp. 1155–1170. ISSN: 1572-9567. DOI: 10.1023/A:1025021521945. (Visited on 07/07/2025).

Brillo, J., I. Egry, and T. Matsushita (Nov. 2006). "Density and Surface Tension of Liquid Ternary Ni–Cu–Fe Alloys". In: *International Journal of Thermophysics* 27.6, pp. 1778–1791. ISSN: 1572-9567. DOI: 10.1007/s10765-006-0121-7. (Visited on 07/10/2025).

Brillo, J. and I. Egry (Aug. 2004). "Density and Excess Volume of Liquid Copper, Nickel, Iron, and Their Binary Alloys". In: *International Journal of Materials Research* 95.8, pp. 691–697. ISSN: 2195-8556. DOI: 10.1515/ijmr-2004-0128. (Visited on 07/07/2025).

Brosh, E., A. Pelton, and S. Decterov (May 2012). "A Model to Calculate the Viscosity of Silicate Melts. Part IV: Borosilicate Melts Containing Alkali Metals". In: *International Journal of Materials Research (formerly Zeitschrift fuer Metallkunde)* 103, p. 537. DOI: 10.3139/146.110639.

Cagran, C., T. HÃ¼pf, G. Pottlacher, and G. LohÃ¶fer (Dec. 1, 2007). "High-Temperature Metallic Melts â€" Resistivity Intercomparison for Space Applications". In: *International Journal of Thermophysics* 28.6, pp. 2176–2187. ISSN: 1572-9567. DOI: 10.1007/s10765-007-0245-4. URL: https://doi.org/10.1007/s10765-007-0245-4 (visited on 08/11/2025).

Chikova, O. A., N. I. Sinitsin, and V. V. Vâ€™yukhin (Oct. 1, 2021). "Electrical Resistivity of Liquid Feâ€"Mn Alloys". In: *Russian Physics Journal* 64.6 (6), pp. 1039–1046. ISSN: 1573-9228. DOI: 10.1007/s11182-021-02426-y. URL: https://link.springer.com/article/10.1007/s11182-021-02426-y (visited on 08/05/2025).

Deng, Y., J. Zhang, and K. Jiao (Sept. 2018). "Viscosity Measurement and Prediction Model of Molten Iron". In: *Ironmaking & Steelmaking* 45.8, pp. 773–777. ISSN: 0301-9233. DOI: 10.1080/03019233.2018.1491171. (Visited on 07/30/2025).

Giordanengo, B., N. Benazzi, J. Vinckel, J.-G. Gasser, and L. Roubi (Aug. 1, 1999). "Thermal Conductivity of Liquid Metals and Metallic Alloys". In: *Journal of Non-Crystalline Solids* s 250–252, pp. 377–383. DOI: 10.1016/S0022-3093(99)00268-9.

Grundy, A. N., I.-H. Jung, A. D. Pelton, and S. A. Decterov (2008a). "A Model to Calculate the Viscosity of Silicate Melts. Part II: The NaO0.5–MgO–CaO–AlO1.5–SiO2 System". In: *International Journal of Materials Research* 99.11, pp. 1195–1209. DOI: doi:10.3139/146.101753. (Visited on 08/22/2023).

Grundy, A. N., H. Liu, I.-H. Jung, S. A. Decterov, and A. D. Pelton (2008b). "A Model to Calculate the Viscosity of Silicate Melts. Part I: Viscosity of Binary SiO2–MeOx Systems (Me = Na, K, ca, Mg, Al)". In: *International Journal of Materials Research* 99.11, pp. 1185–1194. DOI: doi:10.3139/146.101752. (Visited on 08/22/2023).

Hixson, R. S., M. A. Winkler, and M. L. Hodgdon (Oct. 1, 1990). "Sound Speed and Thermophysical Properties of Liquid Iron and Nickel". In: *Physical Review B* 42.10, pp. 6485–6491. DOI: 10.1103/PhysRevB.42.6485. URL: https://link.aps.org/doi/10.1103/PhysRevB.42.6485 (visited on 07/31/2025).

Hundermark, R. (2003). "The Electrical Conductivity of Melter Type Slags". Master of Engineering, MEng. Cape Town, South Africa: University of Cape Town.

Jimbo, I. and A. W. Cramb (Feb. 1993). "The Density of Liquid Iron-Carbon Alloys". In: *Metallurgical Transactions B* 24.1, pp. 5–10. ISSN: 0360-2141, 1543-1916. DOI: 10.1007/BF02657866. (Visited on 04/12/2023).

Kim, W. Y. (Aug. 2011). "Modeling Viscosity of Molten Slags and Glasses". PhD thesis. École Polytechnique de Montréal. (Visited on 09/11/2024).

Kim, W.-Y., P. Hudon, and I.-H. Jung (Mar. 1, 2021a). "Modeling the viscosity of silicate melts containing Fe oxide: Fe saturation condition". In: *Calphad* 72, p. 102242. ISSN: 0364-5916. DOI: 10.1016/j.calphad.2020.102242. URL: https://www.sciencedirect.com/science/article/pii/S0364591620305058 (visited on 10/18/2024).

Kim, W.-Y., P. Hudon, and I.-H. Jung (Mar. 1, 2021b). “Modeling the viscosity of silicate melts containing Fe oxide: FeO/Fe2O3 containing system”. In: *Calphad* 72, p. 102244. ISSN: 0364-5916. DOI: 10.1016/j.calphad.2020.102244. URL: https://www.sciencedirect.com/science/article/pii/S0364591620305071 (visited on 08/22/2023).

Kim, W.-Y., A. D. Pelton, and S. A. Decterov (2012a). “A Model to Calculate the Viscosity of Silicate Melts. Part III: Modification for Melts Containing Alkali Oxides”. In: *International Journal of Materials Research* 103.3, pp. 313–328. DOI: doi:10.3139/146.110637. (Visited on 08/22/2023).

Kim, W.-Y., A. D. Pelton, and S. A. Decterov (2012b). “A Model to Calculate the Viscosity of Silicate Melts. Part III: Modification for Melts Containing Alkali Oxides”. In: *International Journal of Materials Research* 103.3, pp. 313–328. DOI: doi:10.3139/146.110637. (Visited on 08/22/2023).

Kita, Y. and Z.-i. Morita (Jan. 1, 1984). “The Electrical Resistivity of Liquid Fe-Ni, Fe-Co and Ni-Co Alloys”. In: *Journal of Non-Crystalline Solids* 61–62, pp. 1079–1084. ISSN: 0022-3093. DOI: 10.1016/0022-3093(84)90684-7. URL: https://www.sciencedirect.com/science/article/pii/0022309384906847 (visited on 07/07/2025).

Mills, K. C., B. J. Monaghan, and B. J. Keene (Jan. 1, 1996). “Thermal Conductivities of Molten Metals: Part 1 Pure Metals”. In: *International Materials Reviews* 41.6, pp. 209–242. ISSN: 0950-6608. DOI: 10.1179/imr.1996.41.6.209. URL: https://doi.org/10.1179/imr.1996.41.6.209 (visited on 07/10/2025).

Mills, K. C. (2002). *Recommended Values of Thermophysical Properties for Selected Commercial Alloys*. 1. publ. Cambridge: Woodhead. ISBN: 978-1-85573-569-9 978-0-87170-753-6.

Mizuno, N., S. Kosai, and E. Yamasue (2020). “Applicability of Wiedemann-Franz Law to Thermal Conductivity of Molten Fieldâ€™s Metal”. In: *Materials Science Forum* 985, pp. 1–9. ISSN: 1662-9752. DOI: 10.4028/www.scientific.net/MSF.985.1. URL: https://www.scientific.net/MSF.985.1 (visited on 08/13/2025).

Mysen, B. and P. Richet (2019). *Silicate Glasses and Melts - 2nd Edition*. 2nd. Elsevier. ISBN: 978-0-444-63709-3. URL: https://shop.elsevier.com/books/silicate-glasses-and-melts/mysen/978-0-444-63708-6 (visited on 10/03/2023).

Ntonti, E., S. Sotiriadou, M. J. Assael, M. L. Huber, B. Wilthan, and M. Watanabe (Jan. 2024). “Reference Correlations for the Density and Thermal Conductivity, and Review of the Viscosity Measurements, of Liquid Titanium, Zirconium, Hafnium, Vanadium, Niobium, Tantalum, Chromium, Molybdenum, and Tungsten”. In: *International Journal of Thermophysics* 45.2, p. 18. ISSN: 1572-9567. DOI: 10.1007/s10765-023-03305-z. (Visited on 08/05/2025).

Ono, Y., K. Hirayama, and K. Furukawa (1976). “Electric Resistivity of Molten Fe-C, Fe-Si and Fe-C-Si Alloys”. In: *Transactions of the Iron and Steel Institute of Japan* 16.3, pp. 153–160. DOI: 10.2355/isijinternational1966.16.153.

Ono, Y. and T. Yagi (1972). "Electric Resistivity of Molten Fe-Ni and Fe-Co Alloys". In: *Transactions of the Iron and Steel Institute of Japan* 12.4, pp. 314–316. DOI: 10.2355/isijinternational1966.12.314.

Sasaki, H., A. Ikari, K. Terashima, and S. K. S. Kimura (July 1, 1995). "Temperature Dependence of the Electrical Resistivity of Molten Silicon". In: *Japanese Journal of Applied Physics* 34 (7R), p. 3426. ISSN: 1347-4065. DOI: 10.1143/JJAP.34.3426. URL: https://iopscience.iop.org/article/10.1143/JJAP.34.3426/meta (visited on 08/27/2025).

Secco, R. A. (Apr. 1, 2017). "Thermal Conductivity and Seebeck Coefficient of Fe and Fe-Si Alloys: Implications for Variable Lorenz Number". In: *Physics of the Earth and Planetary Interiors* 265, pp. 23–34. ISSN: 0031-9201. DOI: 10.1016/j.pepi.2017.01.005. URL: https://www.sciencedirect.com/science/article/pii/S0031920116301832 (visited on 08/08/2025).

Seydel, U. and W. Fucke (1977). "Sub-microsecond pulse heating measurements of high temperature electrical resistivity of the 3d-transition metals Fe, Co, and Ni". In: *Zeitschrift für Naturforschung A* 32.9, pp. 994–1002. ISSN: 1865-7109. DOI: 10.1515/zna-1977-0913. URL: https://www.degruyterbrill.com/document/doi/10.1515/zna-1977-0913/html (visited on 08/11/2025).

Tesfaye, F. and P. Taskinen (2010). *Densities of Molten and Solid Alloys of (Fe, Cu, Ni, Co)-S at Elevated Temperatures - Literature Review and Analysis*. Aalto University Publications in Materials Science and Engineering. ISBN: 978-952-60-3272-6. (Visited on 07/09/2025).

"Thermodynamics Research Center" (Apr. 2009). In: *NIST*. (Visited on 08/14/2025).

Thibodeau, E. (2014). "Modeling the molar volume and electrical conductivity of oxide melts". MA thesis. Montreal, Canada: McGill University. (Visited on 06/26/2023).

Thibodeau, E. (Feb. 2016). "A structural electrical conductivity model for oxide melts". en. In: *METALLURGICAL AND MATERIALS TRANSACTIONS B* 47, pp. 355–383.

Thibodeau, E., A. E. Gheribi, and I.-H. Jung (2016a). "A Structural Molar Volume Model for Oxide Melts Part I: Li2O-Na2O-K2O-MgO-CaO-MnO-PbO-Al2O3-SiO2 Melts—Binary Systems". In: *Metallurgical and Materials Transactions B* 47.2, pp. 1147–1164. DOI: doi:10.1007/s11663-015-0548-y. (Visited on 06/13/2023).

Thibodeau, E., A. E. Gheribi, and I.-H. Jung (2016b). "A Structural Molar Volume Model for Oxide Melts Part II: Li2O-Na2O-K2O-MgO-CaO-MnO-PbO-Al2O3-SiO2 Melts—Ternary and Multicomponent Systems". In: *Metallurgical and Materials Transactions B* 47.2, pp. 1165–1186. DOI: doi:10.1007/s11663-015-0543-3. (Visited on 06/13/2023).

Thibodeau, E., A. E. Gheribi, and I.-H. Jung (2016c). "A Structural Molar Volume Model for Oxide Melts Part III: Fe Oxide-Containing Melts". In: *Metallurgical and Materials Transactions B* 47.2, pp. 1187–1202. DOI: doi:10.1007/s11663-015-0549-x. (Visited on 06/13/2023).

Watanabe, M., M. Adachi, M. Uchikoshi, and H. Fukuyama (July 1, 2019). "Thermal Conductivities of Fe-Ni Melts Measured by Non-contact Laser Modulation Calorimetry". In: *Metallurgical and Materials Transactions A* 50.7, pp. 3295–3300. ISSN: 1543-1940. DOI: 10.1007/s11661-019-05250-9. URL: https://doi.org/10.1007/s11661-019-05250-9 (visited on 08/06/2025).

Yamasue, E., M. Susa, H. Fukuyama, and K. Nagata (May 1, 2003). "Deviation from Wiedemannâ€"Franz Law for the Thermal Conductivity of Liquid Tin and Lead at Elevated Temperature". In: *International Journal of Thermophysics* 24.3, pp. 713–730. ISSN: 1572-9567. DOI: 10.1023/A:1024088232730. URL: https://doi.org/10.1023/A:1024088232730 (visited on 08/13/2025).

Zhao, A. Z. and J. E. Garay (Oct. 1, 2023). "High Temperature Liquid Thermal Conductivity: A Review of Measurement Techniques, Theoretical Understanding, and Energy Applications". In: *Progress in Materials Science* 139, p. 101180. ISSN: 0079-6425. DOI: 10.1016/j.pmatsci.2023.101180. URL: https://www.sciencedirect.com/science/article/pii/S0079642523001123 (visited on 07/11/2025).

Ziman, J. (2001). *Electrons and Phonons: The Theory of Transport Phenomena in Solids*. International Series of Monographs on Physics. OUP Oxford. 554 pp. ISBN: 978-0-19-850779-6. URL: https://books.google.co.za/books?id=UtEy63pjngsC.

Zytveld, J. B. V. (Aug. 1, 1980). "ELECTRICAL RESISTIVITIES OF LIQUID TRANSITION METALS". In: *Le Journal de Physique Colloques* 41.C8, pp. C8–506. ISSN: 0449-1947, 2777-3418. DOI: 10.1051/jphyscol:19808126. URL: http://dx.doi.org/10.1051/jphyscol:19808126 (visited on 07/31/2025).

Glossaries

Acronyms

BF-BOF Blast Furnace-Basic Oxygen Furnace 2

GGS Groeien met Groen Staal i, 2

MQM Modified Quasichemical Model 4, 9, 11–13, 20, 42, 43, 45, 46, 49

REF Reducing Electric Furnace i, 2, 64

Advancing Through Insight